The ELK global emission inventory for the transport sectors

Mattia Righi[1], Simone Ehrenberger[2], Sabine Brinkop[1], Johannes Hendricks[1], Jens Hellekes[3], Paweł Banyś[4], Isheeka Dasgupta[2], Patrick Draheim[5], Annika Fitz[6], Manuel Löber[7], Thomas Pregger[5], Yvonne Scholz[5], Angelika Schulz[8], Birgit Suhr[9], Nina Thomsen[8], Christian Martin Weder[10,11], Peter Berster[10,11], Maximilian Clococeanu[10,11], Marc Gelhausen[10,11], Alexander Lau[10,11], Florian Linke[10,11], Sigrun Matthes[1], and Zarah Lea Zengerling[10,11]

[1]Deutsches Zentrum für Luft- und Raumfahrt (DLR), Institut für Physik der Atmosphäre, Oberpfaffenhofen, Germany
[2]Deutsches Zentrum für Luft- und Raumfahrt (DLR), Institut für Fahrzeugkonzepte, Stuttgart, Germany
[3]Deutsches Zentrum für Luft- und Raumfahrt (DLR), Institut für Methodik der Fernerkundung, Oberpfaffenhofen, Germany
[4]Deutsches Zentrum für Luft- und Raumfahrt (DLR), Institut für Kommunikation und Navigation, Neustrelitz, Germany
[5]Deutsches Zentrum für Luft- und Raumfahrt (DLR), Institut für Vernetzte Energiesysteme, Stuttgart, Germany
[6]Deutsches Zentrum für Luft- und Raumfahrt (DLR), Institut für Maritime Energiesysteme, Geesthacht, Germany
[7]Deutsches Zentrum für Luft- und Raumfahrt (DLR), Institut für Verbrennungstechnik, Stuttgart, Germany
[8]Deutsches Zentrum für Luft- und Raumfahrt (DLR), Institut für Verkehrsforschung, Berlin, Germany
[9]Deutsches Zentrum für Luft- und Raumfahrt (DLR), Institut für Raumfahrtsysteme, Bremen, Germany
[10]Deutsches Zentrum für Luft- und Raumfahrt (DLR), Institut für Luftverkehr, Hamburg, Germany
[11]Deutsches Zentrum für Luft- und Raumfahrt (DLR), Institut für Luftverkehr, Cologne, Germany

Correspondence: Mattia Righi (mattia.righi@dlr.de)

Abstract. The transport sectors, comprising land transport, shipping and aviation, are major contributors to climate change and have a detrimental impact on air quality, with adverse consequences for human health. The emissions from transport, already contributing 23 % of total anthropogenic CO_2 emissions in 2019, are projected to continuously grow in the future, challenging the achievement of climate protection and pollution reduction targets. A major goal of transport research on climate and air quality is the accurate assessment of its impacts, which requires detailed emission data to drive atmospheric models and calculate projections for future scenarios. This paper presents the ELK global emission inventory for the transport sectors. The inventory is developed using a consistent bottom-up approach fed with a wide range of input data to model the transport fleets of land transport, shipping and aviation. It provides several major improvements over existing datasets, such as the explicit resolution of the emissions at the subsector level, the consideration of transport-specific quantities and emission species, and the quantification of major transport-related emissions from the energy sectors. The emission data is complemented by an uncertainty score, based on a detailed expert-judgement analysis along the modelling chain, from the activity data to the emission factors. The emission data is validated by comparing it with other, well-established global inventories, and biases are discussed and, where possible, explained in terms of the different assumptions and features of the underlying emission models. The ELK dataset is released under an open-source license to encourage their use in the atmospheric modelling community (https://doi.org/10.15489/d9dswthdix21, Ehrenberger et al., 2025, for land transport; https://doi.org/10.15489/lhqawfes5755, Banyś et al., 2025, for shipping;

https://doi.org/10.15489/86s8uwpxik95, Weder et al., 2025, for aviation; https://doi.org/10.15489/gixadaq6ds98, Draheim et al., 2025, for energy-for-transport).

1 Introduction

The emissions from the transport sectors contribute significantly to climate change. According to the sixth assessment report of the Intergovernmental Panel on Climate Change (IPCC; Jaramillo et al., 2022), transport was responsible for 8.7 Pg of CO_2-equivalent emissions in 2019 and shared 23 % of global energy-related CO_2 emissions. Land-based transport emissions represent the largest transport source (77 %), while shipping and aviation account for 11 % and 12 %, respectively. A major concern of the transport emissions are their large growth rates: according to Lamb et al. (2021), the greenhouse gas (GHG) emissions of the transport sectors grew at a global rate of about 2 % per year in the last three decades, with considerable differences between developed and developing countries: the CO_2-equivalent emissions of transport in East Asia, for instance, grew by a factor of 6 between 1990–2018, but only by 20 %–30 % in Europe and North America during the same period. Emissions scenarios project a continuous increase in the future, in particular for the shipping and aviation sectors which are hard to defossilise (Feng et al., 2020; Lund et al., 2020). In addition to CO_2 emissions, the combustion process of fossil fuels, still driving the vast majority of the fleet, leads to the formation of several short-lived climate forcers (SLCFs; Szopa et al., 2021), including NO_x ($=NO+NO_2$), CO, non-methane volatile organic compounds (NMVOC), SO_2, and aerosol particles (such as black and organic carbon). These compounds can have significant climate effects (Righi et al., 2023; Mertens et al., 2024) and, at the same time, be harmful for air quality (Fiore et al., 2012). The introduction of policy measures and the evaluation of their effectiveness is therefore challenging, because the impacts on both climate and air quality, as well as their trade-offs, need to be considered. Furthermore, some measures are applied on national or regional scale, especially for land-based transport, while sectors like shipping and aviation are regulated at the international level.

To address these scientific and policy-making challenges in the transport research, geographically resolved inventories for the emissions of all relevant compounds are essential. Given the global nature of the emissions and of the resulting climate impacts, a global data coverage is a key requirement, although regional inventories at higher resolution are also necessary for air quality studies. These datasets are the starting point for quantifying the effect of transport on climate and air quality, for developing scenarios of future emissions, and for assessing policy- and technology-based mitigation strategies to protect climate and improve air quality. State-of-the-art global inventories of anthropogenic emissions commonly used in climate science (e.g. Hoesly et al., 2018; Crippa et al., 2024; Soulie et al., 2024) include data for the transport sectors, often aggregated at the sector level, i.e. land-based transport (road and rail), shipping (international and domestic) and aviation. Being general-purpose inventories of anthropogenic emissions, however, these datasets do not usually provide information on transport-specific quantities, which are relevant to address the challenges of transport research outlined above. Such quantities include, for instance, water vapour emissions from aircraft (required for aviation contrails modelling; Burkhardt and Kärcher, 2011; Bickel et al., 2025) or highly resolved sectoral emissions (e.g. different vehicle or aircraft types). Most of the available inventories also do not report the transport-related share of emissions from other sectors, like the emissions from oil refineries and their share driving the transport fleet, as these are usually integrated in the emissions from the energy and/or the industry sector. This information is of key importance for a comprehensive assessment of the transport impacts and will be even more so in the future, with the expected shift of the road vehicle fleet towards alternative energy sources, with no or reduced direct (tailpipe) emissions from vehicles (Ghosh, 2020).

The goal of the project ELK (*EmissionsLandKarte*, en.: Emissions Map) of the German Aerospace Center (DLR) is to develop a consistent, complete, comparable and transparent global emission inventory of greenhouse gases and short-lived climate forcers (SLCFs) for the transport sectors and their relevant subsectors, while also accounting for major indirect emissions of transport in the energy sector. The ELK inventory described in this paper aims at providing the following improvements and added values over the existing datasets:

1. A consistent quantification of the emissions from all transport sectors with a bottom-up approach, using state-of-the-art emission models and a wide range of input data from different sources to drive these models.

2. The explicit resolution of the emission data at the subsector level, considering the emissions in 7 subsectors for the land transport emissions (cars, heavy-freight trucks, light commercial vehicles, buses, 2-wheelers, passenger rail, and freight rail) and in 4 subsectors for aviation (wide-body, single-aisle, regional, cargo). Shipping emissions are resolved between international (ocean-going) shipping and domestic navigation.

3. The inclusion of transport-specific quantities and emissions species, such as flight distance, propulsion ef-

ficiency and water vapour emissions from the avia-
tion sector (necessary for contrail modelling) and non-
exhaust emissions from the land transport sector.

4. An estimate of the indirect emissions of transport result-
ing from the energy sector via oil refineries.

5. An advanced assessment of the uncertainties along the
whole modelling chain, providing an uncertainty score
at the country level (for land transport) and in the IPCC
regions (for the other sectors), thus informing data users
about the quality of the data.

The ELK inventory considers present-day conditions, pro-
viding emission data for the year 2019 (hereafter, the refer-
ence year). The emission model chain is structured in a way
that it can also be used to project future emissions according
to given scenarios or including new fuel types and technolo-
gies that might be used for an energy transition in transport.
For example, considering new fuel types, this means to allow
to modify the emission species and their emission factor, and
also to include additional species such as hydrogen (H_2).

The ELK inventory is generated using common data stan-
dards for gridded emissions, to facilitate their use in cli-
mate and air quality models. The datasets are made avail-
able as CF-compliant NetCDF files, including standard meta-
data and units defined according to SI-standard. Furthermore,
a common grid with a resolution of $0.1° \times 0.1°$ is consid-
ered for all sectors, so that spatial aggregations across the
sectors can be calculated consistently without the need of
regridding. The temporal resolution of the data is monthly,
although hourly data is provided for some specific cases.
Aviation data is provided on a three-dimensional grid, fur-
ther including 48 vertical layers from the surface to an al-
titude of 47 000 ft (~ 14.3 km) above the mean sea level,
with a vertical resolution of 1000 ft, representing the main
flight levels of the commercial fleet. To reduce the signifi-
cantly larger amount of data required by a three-dimensional
grid, aviation data is provided at a reduced horizontal res-
olution ($0.25° \times 0.25°$) and temporal resolution (annual and
two seasonal averages over the November–March and April–
October periods). If necessary, the ELK emission models are
capable of modelling individual sectors at a higher resolu-
tion. To increase the internal consistency of the ELK dataset,
the same underlying framework data (e.g. population, gross
domestic product, trade flows, globally aggregated energy,
and fuel consumption) and the same methodology is applied
across the sectors where possible.

This manuscript serves as the main reference for the ELK
inventory. The methods for generating the emission data of
each sector are described in Sect. 2. Section 3 describes the
method applied for the assessment of the uncertainties in the
emission data. The results are presented in Sect. 4 for se-
lected species and compared with the transport emissions of
other well-established global inventories (additional species

are shown in the Supplement). The main conclusions of this
work are summarised in Sect. 6.

2 Methods

2.1 Land transport

2.1.1 Method overview

Land transport includes most of the everyday movement
of people and goods and hence contributes significantly to
transport-related emissions, with the largest share originat-
ing from road-based transport. However, due to its nature,
which is characterised by individual movements on large net-
works with a large, heterogenous vehicle fleet, the creation
of an emission inventory proves to be a challenging task.
On a global level, the transport sector has been modelled
by integrated assessment models (IAMs) and transport spe-
cific models. These models differ in their modelling frame-
work, in the underlying country-specific data and considered
emission factors (Yeh et al., 2017). A benchmark emission
stock is Emissions Database for Global Atmospheric Re-
search (EDGAR; Crippa et al., 2023) which have been devel-
oped over the past 20 years and which include the land trans-
port sector among others. The EDGAR group acknowledges
the huge challenge of collating and harmonizing datasets of
countries for road transport (Lekaki et al., 2024) and provides
the data sources for emission factor databases, vehicle stock
and assumptions for country-specific unavailable data.

Given the focus on transport of the ELK inventory, the ob-
jective is to build on and improve previous methodologies
to provide vehicle category specific datasets for both exhaust
and non-exhaust emissions, together with uncertainty metrics
and also to improve the methodology for spatial disaggrega-
tion of emissions. The vehicle categories considered in the
ELK inventory are passenger cars, 2-wheelers, buses, light
commercial vehicles (LCVs), heavy freight trucks (HFTs),
passenger and freight rail. The inventory contains emis-
sions of black carbon (BC), organic carbon (OC), CH_4, CO,
CO_2 (both fossil-fuel-based emissions and total emissions in-
cluding biofuels), hydrocarbons (HC), NMVOC, NH_3, N_2O,
NO_2, NO_x, particulate matter (PM_{10} and $PM_{2.5}$), particulate
number (PN), and SO_2. Emissions from non-exhaust species
include PM_{10} and $PM_{2.5}$ from tire wear and brake wear, and
PN from brake wear.

Two methods are developed in the ELK project using the
following approaches: (i) a global inventory is generated
based on a proxy data set and traffic counts for spatial disag-
gregation; and (ii) a European inventory is generated based
on a transport model. Figure 1 shows a schematic overview
of the methods, which differ primarily in the spatial distribu-
tion of the transport activity. The global approach calculates
the total emissions per country and species based on activity
and emission factors and then spatially disaggregates them
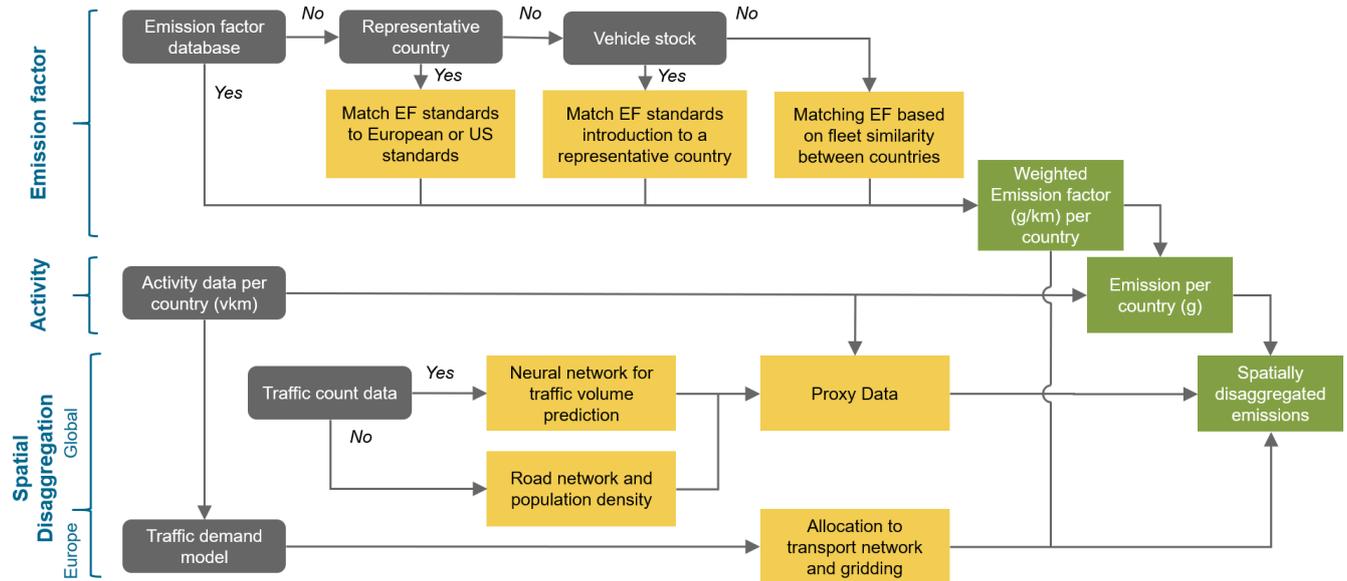on a grid using proxy data. For selected countries with good

Figure 1. Schematic of the emission computation for a given vehicle category.

quality data for validation, a model to spatially disaggregate emissions based on traffic counts is applied. While this approach is suitable for the estimation of emission sources on a larger scale with scarce calibration data sources, forecasting and the calculation of scenarios requires dedicated transport models describing travel behaviour (as demonstrated by Matthias et al., 2020). This is why, as a proof of concept for the correct allocation of emission sources, an additional emission inventory is created for Europe, where transport activity is first distributed on the road network, before aggregating the resulting emissions on a grid. Still, both approaches share the following major components: (i) transport activity data by vehicle category on the country level, including passenger and freight transport; (ii) emission factors on a country level; and (iii) a spatial disaggregation model. These three components are described in the following.

2.1.2 Activity data for land transport

Emissions from land transport are defined by transport activity, or travel demand, which constitutes transport volume by people (person kilometres travelled) and goods (tonne kilometres travelled). Therefore, a global activity database for the reference year 2019 is created based on data for population and economic development.

For passenger transport, the calculation of transport volumes follows the methodology described by Thomsen and Schulz (2024). The first step is the determination of national vehicle fleets. Based on historical data, correlating motorisation to the gross domestic product per capita (GDPpC) growth for representative countries, the parameters of Gompertz functions for different world regions are estimated. The Gompertz functions are used due to their typical s-shaped

curve, which allows to parametrise the point where a plateau for motorisation is reached. Applying these functions to the GDPpC in the reference year yields a motorisation rate (vehicles per capita), which is multiplied with the total population to generate the total vehicle fleet per country. Using reference values from literature for mean annual mileage per vehicle and world region, the total vehicle kilometres travelled per country are generated. Applying occupancy rates then yields the transport volume for car transport. The transport volumes for other modes are then calculated based on these car transport volumes by applying representative modal splits from national statistics, such as BMV (2025), and international data, such as OECD (2025).

Concerning freight transport, data for various countries of the world is available from sources like Eurostat or OECD. Since this data is regularly reported only for OECD countries, other countries are assigned to reference countries based on their similarities in GDPpC development. Freight transport performance on the road and, where available, on the railways is then modelled for the reference year using regression models. Data up to 2013 is used as training data for the regression and the model is applied using population and GDP data for 2019. The comparison of the 2019 observations revealed some significant deviations between the modelled and observed data in both directions. In cases where observations are available, these are used as activity data, otherwise correction factors describing the relationship between modelled and observed data is derived. These factors are then used to adjust the transport performance in countries without observed values, using the correction factors of the representative country.

The final inventory contains a small number of data gaps, mainly resulting from the lack of input data for certain coun-

tries with contested political status (e.g. Kosovo). These gaps may be mitigated in future work by incorporating alternative data sources.

2.1.3 Emission factors for land transport

The methodology used to calculate emission factors of vehicles per country, vehicle category and species is shown in Fig. 1. Weighted emission factors represent the emission factor for a specific vehicle category and species, taking into account the distribution of drivetrain types, segment and vehicle ages within the fleet for the reference year. If country-specific emission factor databases with integrated vehicle stock information are available, like HBEFA for Germany (INFRAS, 2026), they are used directly for calculating the weighted emission factors. If not, vehicle stock data of a country combined with emission factor (EF) standards is used to calculate the weighted emission factors. If no vehicle stock data is available then assumptions from similar countries are used to for assigning emission factor values.

The main data source for the vehicle stock data for the year 2021 is acquired from S&P Global Mobility (2021), which covers 76 country fleets worldwide. A key feature of the dataset is that the number of registered vehicles in the stock data is provided differentiated by vehicle category, segment or weight class, drivetrain or fuel type, and vehicle age or year of initial registration. Since emission factor datasets have a similar or identical structures, the core idea is to link the vehicle stock datasets with emission factor datasets via country-specific emission factor standards so that weighted, fleet-average emission factors can be calculated for these countries.

Emission factor databases with integrated vehicle stock of road vehicles are less widely available than vehicle stock data. Thus, the emission factors of a vehicle are determined by its emission standard, according to which it is type-tested and registered. Globally, there are essentially two major sets of rules for regulating pollutant emissions from road vehicles, differing by the year of their implementation in a given country/area. These are the European or UN-ECE based regulation with corresponding Euro 1–6 levels and the US regulation according to EPA or CARB which applies to North, Central and partly South America. Thus, two basic emission factor datasets are prepared for the global emission factors database: one for Euro-based vehicles from HBEFA (INFRAS, 2026) and one for US-based vehicles, from the California EMFAC model (CARB, 2021).

For the 6 European countries covered by HBEFA and for USA, the respective country-specific emission factor database or model-internal data included are considered for the calculation of the weighted emission factors. For all other countries for which S&P Global Mobility stock data is available, the emission factors are calculated on the basis of the global Euro- or US-based data. Different emission classes or Euro levels are introduced and implemented at different years

in respective countries. The goal was to assign a matching emission factor for each vehicle listed in the stock data by researching the applicable emission standard for each vehicle registration year in the period between 1971–2021. This mapping is implemented for the vehicle markets of representative countries for which information on emission standards are available (Argentina, Brazil, Canada, China, (rest of) Europe, India, Japan, Mexico, Russia, South Africa, South Korea, and US). Assumptions of emission factor standards are made for the remaining countries which are available in the S&P Global Mobility dataset by assigning to one of the representative countries, for which similar emission standards apply demonstrably or by assumption (i.e. the same emission standard is assumed for the same registration year). The remaining countries of the world, for which no stock data is available, are assigned weighted emission factors from one of the 76 bottom-up calculated countries. Similarities in emissions regulations and geographical correlations are considered. As a result, calculated NO_x emission factors are shown in Fig. 2a with vehicle-age-related contributions of passenger cars to their resulting NO_x emission factor using the vehicle stock, assumed age-related mileage driven curves, emission standards and introduction year of the particular country. This is relevant for policies like vehicle age-related circulation bans and understanding stock turnover effects.

A similar approach is adopted to obtain emission factors of commercial vehicles of LCVs and HFTs, although these vehicles have an additional parameter related to their weight class, whose definition varies across datasets available. To finalize these definitions, several options are considered for the vehicle allocation in each case. Representative vehicles from HBEFA and EMFAC are selected which correspond as closely as possible to the S&P Global Mobility vehicle categories. For this purpose the weight classes with the given weight ranges are considered as closely as possible and global information on CO_2 tailpipe emissions of commercial vehicles is used for comparison. Figure 2b shows the share of NO_x emissions calculated by the above described methodology from passenger cars and commercial vehicles in representative countries. The relative contributions are influenced by the diesel share of passenger cars in the stock and their age which determines the emission standard they conform to and also vehicle activity. NO_x emissions are heavily dominated by heavy freight trucks, which further support the need of vehicle category specific inventories and policies.

For other transport modes, such as passenger and freight rail, two-wheelers, and buses, the technology shares (including train-type distributions) and corresponding energy efficiencies for major countries are taken from earlier work (Teske et al., 2019). The countries covered include Australia, Brazil, China, Germany, India, Japan, Russia, South Africa, and the US. Emission factors for each technology in the reference year are derived from the most recent country-specific literature. For non-exhaust emissions of PM_{10} and $PM_{2.5}$ from tire wear and brake wear, the values are taken
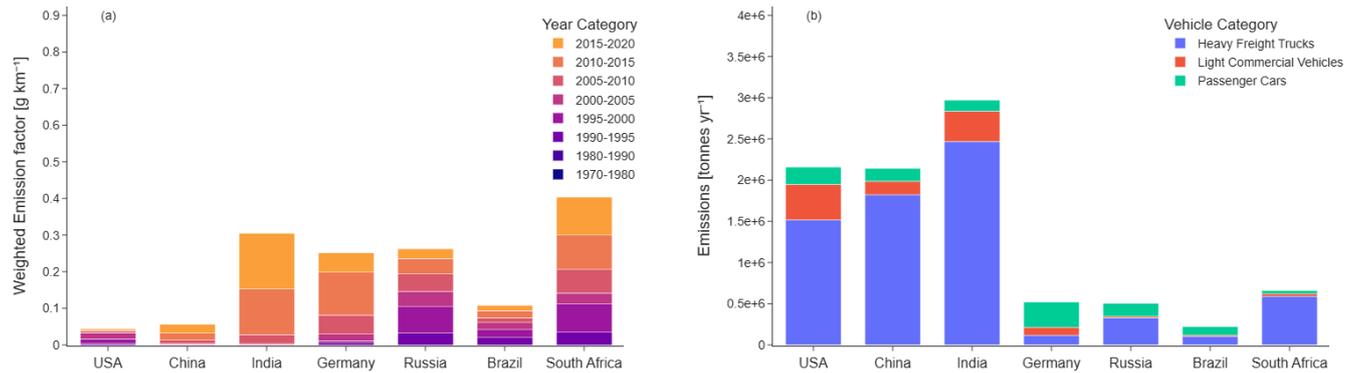
Figure 2. (a) Contribution to the NO_x emission factor by different passenger car ages; **(b)** NO_x emissions from vehicle categories in representative countries in 2019.

from Monks et al. (2019), including cars, 2-wheelers, buses, LCVs and HFTs differentiated by road type for the 6 European countries of HBEFA and uniformly across all other countries. Values of PN from brake wear stem from Perricone et al. (2020). For rail transport Fruhwirt et al. (2023) is used as a reference for non-exhaust emissions.

It should be noted that in addition to a vehicle emission standards, there are other country-specific, in-vehicle and out-of-vehicle characteristics that can determine or influence its real-world emission level. These include vehicle size and engine size, traffic conditions, ambient temperatures, and fuel quality among others. In principle, this approach produces global emissions inventories for country fleets with annual resolution. Due to this rather low level of detail, it is assumed that, apart from individual exceptions, the influencing factors mentioned are negligible. The effects of these parameters and other stock data quality influencing errors are considered in the uncertainty analysis described in Sect. 3.1.2. As a note, the stock data year (S& P Global Mobility, 2021) is slightly inconsistent with the reference year for the ELK inventory, but the differences between 2019–2021 are expected to be minimal.

2.1.4 Spatial disaggregation of land transport emissions

With emissions resulting from transport activity, which itself results from travel demand, applying a transport model for the spatial disaggregation is the logical approach. However, these models require a large amount of data for application as well as calibration and validation. Especially behavioural data, like National Household Travel Surveys (NHTS), is not widely available. Therefore, an approach using proxy data is used globally, while a simplified transport distribution model is applied for Europe. These methods are described in the following.

For the spatial disaggregation at the global level, existing transport inventories usually consider road type and density as well as population to disaggregate country-level emissions to its respective grid cells (Janssens-Maenhout et al., 2019).

This has been found to lead to an underestimation in high traffic roads in remote areas and suburban areas and thus an overestimation in urban areas with high population densities (McDonald et al., 2014; Gately and Hutyra, 2017). An alternative methodology is implemented in the ELK inventory to develop spatial proxies for passenger cars to disaggregate emissions in a country. A graph neural network is trained and tested to predict traffic counts in countries where traffic count data is openly and widely available. The approach relies on passenger car traffic count data collected on major roads in the US, Germany and UK. For model training and validation, US traffic count data from 2019 are used, comprising 5648 data points, of which 2400 located on interstate highways (FHWA, 2022a, b). For Germany, 1170 cleaned traffic count data points from 2022 on major roads are utilized (BASt, 2019). For the UK, traffic count data are obtained from a total of 13 900 data points (DfT, 2014, 2019). From each of the three datasets, approximately 1000 data points are selected to avoid introducing model bias.

The features used are population at different spatial scales (aggregated population at different distance buffers around a point), road density, population density, proximity to urban centres, and engineered in-betweenness features. In-betweenness features incorporate population and distance information of the surrounding cities and their contribution to traffic flow at a particular point. The model is thus able to predict the observed traffic flow in remote areas with high traffic flow by incorporating these features. Further details of this methodology will be provided in a separate publication. This methodology can be easily implemented for other developing countries if traffic count data becomes available. For the other modes like trucks (road type 1 and 2; Meijer et al., 2018) and 2-wheelers (road type 3, 4, and 5 multiplied by population) and buses (road type 2, 3, and 4 multiplied by population), proxies of road density of certain types combined with population are used globally and need further research and improvement on their applicability and country-wise relevance.

As mentioned above, a more detailed spatial distribution method was applied for Europe as a proof of concept (see Supplement). The spatial disaggregation for Europe is based on the universal transport distribution model ULTImodel (Thomsen, 2023) and described in Thomsen and Seum (2021) and Thomsen and Schulz (2024). Here, the transport volumes of the considered countries are distributed between cells using a gravity model and allocated to a higher-level road network with a network assignment. As reference cells, the NUTS 3 regions (Nomenclature of Territorial Units for Statistics; Eurostat, 2022) are used and the road network is generated from Open Street Map (https://www.openstreetmap.org/, last access: 10 June 2025). The distribution is based on the travel times and distances between cells, and their attractiveness as origins or destinations of trips is derived from their population and industrial sites. Transport volumes in the subordinate road network can be disaggregated at cell level. The results of the model run are then intersected with the inventory grid and aggregated per pixel by route type, whereupon the emissions are calculated using weighted emission factors.

The resulting spatial distributions with the two methods are shown in Fig. S1 in the Supplement for CO_2, while the total emissions over the domain of the European inventory are compared in Table S1 in the Supplement. Note that in the following only the global data will be discussed and validated, as this is the main focus of this work.

2.2 Shipping

For the shipping sector, the ELK inventory distinguishes between all ship movements in maritime environment (Sect. 2.2.1) and inland navigation (Sect. 2.2.2), for which different input data structures and modelling approaches are applied. For consistency with the IPCC definitions (IPCC, 2006), we use the terms international shipping (IPCC sector 1.A.3.d.i) and domestic navigation (IPCC sector 1.A.3.d.ii) to distinguish these two subsectors. Note, however, that domestic navigation in the ELK inventory only includes inland waterways, while short-range coastal shipping is part of the international shipping sector, although this is not fully consistent with the sector definitions.

2.2.1 International shipping

Maritime emissions and their environmental effects have been an important topic of research worldwide. The first study aimed at calculating emissions originating from vessels which took into consideration operational activities of the fleet applied a top-down approach (Corbett and Fischbeck, 1997). In that study, the authors based their analysis of air pollution on the research done by the International Maritime Organization (IMO). They concluded that the maritime sector is a significant source of air pollution on a global scale. Another interesting study of maritime emissions was completed by Eyring et al. (2005), who analysed five decades of civilian and military fleet movements and used them for global modelling of tropospheric chemistry. Various research activities were focused on predictions of future maritime emissions, too. An example analysis of the global maritime emissions and marine fuel consumption including future scenarios for 2050 was carried out by Paxian et al. (2010), considering the opening of Arctic polar routes as the aftermath of projected sea ice decline.

After the introduction of the Automatic Identification System (AIS; IMO, 2004), it became easier to track vessel positions and to store their movements in big-data archives. One of the first attempts to utilise AIS data for computation of maritime emissions was undertaken by Jalkanen et al. (2009) using the Ship Traffic Emission Assessment Model (STEAM) and focusing on the Baltic Sea. Since then, the method has been developed further (Johansson et al., 2017) and used by internationally recognised research projects like the Copernicus Atmosphere Monitoring Service (CAMS; Soulie et al., 2024). The STEAM model takes into account the environmental factors which interact with vessel movements, such as currents, waves, winds and ice conditions. Such approach has a high demand for computational power and is sensitive to various uncertainties related to the estimation of dynamic environmental influences depending on time and location. Within the scope of the STEAM model, it was assumed that considering the aforementioned factors could lead to an increase in the global annual fuel consumption estimates by as much as 5 %–15 % (Johansson et al., 2017).

In 2020 the IMO published the fourth edition of their comprehensive assessment of maritime emissions between 2012–2018 (Faber et al., 2020). The work also presents a revised algorithm for calculating maritime emissions, built upon the STEAM model. The IMO researchers reduced the complexity of the original model and generalised dynamic environmental factors in reference to aggregated classes of vessel type and size. Thanks to its lower requirement for computational power, the IMO algorithm is chosen for calculating maritime emissions for the ELK inventory, considering the global vessel traffic for the reference year 2019. A schematic overview of the applied method is depicted in Fig. 3.

The relevant input data includes two datasets, describing vessel traffic and vessel particulars, respectively. The vessel traffic data originates from the AIS. The AIS data was purchased from FleetMon (https://www.fleetmon.net/, last access: 10 June 2025). It contains over 76 billion vessel positions registered around the world in 2019 by the shore-based and satellite-based AIS reception systems. In addition, AIS data includes basic technical details, such as for instance the hull size, the vessel type and the current draught. The following AIS messages are utilised for the emission computation (ITU, 2014, p. 105–106): class A position report (IDs 1, 2, and 3), class B position report (ID 18), long-range position report (ID 27), and class A static and voyage related data (ID 5).
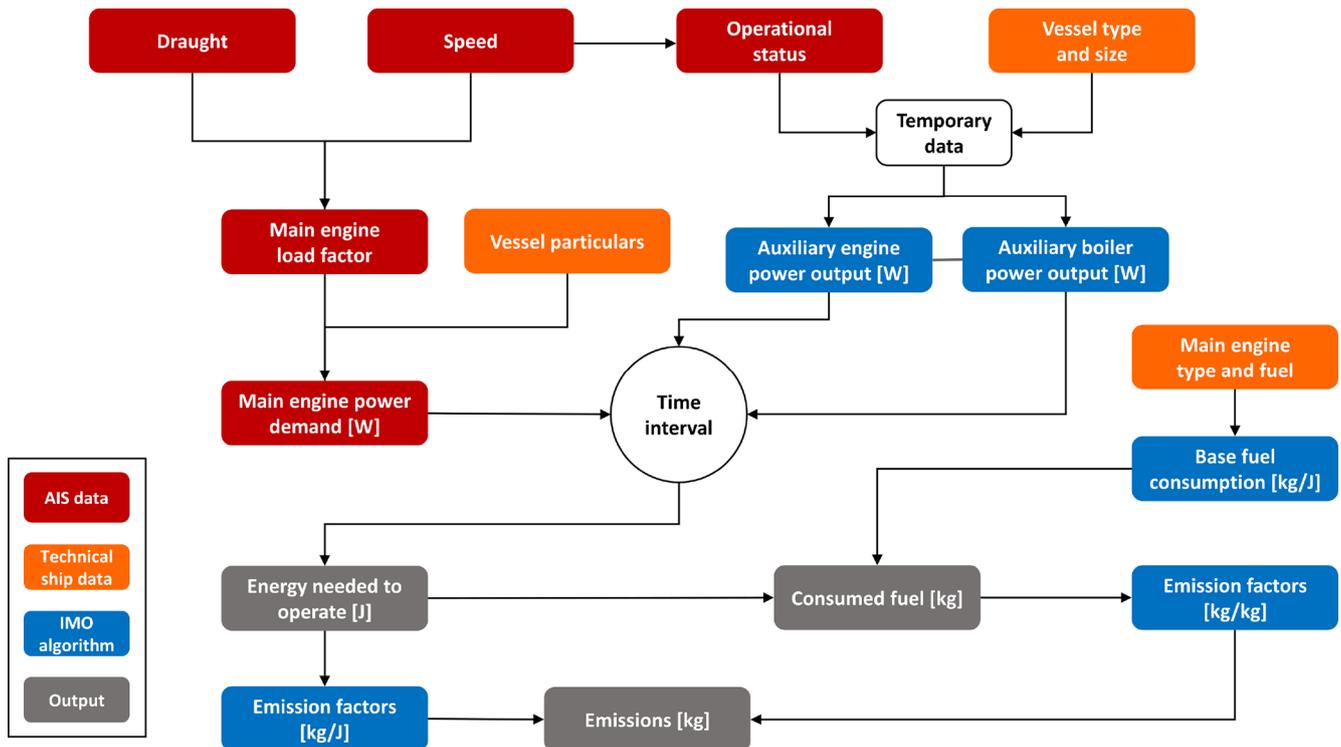
Figure 3. Schematic overview of the method applied for calculating the emissions from international shipping.

The vessel particulars dataset was purchased from Clarksons Research (https://www.clarksons.com/research/, last access: 10 June 2025). As of 16 May 2023, the vessel particulars contain technical details of 197 650 vessels. The dataset lists both vessels in operation and historical craft. This particular data mixture is helpful for the gap-filling of technical data because it allows to search for fleet similarities among sister or near-sister vessels to complete missing technical details, especially in regard to engine and fuel parameters. The number of vessels which were engaged in voyages during 2019 and could be identified both in AIS data and the vessel particulars database amounts to 86 192. According to the vessel particulars dataset 50.4 % of the above-mentioned fleet uses heavy fuel oil (HFO) and about 48.6 % uses marine diesel oil (MDO). The remaining 1 % of those vessels use either liquefied natural gas (LNG) or methanol. The vessel particulars dataset includes the following parameters: vessel identification, be it the Maritime Mobile Service Identity (MMSI), IMO number or call sign; construction year; vessel type and sub-type; reference power output of the main engine, main engine model, revolutions per minute (RPM) rating and engine design; fuel type; cargo capacity; maximum draught and maximum speed. With vessel identification data, especially MMSI, it is possible to merge the AIS data describing vessel movements with their technical parameters.

It is worth mentioning that a total number of MMSI spotted within the dynamic AIS position reports stored in the 2019 AIS dataset stands at 1 830 316. However, from as many as 790 653 (43.1 %) vessels only one dynamic AIS position report was ever received and stored in the AIS dataset. This makes all those vessels, even if they existed in the vessel particulars dataset, unusable for the emission calculation because no movement can be reconstructed from their AIS data. Moreover, in terms of all vessel positions (76 508 329 255) stored in the AIS dataset of 2019 about 50.3 % originate from the above-mentioned 86 192 vessels which could be fully identified for the purpose of emission calculation. The remaining 49.7 % of vessel movements, according to their static and voyage related AIS data, come from small craft, be it pleasure boats, tenders or special-purpose vessels, which have a limited range of operation and are not significant for the global trade and flow of cargo.

The process chain for calculating the shipping emissions in the ELK inventory can be generalised as follows:

1. computation of the current power demand of the main engine;

2. calculation of the corresponding power demand of auxiliary engine and auxiliary boiler based on the operational phase of a voyage;

3. computation of energy necessary to move a vessel between two positions during a period;

4. query of the baseline fuel consumption parameters based on the main engine type, the fuel type and the year of construction;

Earth Syst. Sci. Data, 18, 1619–1664, 2026

https://doi.org/10.5194/essd-18-1619-2026

5. calculation of the specific fuel consumption based on the current engine load;

6. assignment of the emission factors based on the engine and fuel parameters of a vessel;

7. computation of the emitted masses of the following species: CO_2, sulphur oxides (SO_x), NO_x, particulate matter (PM_{10} and $PM_{2.5}$), CO, NMVOC, and BC.

It should be emphasised that there is currently no technical possibility to obtain the engine performance and fuel consumption data directly from AIS. Therefore, these parameters have to be averaged based on aggregated vessel types and sizes. The current load of the main engine $L(t)$ on board a vessel is calculated using the following equation (Faber et al., 2020):

$$L(t) = \left(\frac{D(t)}{D_{\mathrm{ref}}}\right)^{2/3} \left(\frac{V(t)}{V_{\mathrm{ref}}}\right)^3, \qquad (1)$$

where $D(t)$ is the current draught of the vessel, $V(t)$ is the current speed of the vessel, D_{ref} and V_{ref} are the maximum draught and maximum speed, respectively, which are obtained from the vessel particulars dataset. The current power demand $W(t)$ of the main engine on board a vessel is calculated based on the so-called Admiralty formula (Faber et al., 2020):

$$W(t) = \frac{\delta_{\mathrm{w}}}{\eta_{\mathrm{w}}\,\eta_{\mathrm{f}}}\, L(t), \qquad (2)$$

where δ_{w} is a speed-power correction factor, η_{w} is a weather correction factor, and η_{f} is a fouling correction factor. The fouling is an overgrowth of invasive aquatic species on the submerged surface of a hull which can increase the friction of vessel movement through water (Townsin, 2003). The current speed of the vessel is calculated as a change in the position divided by the duration of a single movement. The change in the position is the distance along the geodetic line between two consecutive positions reported by the AIS transponder of the vessel. The duration of the movement is obtained from the absolute timestamps of the AIS position reports. It should be noted that the speed over ground (SOG) is an integral part of the dynamic AIS position report (ITU, 2014) and it can directly be used in the Admiralty formula. However, the design of AIS allows some data to be missing prior to a transmission of the AIS message. The AIS transponder, not to waste its reserved time slot for the upcoming AIS broadcast, automatically replaces unavailable parameters with default values, which explicitly indicate that certain sensor data on board a vessel are currently unknown. All parameters contained within a dynamic AIS position report except for MMSI are allowed to have an unknown value (ITU, 2014). Various analyses have shown that position reports containing unknown values of latitude and longitude have the lowest relative frequency of occurrence

(Banyś et al., 2020). Therefore, the likelihood that a vessel's speed, derived from two consecutive positions, is available for emission calculation is quite high.

The weather and the fouling correction factor for different vessel types and sizes are taken from Faber et al. (2020). These factors account for the impact of meteorological conditions and hull fouling on a vessel's power demand. The speed-power correction factor is applied to cruise vessels irrespective of their size and to container carriers which have a capacity of at least 14 500 twenty-foot equivalent units (TEU), again based on Faber et al. (2020). Analyses show that container vessels of this size are usually equipped with large engines but rarely proceed at their maximum speed, preferring rather an economical speed at lower engine load levels (Faber et al., 2020). The speed-power correction factors help to avoid an overestimation of the current power demand of those vessels.

The operational phase of a vessel is estimated based on its current speed and engine load as follows: *at berth* (when $V(t) \leq 1\,\mathrm{kn}$), *anchored* (when $1\,\mathrm{kn} < V(t) \leq 3\,\mathrm{kn}$), *manoeuvring* (when $3\,\mathrm{kn} < V(t) \leq 5\,\mathrm{kn}$), and *voyage* (when $V(t) > 5\,\mathrm{kn}$). The current power demand of auxiliary engines and auxiliary boilers fitted on board a vessel are categorised into different vessel types, sizes and operational phases. The following three conditions might occur:

– if the main engine power is not higher than 150 kW, then the current power demand of auxiliary engines and auxiliary boilers is set to zero,

– if the main engine power is between 150 and 500 kW, then the current power demand of auxiliary engines is set to 5 % of the main engine power and the current power demand of auxiliary boilers is taken from the power demand parameter table,

– if the main engine power is higher than 500 kW, the power demand parameter table is applied to both auxiliary engines and auxiliary boilers.

The energy demand is computed as a product of the current power demand $W(t)$ of the main engine on board a vessel and the time Δt needed to move between two consecutive positions reported by the AIS transponder:

$$E(t) = W(t)\,\Delta t. \qquad (3)$$

The baseline fuel consumption F of a vessel is obtained from a parameter table which contains aggregated constant values in relation to the main engine type, the fuel type and the year of construction of a vessel (Faber et al., 2020). To compute the specific fuel consumption $S(t)$, a main engine load correction factor $C(t)$ based on the current engine load $L(t)$ is applied:

$$S(t) = C(t)\,F, \qquad (4)$$

where the load correction factor $C(t)$ is provided by Faber et al. (2020) as:

$$C(t) = 0.455\,L(t)^2 - 0.71\,L(t) + 1.28. \qquad (5)$$

The load correction factor $C(t)$ is a simplified attempt to indicate that every vessel has a certain optimal engine load level at which the fuel consumption reaches its minimum (Al-Falahi et al., 2018). It is assumed that the specific fuel consumption shows a parabolic response to engine load levels. The fuel consumption curve is a specific property of each vessel. Here, we assume that the fuel consumption of the auxiliary engines and the auxiliary boilers does not depend on the engine load. The fuel consumption of the main engine and thus its emissions are set to zero if the main engine load $L(t)$ drops below 7 %. This kind of situation usually occurs at berth when the auxiliary engines and the auxiliary boilers are the only source of emissions. The mass of fuel consumed during a single movement is then obtained as a product of the specific fuel consumption $S(t)$ and the energy demand $E(t)$ as reported by AIS.

The final step of calculation of the emission fluxes followed one of the two alternative approaches: a computation based on energy demand $E(t)$ is applied for NO_x, CO, PM_{10}, $PM_{2.5}$, and NMVOC, whereas a computation based on specific fuel consumption $S(t)$ is applied for CO_2, SO_x, and BC. Depending on the applicable approach, either the energy demand or the specific fuel consumption is multiplied by the emission factor of the species provided in the factor lookup tables (Faber et al., 2020). The result is the mass of the species emitted by a given vessel during a single movement. The calculated masses of species are stored in a temporary database format, enabling the accumulation of raw emission values based on grid coordinates, time of occurrence, species, and vessel type. The raw emission data is then converted into the NetCDF files containing gridded emissions at the resolution of $0.1° \times 0.1°$. The intermediate database storage of raw emission data allows the creation of emission inventories for all vessel movements available in AIS data, as well as for selected fleets of specific vessel types.

2.2.2 Domestic navigation

In contrast to the international shipping sector, AIS data availability is more limited on inland waters. Fewer land-based antennas along rivers compared to coasts, shading through the terrain and terrestrial installations, restricted data sharing and regulatory differences between regions lead to a generally lower coverage. Therefore, bottom-up inventories using AIS data have been generated only on prominent waterway sections, which provide a higher density of AIS signals (e.g. Huang et al., 2022; Segers, 2021), but not on a larger scale. Top-down approaches use transportation statistics as an alternative to AIS data. Knörr et al. (2013) developed a top-down inland ship emission model utilising transport statistics of the German transportation emission model TREMOD (Allekotte et al., 2020). Based on goods statistics reported in ports and water locks by the Federal Statistical Office of Germany, the voyage and transport performance is assessed and differentiated by ship and cargo characteristics. Ship-type-specific energy demand and emission factors are developed to derive the total fuel consumption and emissions. The model, however, does not provide a spatial resolution of emissions in terms of an emission map. To address the problematic of low reliability in AIS for inland waters, Peng et al. (2024) proposed a combination of AIS and transportation data. While AIS and ship technical data were used to reconstruct characteristic ship behaviour, statistics from the Ministry of Transport of the People's Republic of China were used to fully capture the activity level. Although this approach seems promising, the input data requirements are high and difficult to realise on a global scale. To the authors' knowledge, there is no spatially resolving global model of domestic navigation emissions available to date. Existing inland ship emission inventories are regionally limited and rely on region-specific data structures. For the global ELK inventory of domestic navigation a method is presented limiting input data requirements to achieve a high regional flexibility while still addressing major differences in waterway systems.

For the ELK inventory the assessment of activity levels on the waterway systems consists of a primary approach, based on transportation data, and two fall back approaches, based on AIS data and on the assumption of homogeneously distributed activity, respectively. The primary approach for determining the activity levels is based on transportation data in tonne-kilometres (tkm) with a high spatial resolution (state-to-state flows). This is the case for Europe, where transportation flows can be obtained from Eurostat (https://doi.org/10.2908/IWW_GO_ATYVEFL, last access: 10 June 2025) on the NUTS2 level (https://ec.europa.eu/Eurostat/web/nuts, last access: 10 June 2025), and for North America, where annual transportation reports between states were published by the Waterborne Commerce Statistics Center (2021). For China similar data is also collected by the Ministry of Transport of the People's Republic of China, as mentioned in Peng et al. (2024), yet they are not publicly available. To achieve a spatial distribution, the transportation flows are modelled on a network graph of each inland waterway system with the Python library networkx (Hagberg et al., 2008). The path between two regions is identified utilising a Dijkstra shortest path algorithm, with the assumption that each ship performing the transportation task chooses the most direct route. Thereby all region-to-region transportation flows are distributed over the river network, thus determining the varying activity levels on each river section. If only total transportation volumes without region-to-region flows can be obtained but there are AIS signals available, the first fallback approach is utilised. Although the AIS signal level is generally not sufficient to reconstruct the full activity level for inland ships, it is used to model the spatial distribution. This approach comes with the drawback that AIS-

blind spots, for example where signals are fully shaded, are ignored in the activity distribution. This approach is applied for the China Yangtze River and Grand Canal region where the overall activity level could be estimated from values for 2018 published by Aritua et al. (2020). For the region of the Pearl River the overall activity level is also obtained from Aritua et al. (2020), however the available AIS dataset does not contain any signals for this river. As the second fallback approach the activity level is distributed homogeneously on the navigable sections of the river. Further waterway systems that are not considered in this dataset due to scarce data availability include the Amazon, Parana, Volga, national waterways of India, Nile, Congo, Mekong and Niger. Yet, the overall proportion in transported goods on these waterways is below 10 % comparing various data sources (Eurostat, 2022; Lewis et al., 2022; Press Information Bureau, Government of India, 2023; Jaghdani and Ketabchy, 2023).

To model the temporal distribution of the emissions, we follow the total waterway transportation volumes reported by the respective institutions. In the US, the Department of Transportation publishes monthly totals (https://data.bts.gov/stories/s/Monthly-Transportation-Statistics/m9eb-yevh/, last access: 10 June 2025), while for Europe quarterly data can be obtained from Eurostat (https://ec.europa.eu/Eurostat/databrowser/product/page/IWW_GO_QNAVE, last access: 10 June 2025). For China no monthly waterway transport statistics are obtained, therefore the temporal distribution is applied homogeneously over the year.

In addition to the actual transportation tasks, ships also perform journeys without carrying any cargo and these are therefore not captured in the transportation statistics. Knörr et al. (2013) observed a difference in the percentage of empty trips between dry and liquid goods carriers by evaluating data from German water locks. Based on this data they concluded that dry cargo ships perform 30 % and liquid carriers 80 % of their trips in unloaded conditions. This coincides with the average value of 47 % for both, liquid and dry cargo, reported in the year 2023 for the Iffezheim water lock (CCNR, 2023). For the other regions no specific information on the percentage of empty trips could be found. To still capture the effect of empty trips, the values of 30 % for dry goods and 80 % for liquid goods are applied to other modelled regions as well, although this estimate might differ from the actual value due to the region-specific trading patterns.

To obtain the energy demand of domestic navigation, the average energy intensity of the transportation tasks is identified for different regions by a literature review. The energy intensity of the transportation task can be affected by multiple parameters, including ship characteristics, loading conditions, conditions of the waterway, water level, and the direction of flow (up- or downstream the river). Since the data availability is not given in all modelled regions, a simplified approach is chosen, utilising the average energy intensity typical for each region based on a literature review. Radmilovic and Dragovic (2007) conducted a study on the

energy intensity of various domestic transportation modes in Europe, concluding that inland waterway transport is the most energy-efficient, with a value of $0.423\,\mathrm{MJ\,t\,km^{-1}}$. This finding aligns with the energy intensity range of 0.38–$0.52\,\mathrm{MJ\,t\,km^{-1}}$ reported by Knörr et al. (2013), who used a bottom-up calculation approach under average loading conditions for ships of different load classes. Consequently, we adopted the value of $0.423\,\mathrm{MJ\,t\,km^{-1}}$ as the reference for Europe. For the US, Bray et al. (2002) studied the energy intensity on different sections of rivers with a top-down approach to transportation statistics, lock data and vessel characteristics, and found an average value of $0.192\,\mathrm{MJ\,t\,km^{-1}}$. A later study by Belzer (2014) reported a lower value of $0.157\,\mathrm{MJ\,t\,km^{-1}}$, which is used in this study. According to these values, the US inland waterway system operates more than twice as efficient compared to the EU system. This may be due to wider and more navigable waterways and fewer locks. Furthermore, the more widespread use of larger, non-propelled barges in push tows enables more efficient transportation. The analysis of the Clarksons Research data showed that while in the US 87 % of the vessels listed are non-propelled barges, in the EU it is only 16 % and 9 % in China. Therefore, the energy intensity for China is assumed to be similar to that of the EU.

Finally, the emission factors are determined based on the regional emission regulations and the age structure of the fleet extracted from Clarksons Research data. It is assumed that vessels built within an emission stage comply with the respective emission limits for NO_x, CO, HC, and PM in each region. It is also assumed that the transportation tasks are distributed equally among the age distribution of the fleet, resulting in the fleet emission factors shown in Table 1. The US result in significant lower fleet emission values due to stricter emission limits of the US Environmental Protection Agency (EPA) and a continuous replacement of vessels. In Europe, on the contrary, the aged fleet leads to higher average emission factors, despite the aligned emission limitations of the EU Non-Road Mobile Machinery (NRMM) regulations to the US EPA regulations. China implements less strict emission limits compared to Europe and the US, starting with stage I only in 2015. Yet the overall younger age structure of the Chinese fleet leads to lower emission factors compared to Europe. In all regions the emission factors before any implementation of emission regulations are assumed to be $11\,\mathrm{g\,kWh^{-1}}$ for NO_x, $5\,\mathrm{g\,kWh^{-1}}$ for CO, $4.7\,\mathrm{g\,kWh^{-1}}$ for HC and $0.4\,\mathrm{g\,kWh^{-1}}$ for PM. Emissions of CO_2, CH_4, N_2O, NMVOC, BC, and SO_x are addressed independently of the emission stage but based on the general combustion characteristics of 4-stroke, high-speed diesel engines operating on distillate diesel oil, which represent the large majority of equipment used in domestic navigation. The values are harmonised with the respective equipment emission factors of the international shipping sector (Sect. 2.2.1). The same energy density of $42.7\,\mathrm{kJ\,kg_{fuel}^{-1}}$ for distillate diesel oil (ma-

Table 1. Average fleet emission factors of regulated pollutants from inland navigation in each modelled region. Units are $g\,kWh^{-1}$.

Species	Unites States	Europe	China
NO_x	5.62	8.5	8.27
CO	4.63	4.8	4.56
HC	2.78	3.87	3.20
PM	0.25	0.28	0.3

rine diesel oil) is applied to quantify the amount of burnt fuel for fuel-based emission factors.

As noted in the analysis of available AIS data for domestic navigation, there is insufficient data in the investigated regions. Therefore, we conclude this section by illustrating a concept for using satellite data that could help identifying vessels on rivers and channels. This concept considers the use of freely available satellite data for scientific research, with a specific focus on optical and Synthetic Aperture Radar (SAR) data. To minimise the number of satellite scenes to be processed, a database is created which contains only those metadata of the radar and optical scenes that have an overlap with inland waterways. A second approach is to use existing ship detection algorithms to identify vessels over terrestrial areas. Ship detection algorithms mostly use land masks to determine whether a raster pixel is land or water. Also for this case, we identify and analyse various data sources in more detail with regard to their usability. As for the first approach, the detected ships are stored in a database and compared with the few existing AIS data to determine only the missing vessels in the AIS detections. These can then be passed on for validation purposes or to supplement missing vessel positions. Since the existing ship detection algorithms are developed for the open sea, the results must be evaluated to identify false or missing detections. When using the existing algorithms, it should also be noted for which satellite data they were developed and which land masks can be used. This may limit the availability of usable, freely accessible satellite data, reducing the number of additional ship positions that can be identified. One of the possible sources are radar data, which, compared to optical data, is almost independent of weather conditions and can record signals even during darkness. Radar data is generated by SAR sensors, which operate in the microwave frequency range of the electromagnetic spectrum (Skolnik, 2008). SAR sensors actively illuminate an area with microwaves and map it in two dimensions. In addition to the position, the ship width and length also play a role in determining the emissions in relation to her class or type, therefore the use of radar signatures of ships to derive ship length and width from the dimensions of the signatures is widespread (Tings et al., 2016). The ship radar signatures in the SAR images usually have larger dimensions than the actual dimensions of the ship. The reason for such dimensional distortions is the higher normalized radar cross section (NRCS) at the boundary between the ship hull and the water surface as well as at the ship superstructure, which lead to different reflection effects (Crisp, 2004; Tings et al., 2016). The smearing of moving point targets also leads to a distortion of the ship dimensions (the so-called azimuth smearing effect; Skolnik, 2008; Tings et al., 2016). The overestimation of the ship dimensions can be reduced by applying analytical and empirical methods (Tings et al., 2016). If AIS data is available for the radar scenes, these can be used to determine the ship dimensions, as they are more accurate than the derivation from the ship radar signatures. There are a large number of research teams working on ship detection based on radar data (Vachon et al., 1997). Since the existing ship detection algorithms are designed for the open sea, their applicability to inland navigation remains uncertain. Limitations include wind speeds, radar angle of incidence, satellite flight direction, ship speed, decay rates of wakes, ship offset in azimuth direction, waves, width of the river compared to the open sea, other metal objects (bridges, bollards, harbour superstructures, quay walls, buildings, etc.) or the ship length. On the open sea, the detectable ship lengths are between 5 and 350 m.

2.3 Aviation

Air transport is essential for long-distance travel in a relatively short time and for the rapid transport of freight between continents. Due to the increasing relevance of environmental effects and climate impacts of air traffic, that is responsible for 3.5 % of global anthropogenic radiative forcing in 2018 (Lee et al., 2021), several studies have focussed on the generation of bottom-up quantification of aviation emissions. The underlying methodology of the ELK inventory for aviation emissions is an advancement of the approach used in the predecessor inventory TraK (Transport und Klima, en: Transport and Climate), where gridded aviation emission inventories for passenger flights for the years 2015, 2019, and 2020 were generated using Reduced Emission Profiles (Linke, 2016), great circle routes and fuel-optimized cruise altitudes. The idea of emission quantification on a subsectoral level including cargo air traffic developed in this work has also been followed in Graver et al. (2020) for the years 2013, 2018, and 2019, but only for CO_2 and without modelling three-dimensional distributed data. Teoh et al. (2024) used detailed trajectories from Automatic Dependent Surveillance – Broadcast (ADS-B) data and EUROCONTROL Base of Aircraft Data model family 3 and 4 (BADA3 and BADA4) flight performance models to derive 3D annual emission inventories for 2019, 2020, and 2021 to evaluate the effects of COVID-19 pandemic on air traffic volume and emissions. Quadros et al. (2022) also investigated pandemic effects and covered the years 2017–2020 based on BADA3 aircraft performance and monthly averages of ADS-B routing data. Eyers et al. (2005), Wilkerson et al. (2010),

and Simone et al. (2013) produced annual bottom-up aviation emission inventories for 2002, 2004, 2005, and 2006.

To model a detailed aviation emission inventory, a traffic demand and fleet scenario in the form of a flight schedule is required to construct the global network. 4D aircraft trajectory profiles, incorporating detailed information on fuel consumption and emission factors for each flight phase, are adjusted for wind affects and projected along actual flight paths to achieve a more realistic spatial distribution. The applied methodology is described in detail in the following subsections.

2.3.1 Air traffic schedule and fleet composition

In the ELK inventory, the air traffic of worldwide scheduled civil commercial passenger flights and large parts of cargo flights have been considered. Non-scheduled passenger flights, business flights, general aviation, governmental flights and military flights are not included. The air traffic network for the reference year 2019 is calculated with the model FORMO (Gelhausen et al., 2019) based on input from several databases like Airport Council International (ACI, 2019), Sabre Market Intelligence (Sabre, 2019), Official Airline Guide (Reed Travel Group, 2019), IATA Air Freight Bills (CASS; IATA, 2019) and Cirium Fleet Analyzer (Cirium, 2019). These databases provide information on the global fleet composition, scheduled commercial passenger flights, transported passengers and ticket fares. For passenger air traffic the model synchronizes the various databases: OAG, Sabre and Cirium to match passenger and flight volume by aircraft type and flight time for passenger transport. Cirium is used to determine the number of aircraft and aircraft type for the corresponding flight movement volume. This involves standardizing and cleaning data and removing data not needed. The data for a global air freight is largely based on aircraft movements derived from the ACI, OAG freight flights on individual routes and freight volumes by origin and destination airport pair from the CASS. Aircraft data from Cirium plays a major role in obtaining information on individual aircraft and airlines. In addition to cargo-only scheduled flights, a large share of air freight is transported as belly freight by passenger aircraft and by dedicated freight integrators like DHL, FedEx or UPS, which do not appear in official flight schedules from Sabre. The major challenge is that there is no standardized and complete database for air freight, so that at least some of the freight flows and related flights need to be modelled by comparing different databases, cleaning data, and modelling missing data. Cross-checking for plausibility and further quality checks are important for a consistent database of air freight. The result consists of global weekly flight plans providing information on origin and destination airport, local departure and arrival time, aircraft type, seat capacity as well as seat load factor (passenger transport only). The public domain airport database OpenFlights (http://www.openflights.org, last

access: 10 June 2025) provides information on location and elevation of the origin and destination airports and the time zones, which are necessary to convert the local departure and arrival time into Coordinated Universal Time (UTC) units. For the ELK inventory, flight plans for both passenger and cargo air transport are created for the week 28 January 2019–3 February 2019, representative of the winter season, and for the week 22 July 2019–28 July 2019, representative of the summer season. These seasonal air traffic data enable an extrapolation to the entire year, by considering five months of winter season (November–March) and seven months of summer season (April–October). To gain a more specific view on the emission quantities by aircraft size, the global fleet of passenger aircraft is split into three subsectors based on the seat number and the maximum range, namely regional (typical number of seats < 100 and maximum range < 2000 nautical miles (NM)), single-aisle ($100 \leq$ typical number of seats < 235 and 2000 NM $\leq$ maximum range < 4500 NM) and wide-body aircraft (typical number of seats $\geq$ 235 and maximum range $\geq$ 4500 NM). If an aircraft exceeds either the maximum range or the seat number threshold, the aircraft is categorized into the next larger category.

2.3.2 Aircraft performance and trajectory modelling

Flight trajectories are modelled with the Trajectory Calculation Module (TCM), an aircraft trajectory simulator developed at DLR Institute of Air Transport based on the Total Energy Model (Linke, 2016). For the atmospheric background data, International Standard Atmosphere (ISA; ICAO, 1993) conditions are used. TCM performs a forward integration in high temporal resolution (typically 10 s) of the aircraft state along a four-dimensional flight trajectory defined by characteristic flight phases. Required aircraft characteristics (e.g. weight, geometry) and flight performance parameters are provided by BADA4 (version 4.2) from EUROCONTROL (Nuic et al., 2010). In order to cover the global fleet to the highest possible extent, we supplement BADA4 data by internally developed aircraft performance models of aircraft types recently put into service (e.g. Airbus A321neo, A330-900neo, A220-300) or missing aircraft type in BADA4 of enhanced relevance for regional air traffic (Canadair Regional Jet 900), see Woehler et al. (2020). To facilitate the calculation of a large set of trajectories in an efficient manner, Reduced Emission Profiles (RedEmP) are derived (Linke, 2016) representing a pre-calculated dataset of relevant flight performance parameters along standardised flight trajectories, starting and ending at sea level and non-georeferenced, with a reduced number of datapoints. The RedEmP database contains trajectories for every available aircraft type with different flight lengths in 100 NM steps, different altitude settings and take-off masses (characterised by load factors), as these factors significantly influence flight performance, fuel consumption and emission factors. Resulting trajectories are then reduced to flight phase characterising data points so that

between 13–25 trajectory points can be used to efficiently describe every trajectory of a given flight plan. The stored parameters contain several state variables, such as altitude, true air speed, thrust, rate of climb and descent, and fuel flow along the entire trajectory. Flight phase dependent emission flows for various species are added to the database of RedEmP in a post-processing step (see Sect. 2.3.3).

Compared to the previously developed RedEmPs (Linke, 2016), here we extend the data set by considering different flight altitudes, namely fuel-optimized cruise altitudes, characterized by a minimum fuel flow and the operation of step climbs in the course of the cruise phase in case the next flight level is more fuel-efficient, and constant cruise altitudes (Zengerling et al., 2022). Furthermore, we improve the resolution of the assumed load factors by covering an interval width of 0.025 for load factors higher than 0.7. Finally, we extend the set of covered parameters by engine thrust and propulsion efficiency. Aircraft performance models from BADA4 and DLR cover more than 97 % of the total annual available seat kilometers (ASK) of the underlying flight plans, thus ensuring a high coverage of the global fleet in the emission inventory. In order to reduce remaining gaps in fleet coverage and to complete the regional and cargo fleet, simplified trajectories from previous performance simulations are applied additionally, using BADA3 models (version 3.11), that are available for plenty of turboprop and piston aircraft models. In previous trajectory simulations, BADA3 vertical profiles of aircraft performance have been forwardly integrated and vertically interpolated to generate simple trajectory segments for climb, cruise and descent phase with a payload-dependent rate of climb and cruise altitude, which have been stored in a database. For the flight missions of the remaining aircraft out of the ELK flight schedules, the preprocessed trajectory segments have been re-used and combined to obtain a complete trajectory, where the emission flows have been added finally.

2.3.3   Emission factors for aviation

CO_2 and water vapour (H_2O) emissions are scaled linearly to fuel consumption with constant emission factors of 3.159 and $1.237 \, \mathrm{kg \, kg_{fuel}^{-1}}$, respectively, assuming a stoichiometric combustion (Wilkerson et al., 2010). For the calculation of non-linear emissions of CO and HC, the Boeing Fuel Flow Correlation Method 2 (DuBois and Paynter, 2006) is applied, while NO_x emissions are derived as NO_2 mass equivalent with the DLR methodology by Deidewig et al. (1996). NMVOC emissions are derived from HC emissions by applying a scaling factor of 1.0947 (Jelinek et al., 2004). For the application of fuel flow correlation methods, the required atmospheric background data is taken from ISA (ICAO, 1993), for NO_x emissions an altitude-dependent humidity profile is assumed (Schaefer and Bartosch, 2013). Emission factors that have been quantified from test bench measurements for four thrust settings as defined in landing-takeoff-cycle (LTO;

ICAO, 2008) are taken from ICAO Engine Emission Databank v29a (EEDB, https://www.easa.europa.eu/domains/environment/icao-aircraft-engine-emissions-databank, last access: 10 June 2025) for jet engines and from piston engine emission data from the Swiss Federal Office of Civil Aviation (FOCA, 2007). For turboprops no thrust-dependent emission factors are available, so constant values are used for NO_x, HC, CO, and BC, as derived from fleet averages in Wilkerson et al. (2010). BC emissions are built on smoke numbers from EEDB and the methodology from Döpelheuer (2002). SO_2 emission quantities scale linearly with the fuel consumption, but the emission factor depends on the regional average fuel sulphur content as analysed in CRC (2012) for year 2010 and is set for each flight individually with regard to the continental area of the departure airport. The OC emission factor is set constant to $0.02 \, \mathrm{g \, kg_{fuel}^{-1}}$ (Stettler et al., 2011). Non-volatile particular matter number (nvPMn) and mass (nvPMm) emission factors for LTO cycle are taken from EEDB for jet engines and interpolated linearly depending on the relative thrust setting from the trajectory simulations. For engines without LTO particle emission data available, fleet average values of $0.080 \, \mathrm{g \, kg_{fuel}^{-1}}$ for nvPMm (Stettler et al., 2013) and $10^{15} \, \mathrm{\# \, kg_{fuel}^{-1}}$ for nvPMn (Schumann et al., 2015; Teoh et al., 2020) are used constantly for all flight phases.

In addition to GHG and SLCF emissions, propulsion efficiency η is a relevant parameter for the contrail modelling and is therefore included in the ELK inventory. The propulsion efficiency depends mainly on the flight phase and can be expressed as a function of thrust setting, speed and fuel flow:

$$\eta = \frac{v_{\mathrm{TAS}} \, T}{\dot{m} \, Q}, \tag{6}$$

with v_{TAS} as true air speed, T as engine thrust, $\dot{m}$ as fuel flow rate and the specific combustion heat for aviation fuel $Q = 43 \, \mathrm{MJ \, kg^{-1}}$ (Schumann, 1996). The resulting emission flows are additionally stored in the RedEmP database enabling a combined evaluation across a given flight plan.

2.3.4   Routing and flight path data

To enhance the realism of routing in the ELK emission inventory, detailed waypoint and altitude profiles of approximately one million global flights operated in year 2019, mainly from week 05 and week 30, are quality-checked, filtered and stored in a database. The actual 3D flight paths are derived from ADS-B mode S data from OpenSky Network (Schäfer et al., 2014; Strohmeier et al., 2021), covering predominantly domestic flights over Europe, North America and some regions in Asia (e.g. Japan, India and Australia) depending on the density of the ADS-B receiver network. Additionally, model 3 data from EUROCONTROL Demand Data Repository 2 (DDR2: Urjais, 2022) with flight path profiles of inner-European flights and intercontinental flights from Europe to various worldwide destinations and vice versa as

well as international flights crossing European airspace contribute to the routing data. For the remaining flights in the schedules, where no flight path profile can be identified in the datasets, the great circle route between the origin and destination airport is used.

2.3.5 Wind impact on aviation emissions

To consider head and tail wind effects on flown ground distance, the statistical approach by Swaid et al. (2024) is used to derive the average of the wind-corrected ground speed based on local annual wind statistics. For this purpose, global grids of horizontal wind data at $0.25° × 0.25°$ resolution on various pressure levels from the ERA-5 reanalysis data (Hersbach et al., 2023) at 00:00, 06:00, 12:00, and 18:00 UTC for every day in the year 2019 are vertically interpolated to obtain a dataset for each flight level from 0 to 44 000 ft altitude (and the same value is applied for higher levels up to 47 000 ft). The vertically interpolated wind data is binned in each grid cell with a wind speed increment of $5 \, \mathrm{m \, s^{-1}}$ and 10° wind direction intervals and converted into an annual wind rose statistic that consists of 1460 values per grid cell. For each origin-destination pair and aircraft type within the weekly flight plans, the great circle route is divided into ten segments of equal length. Their mean headings, the aircraft specific mean cruise v_{TAS} at the mean fuel-optimized cruise altitude are then used to derive the resulting statistical distribution of ground speed, incorporating the local annual wind statistics. To obtain a dimensionless wind impact scaling factor ϵ, the flight's mean cruise v_{TAS} is divided by the average of the segment specific ground speed (GS) distribution:

$$\epsilon(i) = \frac{v_{\mathrm{TAS}}(i) \, t(i)}{v_{\mathrm{GS,ave}}(i) \, t(i)} = \frac{\mathrm{d_{air}}(i)}{\mathrm{d_{ground}}(i)}, \tag{7}$$

with $v_{\mathrm{TAS}}(i)$ the mean cruise true air speed in a trajectory segment i, $v_{\mathrm{GS,ave}}(i)$ the mean ground speed depending on the wind statistic along the trajectory segment i, t the flight time of the trajectory segment i and d_{air} and d_{ground} the air and ground distance of the trajectory segment i, respectively. A value of $\epsilon > 1$ ($\epsilon < 1$) represents head (tail) wind situations. The mean wind effect scaling factors ϵ are used to adjust the air distance for the trajectory segments of each route in the flight plan.

2.3.6 Aviation emissions model workflow

For each flight that is scheduled in the seasonal weekly flight plans, the flight route database is scanned, and up to eight appropriate flight path datasets for the respective origin and destination pair are selected in a random-pick approach (see Sect. 2.3.4). Based on the wind-corrected distance, the load factor and aircraft type, the best-fitting RedEmP is picked or if not available, a simple trajectory is generated out of the simplified BADA3 trajectory segments (see Sect. 2.3.2). The

cruise altitude of the RedEmP is assumed fuel-optimized including step climbs during longer flight distances for the first four selected flight path profiles and for the remaining flight path profiles RedEmPs with constant discrete cruise flight levels are used, that have been identified as the main cruise flight level of the route profile. For all available routes, the cruise phase of the selected RedEmP with a discrete distance (100 NM steps) is extended or truncated to the actual flight length and the climb and descend phases are adjusted to the elevation of the origin and destination airports. Subsequently, all available route profiles are averaged with equal weights to represent one single flight. The final emission inventory thus consists of 50 % of trajectories with fuel-optimized cruise altitudes and 50 % of various constant altitudes each. Emissions on ground caused by taxiing at the airports are derived with the measured emission factors and fuel flow in idle mode from the underlying emission factor databases (see Sect. 2.3.3) and multiplied with the airport-specific median taxiing times from the EUROCONTROL seasonal statistics for year 2019 (https://www.eurocontrol.int/publication/taxi-times-summer-2019, https://www.eurocontrol.int/publication/taxi-times-winter-2018-2019, last access: 10 June 2025). These times are available for more than 400 airports worldwide, otherwise intervals of 19 min for taxi-out and another 7 min for taxi-in as defined in LTO cycle (ICAO, 2008) are applied. For all flights, take-off emissions are represented by engines running 0.7 min in take-off mode, also following the LTO cycle. The resulting emission quantities are attached at the beginning and at the end of the emission profile at the airport location and allocated to the grid layer of the respective airport elevation. Due to the unavailability of LTO cycle emission factors for turboprop engines, taxiing emissions cannot be taken into account for flights operated by turboprops. Finally, the modified emission profile is projected on the georeferenced route and converted to the 3D numerical grid with a resolution of $0.25° × 0.25° × 1000$ ft. The grid layers are arranged in a way so that each discrete flight level (FL) is located in the centre of each grid layer (e.g. grid cell layer from 36 500 ft to 37 500 ft for FL 370), starting from sea level at the lowest layer. The annual total emission inventory is derived by an upscaling and weighted mean of the seasonal weekly inventories (see Sect. 2.3.1). A more detailed temporal discretisation of emission grids in up to hourly resolution is performed to show diurnal effects of air traffic volume on emission distribution. The entire model workflow including the required input datasets and the preprocessing steps is depicted in Fig. 4.

2.4 Energy for transport

This section describes the estimation of global emissions from major energy-related production processes of fuels for the transport sector, that is, the indirect emissions from transport in the energy sector. According to the International
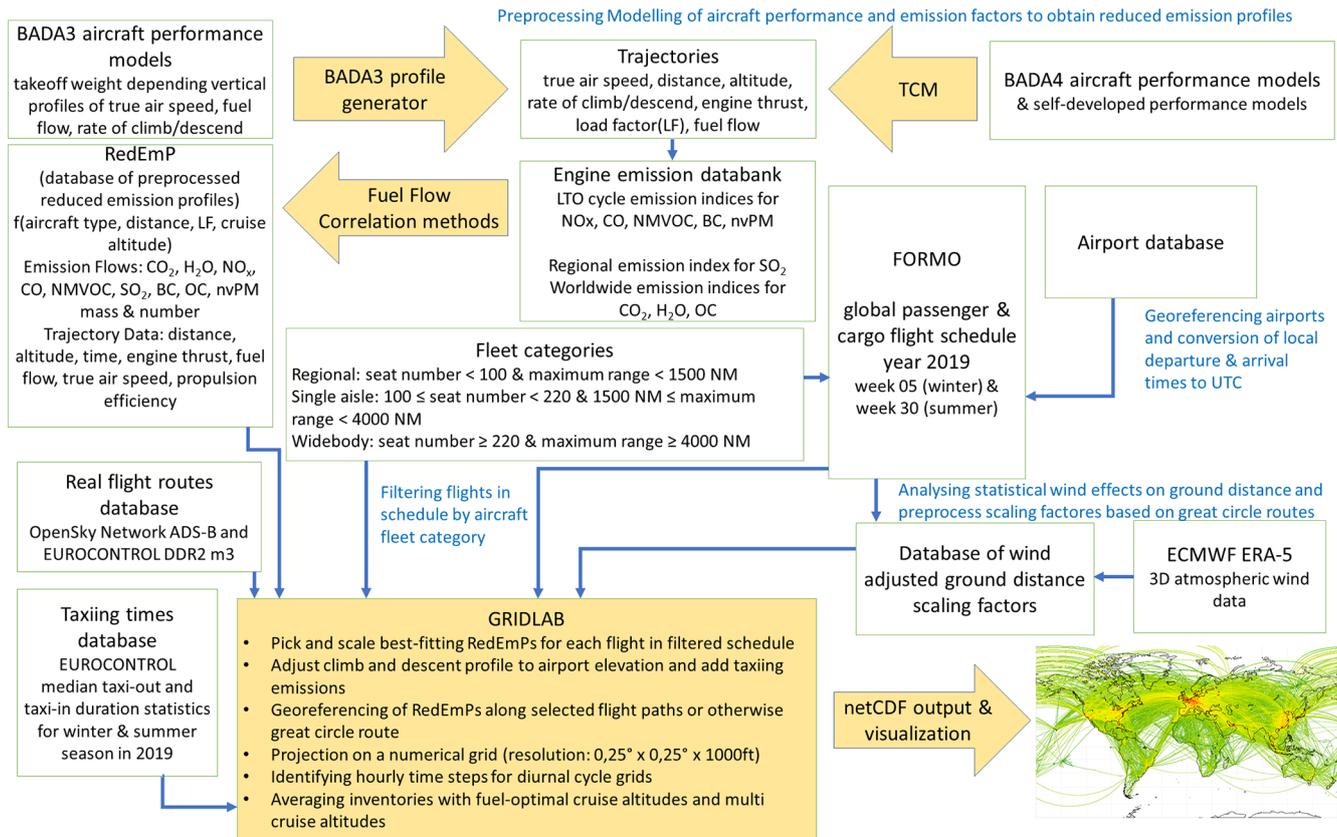
Figure 4. Workflow of the aviation emissions model, showing the required input data and a schematic depiction of the methodology.

Energy Agency (IEA), in the reference year 2019 about 91 % of the fuels used in the transport sector were based on petroleum, while only 4 % of the final consumption was natural gas, 3 % biofuels and around 1 % of the transport fuels were based on electricity (https://www.iea.org/data-and-statistics/charts/energy-consumption-in-transport-by-fuel-in-the-net-zero-scenario-2000-2030, last access: 10 June 2025). Thus, although the share of non-petroleum-based energy carriers and especially e-fuels is expected to increase in the future, we focus here on petroleum-based fuels as the main energy carriers for global transport in 2019. Different studies indicate that refining represents the most important sector in terms of indirect emissions of petroleum-based transport fuels, although to varying degrees. According to Rahman et al. (2015), refining is responsible for 56 % of GHG emissions for gasoline production in a North American refinery, while 25 % and 15 % were allocated to crude oil recovery and fugitive emissions, respectively. In a similar study for gasoline production in Chile, 87 % of indirect GHG emissions from gasoline production stem from refining activities, and 13 % from oil extraction activities (Morales et al., 2015). That study also suggested that refining is the most important sector for indirect emissions when considering all other environmental impact categories (e.g. terrestrial acidification). However, not all emissions from refining can be allocated to the transport sector. Although the majority of refinery products is usually used for transportation purposes, there are also other uses of fuels (e.g. electricity generation) and other refinery products besides fuels (like lubricants and chemical base materials) which are dependent on oil refining. Against this background, for the estimation of indirect emissions from the transport sector in the ELK emission inventory, we determine transport-induced global emissions from crude oil refining. Emissions from other upstream processes (e.g. fugitive emissions or crude oil recovery) were omitted because they are difficult to quantify and distribute geographically on a global scale. We first estimate total emissions from crude oil refining on refinery level for refineries worldwide. We then calculate the share of these emissions which can be attributed to the fuels used in the transport sector, deducting emissions for refinery products which are consumed in other sectors. Overall, we estimate transport-induced emissions for 85 countries and distribute them to 549 refineries based on their capacity. In doing so, we cover at least 99.75 % of total refinery emissions from combustion, based on refinery activities given in the IEA Extended Energy Balances (https://www.iea.org/data-and-statistics/data-product/world-energy-balances, last access: 10 June 2025).

In the following, we first describe the methodology used to estimate the emissions for 2019. We then explain the approach of determining the share of transport-induced refinery products. Finally, we show how this share is applied to the total amount of refinery emissions to obtain only transport-induced refinery emissions. Further details on the methodology are provided in the Supplement.

2.4.1 Refinery-level emission data

The majority of refinery emissions originates from combustion processes, according to Sun et al. (2019) who analysed US-American refinery emissions in 2014. For the species considered in the ELK inventory, 66 % to 87 % of all emissions were caused from combustion with the exception of NMVOC, where this applies to only 9 % of the emissions. As a result, fugitive emissions and emissions from other refining processes play a minor role. Estimating these emissions consistently on a global scale is both complex and highly uncertain due to variations in individual processes and plant configurations. Therefore, to ensure a more consistent and well-founded inventory, only emissions related to combustion are taken into account.

Depending on data quality and availability, four approaches are employed to estimate refinery-level combustion emissions on a global scale. First, whenever possible, publicly reported emission data on refinery-level for 2019 or a similar year are used, as they are considered to provide high-quality emission estimates. These are available for refineries in EU countries from the European Pollutant Release and Transfer Register (E-PRTR; https://www.eea.europa.eu/data-and-maps/data/member-states-reporting-art-7-under-the-european-pollutant-release-and-transfer-register-e-prtr-regulation-23/european-pollutant-release-and-transfer-register-e-prtr-data-base, last access: 10 June 2025), the National Emissions Inventory of the US (https://www.epa.gov/air-emissions-inventories/2017-national-emissions-inventory-nei-data, last access: 10 June 2025) and the National Pollutant Release Inventory of Canada (Greenhouse gas reporting: facilities; https://www.canada.ca/en/services/environment/pollution-waste-management/national-pollutant-release-inventory.html, last access: 10 June 2025). If certain pollutants are not reported due to thresholds defined in the reporting guidelines, a gap-filling routine using species-to-species ratio factors is applied. Second, aggregated country-level data for the refinery sector (IPCC sector 1.A.1.b) from reported emission data of the United Nations Framework Convention on Climate Change (UNFCCC; https://www.unfccc.int/ghg-inventories-annex-i-parties/2023, last access: 10 June 2025) and the Convention on Long-Range Transboundary Air Pollution (CLRTAP; https://www.eea.europa.eu/en/datahub/datahubitem-view/5be6cebc-ed2b-4496-be59-93736fc4ad78, last access: 10 June 2025) are used for several countries. Third, if no

other data is available, emissions are estimated based on refinery consumption data taken from the IEA Extended Energy Balances (https://www.iea.org/data-and-statistics/data-product/world-energy-balances, last access: 10 June 2025) and the default emission factors for the refinery sector from EMEP/EEA guidelines 2023 for energy industries (https://www.eea.europa.eu/en/analysis/publications/emep-eea-guidebook-2023, last access: 27 February 2026). Finally, a separate approach is chosen for India, where emission factors are derived from country-specific emission limits for refineries and emissions calculated with consumption data from the IEA energy balance of India. If emissions are only available at the country level (cases 2–4), they are distributed to refineries based on their oil processing capacity, using refinery data from the Global Energy Observatory (https://globalenergyobservatory.org/list.php?db=Resources&type=Crude_Oil_Refineries, last access: 10 June 2025).

2.4.2 Transport-induced refinery products

Using the IEA Extended Energy Balances, a method has been developed to determine how much of the refinery output of each country is used in the domestic transport sector for each country. Since refinery products are often exported (e.g. to countries which do not have refineries, among others), fuel export data from Eurostat database for EU countries (https://ec.europa.eu/eurostat/web/international-trade-in-goods/database, last access: 27 February 2026) and UN Comtrade database (https://comtradeplus.un.org/TradeFlow, last access: 10 June 2025) for the reference year 2019 are used in combination with the IEA Extended Energy Balances from 2019 to also consider fuels produced in domestic refineries which are consumed by the international transport sectors. For each country, it is possible to estimate the share of domestically produced fuels from refineries which are consumed for transportation purposes domestically or in transport sectors of other countries.

2.4.3 Merging refinery-level emission data and transport-induced refinery output

As the last step, the fuel-specific share of transport-induced refinery output has to be combined with the refinery-level emission data. The refinery-level emissions are distributed to the refinery products to get the fuel-specific emissions of each refinery first. This distribution is carried out for each refinery based on the energy content of the different refinery products generated in the year 2019 in the country where the refinery is located. By multiplying the resulting fuel- and refinery-specific emissions with the shares of transport-induced fuels, we obtain the transport-induced share of global refinery emissions for the year 2019.

3   Uncertainty assessment

The components and assumptions used in the compilation of the ELK emission inventory are uncertain to varying degrees. Uncertainty estimates are a relevant tool for inventory development, as they identify where data and methodology need to be improved. Furthermore, as emission levels are expected to change in the future, it is important to pay more attention to estimating uncertainty to better understand which areas of emission calculation need to be enhanced to prevent inaccurate data from misleading trends or influencing policy decisions in a suboptimal way. Therefore, the information on uncertainty is not intended to dispute the validity of inventory estimates, but to help set priorities for improving accuracy in the future. However, uncertainty reporting is challenging: a formal sensitivity analysis does not guarantee that all sources of uncertainty are captured or quantified. Per IPCC guidelines, quantitative GHG uncertainty estimates focus only on parameter uncertainty and do not consider structural uncertainty in models used for estimation or the potential uncertainty from incorrect data reporting or missing emission sources (Smith et al., 2022). Correlation of errors across sectors or countries can increase uncertainty estimates, but this is difficult to estimate and may not be considered in a quantitative uncertainty analysis (Solazzo et al., 2021). Furthermore, some sources of uncertainty (sampling error, instrument accuracy) may generate well-defined estimates of the range of potential error, while other sources may be much more difficult to characterise. Overall, the multidimensional nature of the uncertainties (in terms of sector, species, time, and space) makes a formal quantification challenging.

For these reasons, we adopt an expert elicitation approach, combining a qualitative evaluation with a rating that categorises identified uncertainties into predefined levels. The elicitation was performed based on initial proposals by the expert for the specific data followed by a group discussion; in the end, the group came up with one agreed score. The experts consulted are involved in non-exhaust measurements on chassis dynamometers for obtaining emission factors, in the development of the models used, and in the compilation of the ELK emission inventories, with the support of atmospheric modellers representing the user's side. According to Hiraishi et al. (2000a, b), a key requirement in making estimates of uncertainty by expert judgements is that all the possible sources of uncertainty are considered. Our concept is inspired by Mastrandrea et al. (2010), who suggested using a calibrated language for key findings and providing comprehensive outlines describing the evaluation process. Therefore, step 1 (characterisation) is based on predefined uncertainty factors to ensure intersubjectivity and comparability across the sectors analysed, and the results are provided as background information for later usage. For step 2 (rating), the experts are guided by a list of criteria to be considered when assigning uncertainty scores. Since emission invento-
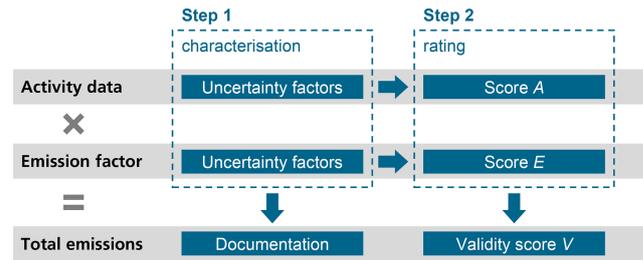

Figure 5. Flow chart for uncertainty assessment in the ELK emission inventories.

ries are principally the product of activity data and emission factors, these two sources of uncertainty are reflected by the assessment procedure displayed in Fig. 5.

Both uncertainty scores A (activity data) and E (emission factors) are based on the qualitative evaluation results and are to be spatially differentiated per area unit i. Since the uncertainty per emission factor n can vary substantially, this is reflected by the resulting validity score V_{ni}. For the calculation of V_{ni} the following equation is used:

$$V_{ni} = \frac{\alpha A_i + \beta E_{ni}}{\alpha + \beta}. \tag{8}$$

The weighting factors α and β can be chosen within a reasonable range to reflect the importance of emission factors and activity data in the emission calculation, but must be identical for each sector to ensure a comparable assessment. For the ELK emission inventory, the weighting factors are set to $\alpha = \beta = 1$. A validity score is only assigned to regions where the emissions by the respective sector are defined (e.g. no uncertainty scores are given for land transport over water bodies).

For step 1, predefined uncertainty factors support the holistic assessment of all sources of uncertainty. Table 2 exhibits the factors common to all sectors as well as the sector-specific ones. Each uncertainty factor is to be addressed for both activity data and all emission factors relevant for the corresponding sector. For step 2, the uncertainty scores for activity data and emission factors are to be differentiated in the spatial dimension. For all sectors except land transport, the IPCC AR6 scientific regions (Iturbide et al., 2020) are used (Fig. S2). For land transport, the amount and quality of input data differ significantly between countries; therefore, the uncertainty scores are obtained at the country level. Table 3 lists the assessment criteria which are intended to guide the expert judgement and make the ratings consistent across species as well as sectors.

The uncertainty is described by one of the qualifiers displayed in Table 4. The uncertainty scores show areas with relatively low ("very robust") to high ("very limited") uncertainties – the assignment of low/high uncertainty is specific for the inventory of a sector (land transport, shipping, aviation, energy for transport). If values are transferred from one

Table 2. Uncertainty factors characterising activity data and emission factors.

Sector	Uncertainty factor	Explanation
All	Delimitation	Does the delimitation to other (sub-)sectors and species lead to double counts or disregarded categories?
	Covariance	Are possible correlations between the activity level and the emission factors inadequately addressed (e.g. elevated emission in the start-up of the equipment)?
	Environmental conditions	Which environmental conditions influence the activity level? Have the emission factors been inadequately addressed?
	Input proxy data	What proxy data is used as input for deriving the activity level or the emission factors?
	Temporal variation	What are the specific uncertainties associated with the calculation of intra-annual values for both activity levels and emission factors?
	Spatial distribution	What are the uncertainties specifically arising from the approach for spatial disaggregation used (2 dimensions for all sectors except aviation, here 3 dimensions)?
Land transport	Type	What uncertainties are specific to freight and passenger transport?
	Mode of transport	What are the specific uncertainties associated with road and rail transport?
	Means of transport	What are the uncertainties specific to the means of transport (car, 2-wheeler, bus, rail vehicles, LCV, HFT)?
Shipping	Operational area	What are the uncertainties specific to domestic navigation and international shipping?
	Means of transport	What are the uncertainties specific for domestic navigation and international shipping vessel categories? How does this affect the magnitude of the uncertainty in the emission inventory?
Aviation	Type	What are the uncertainties specific to freight and passenger transport?
	Means of transport	What are the uncertainties specific for regional, single aisle, wide body, and cargo aircraft?
Energy	Type	What are the uncertainties specific to products from refineries?

n to another due to the lack of reference data, the uncertainty score will be at least one unit higher than for the study region.

The characterisation of uncertainties provides the rationale for assigning uncertainty scores for activity data and emission factors that are differentiated by geographic regions. To identify the major drivers of uncertainty in the resulting inventories, the effort devoted to characterising uncertainty factors should be proportional to their importance.

3.1 Land transport

In comparison to other modes of transport, land transport is less regulated and more influenced by human behaviour. The lower degree of organisation at the international level results in the absence of comprehensive timetable data of vehicle movements. Consequently, the reconstruction of activity data from diverse sources of varying quality is necessary. This process inevitably introduces gaps in the data, particularly in land-based freight transport.

3.1.1 Activity data for land transport

The driving behaviour and conditions under which trips are made are only partially considered: while the discrepancy between emissions during a measurement cycle and in real world is known, it is only partially reflected by the applied emission factors and thus in the inventory. For internal combustion engine (ICE) vehicles, the emission factors are increased in the cold start phase. Since the number of trips and their distribution over time are not reflected by the activity data, the total emissions are slightly underestimated. For temporal disaggregation of the annual volumes from both passenger and freight transport, the monthly time series from EDGAR per world region are used (Crippa et al., 2020). Since they do not capture the variations of individual coun-

Table 3. Assessment criteria to be considered in the evaluation of uncertainty scores A and E.

Aspect	Explanation
Coherence	Are the data geographically coherent?
Consistency	Is there a high degree of consistency with other data sources? What are the areas of consensus and what are places where no consensus exists?
Data origin	Are these model results, (in-situ) measurements, or expert judgements? Do measurement or sampling errors play a substantial role?
Standardization	Is the method a de-facto standard in the community?
Traceability	Can the origin of the data be traced?
Up-to-dateness	Are the data up to date for the reference year or outdated?

Table 4. Values and interpretation of uncertainty scores.

Score value	Qualifier	Interpretation
1	very robust	This uncertainty score is assigned to those areas that have values with the lowest uncertainty. This uncertainty score identifies areas of least concern regarding the validity of the resulting emissions.
2	robust	This uncertainty score is assigned to those areas that have values with a low uncertainty. This uncertainty score identifies areas of minor concern.
3	neither limited nor robust	This uncertainty score is assigned to those areas that have values with a medium uncertainty (e.g. a range can be given). This uncertainty score identifies areas of moderate concern.
4	limited	This uncertainty score is assigned to those areas that have values with a relatively high uncertainty.
5	very limited	This score is assigned to those areas that have values with the highest uncertainty (e.g. only an order of magnitude can be given). This uncertainty score identifies areas of major concern.

tries, it is expected that the emissions for some periods are moderately underestimated, while in others they are overestimated. As this only affects the monthly share, this has no impact on the annual emissions. The possible effect of border controls and customs on the cross-country flow of passengers and goods could not be quantified with the described modelling framework due to a lack of data. This is less relevant within the Schengen area; for other regions, it is expected that the emissions along the major border crossings are slightly overestimated.

Given the limited statistical data on passenger transport from a global perspective, the travel volumes for cars are derived from the motorisation rate based on GDPpC. This comes at the cost of not being able to study trip purposes and travel behaviour. It is expected that both under- and overestimation of the activity occurs, albeit the magnitude cannot be assessed. It has a significant impact on the resulting in-

ventories, given the bottom-up calculation approach. After the car traffic is calculated, the volumes for other means of transport are derived based on the average share per world region. Since car transport is the primary contributor to land-based emissions, the effect of over- and underestimations for the remaining subsectors on the resulting inventories is rather low. The new approach for spatial disaggregation, which is currently implemented only for Germany, UK and the US due to the availability of count station data, leads to a better understanding of the distribution of transport activity and emissions. For the rest of the world, an approach based on population density and the major road network is chosen, which causes underestimation along motorways in remote areas. At the same time, emissions in densely populated areas are overestimated, as alternative modes with lower emissions (such as public transport, cycling, and walking) have a higher share of usage. As a result, the emissions sum up to the target

value for a country, but the spatial disaggregation may be inaccurate by a factor of two. Only for countries with activity data for rail transport published, the associated emissions are calculated. As the mode share of this subsector is generally low, this causes a slight underestimation of the total railway emissions.

For about 50 countries the activity data for freight transport is known and easily accessible. For the remaining countries, a modelling approach based on GDPpC is chosen. However, for some countries structural differences in the relationship between GDPpC and the freight transport performance are observed. Overall, this leads to both over- and underestimations with a high impact on the resulting inventories since the activity data is the baseline for bottom-up calculations. For European countries, only the transport performance of HFTs is reported in official statistics. The volumes for LCVs and their resulting emissions are thus estimated based on typical shares of the vehicle classes (IEA, 2017). However, the delimitation between vehicles used for passenger and freight transport is fuzzy when it comes to the usage of pick-up trucks (especially in the US) and similar vehicle classes (e.g. informal transport systems in African countries). This is because of the lack of metadata for many countries with freight data reported. This may result in a slight shift in emissions between the subsectors. In addition, an educated guess is required to combine the activity data of fuzzy subsectors with the corresponding emission factors. The transport performance via railway is known only for a small number of countries (EU countries, Australia, USA, China, Japan and Mexico). The volume is inferred for remaining countries with a railway network, but without detailed volumes published, by applying modal shares observed in reference countries. As a tendency, this causes overestimation with low impact given the small share of the mode.

3.1.2 Emission factors for land transport exhaust emissions

The methodology for emission calculation relies on the vehicle stock data of 76 countries; for the remaining countries, assumptions are made regarding the vehicle stock and the vehicle age-related mileage. These assumptions may result in an inaccurate representation of the circulation of older vehicles, specifically those manufactured to comply with Euro 2 emission standard or earlier. As a result, the assumptions have a high impact on CO, HC, and NO_x emissions of gasoline vehicles in the reference year. Furthermore, the proportion of diesel vehicles have a high impact on NO_x and PM emissions. The resulting validity scores account for the effect of non-available country-specific emission factors and stock data.

All emission factors are taken from HBEFA or EMFAC databases. Consequently, for countries not covered in these databases, a number of factors that could potentially influence emissions are not captured due to the lack of informa-

tion: the vehicle mass and the related fuel consumption, the effects of driving shares on highways, rural and urban roads, the road conditions, and age-based deterioration. For SO_2, in addition, the resulting validity score reflects the range and availability of data about fuel quality and country-specific sulphur content.

As mentioned in Sect. 3.1.1, the emission calculation model does not model cold starts explicitly or their spatial distribution. For instance, HBEFA emission factors were used at average temperatures. Since catalytic converters are not fully heated up and the combustion process is incomplete in the cold start phase, CO, CO_2, and HC emissions are increased and thus underestimated at lower temperatures. Thus, the effect of lower temperatures in countries due to for cold start is also accounted for in the assignment of validity scores for each pollutant and drivetrain.

3.1.3 Emission factors for land transport non-exhaust emissions

Determining emission factors for brake and tire wear PM is a complex task as they are influenced by many parameters. For tire wear, apart from driving performance, vehicle weight is the most important factor, followed by the type of road surface. Therefore, countries with a higher share of heavy vehicles and low road quality experience higher emission factors. Climatic conditions are also important, as higher temperatures cause higher wear rates. Furthermore, in countries with cold climate, studded tires are often used (e.g. Scandinavia or Switzerland). The use of these tires also increases the uncertainty of the PM emission factor.

For brake wear PM, vehicle weight and driving style are important factors which increase the emission rate. In general, brake wear emissions are expected to be higher in mountainous areas, as more frequent braking and higher brake pad temperatures also lead to higher wear rates.

There is no standardised measurement method for brake wear PN, and the available values from the literature cover a wide range from 10^9 to 10^{13} particles/vehicle-km, mostly due to the large effect of brake temperature on PN emissions (Mathissen et al., 2023). Therefore, the emission factors used are subject to high uncertainty, while their effect on the resulting emissions is unclear. Less accurate emission factors are available for other vehicle types such as 2-wheelers and buses. Since in some world regions (especially some Asian countries) motorcycles account for a high percentage of road traffic, uncertainty on the overall emissions is increased.

Compared to brake wear PN emission factors, existing data about tire wear PN is less reliable. This is partly because it is challenging to distinguish particles generated by the tire from those produced by the pavement. While frictional brakes can be easily encapsulated, this is not possible for tires. Existing literature suggests particle emissions range from 10^{10} to 10^{11} particles/vehicle-km (Löber et al., 2024;

Dahl et al., 2006). Due to these high uncertainties, tire wear PN is not included in ELK.

Despite higher ranges of emissions from brake wear, the testing methodology for brake wear is more reliable than tire wear and hence only brake wear PN emissions are included.

3.2 Shipping

Maritime shipping is inherently influenced by global economic fluctuations, which shape cargo flows worldwide. Nowadays, vessel movements can be tracked by analysing AIS data. AIS is limited by its design and provides only basic data related to the vessel identification, position and movement. Any access to additional information about cargo and vessel operations as well as internal voyage reports is highly restricted and cannot be used for emission estimation. The acquisition of AIS data depends not only on the technical capabilities of shore-based and satellite-based data reception networks, but also on legal restrictions. For example, the General Data Protection Regulation (GDPR) in the European Union aims to protect the privacy and personal data, which can impact AIS data availability. This may also apply to crew members working or living on board vessels. Moreover, access to AIS data may be blocked due to various aspects of national security like, for example, in case of the new Data Security Law (DSL) and Personal Information Protection Law (PIPL) in China.

Other details relevant for emission estimation such as the current engine use and fuel consumption are not included in the AIS messages. Therefore, accessing a vessel particulars dataset is essential. Such datasets provide shipyard-grade technical specifications for vessels and are compiled by maritime intelligence companies like Clarksons Research. The vessel particulars include detailed engine, fuel and propulsion parameters which are crucial for the emission calculation of a given vessel.

3.2.1 Activity data for international shipping

The vessels engaged in international voyage are selected based on the types of AIS messages broadcast by their AIS transponders. Special focus is placed on filtering out AIS message type 26 which is generally transmitted by AIS transponders on board inland vessels and should not be used by vessels engaged in international voyage. To address problems related to interferences of AIS data which may lead to erroneous vessel positions, a land mask is applied globally to exclude unfeasible vessel movements which, as reported by faulty AIS transponders, are spotted on land. Despite careful examination of vessels belonging to the inland fleet, one cannot exclude a possibility of a data overlap: this is because many vessels operate on inland as well as international waterways, and their emissions might be included in both inland and international emission repositories.

The current engine load of a vessel is not reported within AIS data. Therefore it has to be estimated using the Admiralty formula in Eq. (2) which derives the current engine load by reckoning how close current speed and current draught of a vessel, obtained from AIS, are to its technical limits (Faber et al., 2020). The vessel particulars database does not contain technical records of all vessels visible in the AIS dataset used for emission calculation. Some of the records have missing data fields. To fill gaps in technical parameters, a statistical approach is applied by matching sister or near-sister vessels and leveraging similarities in their technical details.

Since the tracking of vessel movements, based on AIS, depends strongly on the quality of GPS positioning input used by AIS transponders onboard vessels as well as the completeness of data within AIS messages, it is necessary to avoid using parameters like, for example, AIS-derived speed over ground (SOG) which show a tendency to remain unknown or missing (Banyś et al., 2020). Therefore, speed over ground of a given vessel is calculated from two consecutive positions and timestamps reported by AIS, disregarding the direct SOG readout provided internally by AIS itself. This approach ensures that latitude and longitude, which are the least frequently missing parameters within the dynamic AIS messages (Banyś et al., 2020), are used for the assessment of vessel movements.

It might be worth mentioning that there are numerous AIS transponders on board vessels worldwide which are used without legal approval of the relevant maritime authority. The users of such AIS equipment configure MMSI numbers which end up in the global AIS data archives as either a sequence of nine randomly chosen digits or, in the worst case, a copy of an existing legally approved MMSI of a legitimate vessel, be it purely accidental or on purpose. As described in Banyś et al. (2024), this situation may lead, to some extent, to an inaccurate assessment of vessel movements in the global scope and affect the estimation of emissions.

It should also be emphasised that a stationary vessel may still use her main engine. There are navigational conditions for stationary vessels, like for example anchoring in constrained tidal waters, which require the main engine to run most of the time to keep the vessel position under control. It is not possible to determine the status of the main engine operation with AIS data alone. Therefore, in numerous cases the emissions of stationary vessels, contrary to reason, may be underestimated.

Another aspect of uncertainties related to vessel tracking includes the parameters of current draught and fuel consumption of the onboard machinery. The current draught is obtained from AIS message type 5, which is manually updated by the vessel's crew. According to the standards of good seamanship, it should be kept up to date, but this is not always the case. An incorrect draught can lead to inaccurate engine load estimations, resulting in errors in emission calculations. Outdated draught, for example, can lead to an underestimation of emissions if a vessel is laden and reports a shallow

draught via AIS, or it can be overestimated if the vessel proceeds under ballast and reports a deep draught.

Ideally, the estimation of maritime emissions would consider prevailing environmental conditions such as currents, wind, and wind-induced surface waves (sea state) measured by the significant wave height parameter. These factors can impact vessel movements in at least two ways. First, external conditions may affect the vessel's current engine load. Second, vessels may intentionally deviate from planned routes to follow adverse weather avoidance procedures. The global distributions of climatological mean significant wave height indicate that major maritime routes, as seen in AIS data, cross the areas of prevailing rough sea conditions, especially in the North Atlantic (Timmermans et al., 2020). In cases of insufficient AIS coverage, especially in remote offshore areas, such route deviations cannot be fully reconstructed and it has to be assumed that vessels proceed along the shortest leg between two AIS-reported positions.

Global modelling of such ocean dynamics and weather patterns would certainly improve the quality of emission calculation but at the same time it would increase the computational complexity beyond the constrained project resources, too. Therefore, the environmental factors are generalised with respect to aggregated classes of vessel type and size. This simplification process might lead to an overall underestimation of emissions.

The tracking of global vessel movements is incomplete due to fragmented AIS data, particularly in remote areas, which is received from a constellation of low Earth orbit (LEO) satellites. Additionally, there are vessels worldwide that are not governed by the International Convention for the Safety of Life at Sea (SOLAS) with its carriage requirements for shipborne navigational systems and equipment (IMO, 2004). Such craft do not have to be equipped with AIS transponders and remain completely invisible for the emission calculation. Moreover, crews are allowed to disable AIS transponder on board their vessels, if their safety cannot be guaranteed, for example, in high-risk piracy areas where a vessel visibility via AIS would pose a hazard. Vessels may be engaged in illegal activities at sea, too. In such situation they often disable their AIS transponders, if they have any on board at all, or manipulate their AIS-reported positions to hide their movements (Paolo et al., 2024). There are attempts to track the movements of vessels which either disable their AIS transponders or do not carry one, for example, using satellite remote sensing (Milios et al., 2019). However, in the scope of project calculations such enhanced appraisal of vessel movements was not possible. In situations where a vessel disappears from the AIS traffic coverage for a longer period, her movements are estimated using a graph constructed from all available position reports stored in the AIS dataset used for emission calculation. Such approach allows for computation of the shortest nautically practicable route connecting two positions within globally navigable waters. Additional uncertainties of emission calculation may be introduced during a route reconstruction if vessels proceed through polar regions of the Northern Hemisphere. The sea ice concentration maps indicate that the changes in the ice coverage may be considered either as constraints of the present time or as new opportunities to overall navigational capabilities of vessels in the future (Rayner et al., 2003). However, there is no guarantee nor a possibility to verify that a vessel followed such a route, especially with fragmentary AIS coverage. Within the scope of the project's calculations it is generally assumed that vessels do not regularly choose the Northwest Passage between the Atlantic and Pacific oceans through the Arctic Ocean. Therefore, in cases of poor AIS coverage, emissions may be underestimated.

A similar tendency applies to vessels navigating within harbours, for example during berthing or unberthing. Vessel handling during manoeuvrers in constrained waters often involves a compulsory tug assistance with the vessel's main engine stopped. Such a situation may lead to an overestimation of emissions. Moreover, the main engine may temporarily run under full load to adjust the speed or to improve the response to the helm. With almost no movement reported by the AIS transponder, a false conclusion might be drawn that the vessel has no emissions from the main engine. Such situations, on the other hand, may lead to an underestimation of emissions.

3.2.2 Emission factors for international shipping

The emission factors used for calculating emissions from the international fleet follow a generalized approach published by the IMO (Smith et al., 2014; Faber et al., 2020). The emission factors depend, first of all, on the vessel typology because the parameters are aggregated based on 18 major vessel types specified by the IMO algorithm (Faber et al., 2020). To apply the emission factors properly, an accurate assignment of the IMO vessel types to the fleet types decoded from AIS data is necessary. Unfortunately, there is no official typology of vessels. Various maritime classification societies have their own categorisation schemes which are detailed up to a subcategory level of fleet types. This multi-level typology is then depicted in their own vessel particulars databases. Mapping this multitude of vessel categories into the predefined set of vessel types used by the IMO algorithm is challenging. This process introduces additional uncertainty into the emission calculations, as vessel type is a crucial input parameter in the computation process.

The emission factors are defined either based on current energy demand of the main engine, which is related to current engine load, or on amount of fuel consumed per unit of time by the main engine. Fuel data of a vessel is obtained from the Clarksons Research vessel particulars dataset. Moreover, the IMO algorithm applies adjustments to emission factors for vessels located within one of the following emission control areas (ECA), as of 2019: Baltic Sea, North Sea, North America, US Caribbean Sea. Before a vessel enters an ECA,

she has to switch completely to an ECA-compliant type of fuel. This process follows vessel-specific procedures through various stages of main engine maintenance and may take up to three days. The duration of such ECA-related fuel transition events is considered during the emission computation. It should be noted that the emission factors provided by the joint IMO researchers do not fully account for how the level of training and good seamanship of the crews, responsible for maintenance of the onboard machinery, may influence the proper and environmental friendly operation of marine engines.

3.2.3 Activity data for domestic navigation

The inland shipping sector is excluded from the maritime shipping sector by the AIS message type 26, typical for domestically operating vessels and applying land masks. Still double counts might be possible especially for coastal vessels that are also involved in transportation tasks on the waterways, leading to a slight overestimation in river mouths when both datasets are combined.

The activity levels on the inland waterway systems are accessed through statistics of region-to-region transportation flows in t km (US, Europe) and the total transportation volume combined with AIS data (China). For the use of AIS data, a higher uncertainty is introduced into the modelling region of China as it comes with the technology-specific restrictions as described for the maritime sector and is additionally strongly affected by data sharing restrictions in China. This leads to blind spots, where no AIS signals are received as well as overestimation and allocation of the transportation proportion of the blind spots to areas with signals. Relying on the AIS data can lead to both under- and overestimation. Further waterway systems of the Amazon, Parana, Volga, India National Waterways, Nile, Congo, Mekong, and Niger are neglected in this dataset due to limited assessment and accessibility of transportation statistics. The overall proportion in transported goods on these waterways is below 10 % comparing various data sources (Eurostat, 2022; Lewis et al., 2022; Press Information Bureau, Government of India, 2023; Jaghdani and Ketabchy, 2023), therefore resulting in a tendency to mildly underestimate the global activity level. Passenger transportation data, including distance and location details, is unavailable for the modelled regions and is therefore not included in the modelling approach. Since passenger transport on inland waterways represents only a small share, its exclusion results in only a slight underestimation of the overall activity level.

The energy intensity for transportation is applied as an average value in MJ t km^{-1} and harmonized for all types of ships and goods transported within a modelling region. This does not cover the variation of operating states and their specific emission behaviour, e.g. entering water locks, as well as navigating upstream or downstream the river. This can lead to over- as well as underestimation and shifting emissions on a modelled track. In contrast to the maritime sector, navigation on rivers is much less affected by storms as no severe wave forming is to be expected. Low water levels, such as those experienced in Europe in 2018, can reduce cargo capacity, necessitate additional trips to move the same amount of cargo, and consequently increase energy intensity. However, for 2019 no low water levels have been reported. We distributed the transportation flows on the waterway network under the assumption that a ship would use the shortest route to fulfil a transportation task. In reality routes may differ due to specific trading patterns and stops along alternative paths, resulting in a possible underestimation. In summary, there is a tendency for the activity level assessment to underestimate the emission inventory for inland shipping.

3.2.4 Emission factors for domestic navigation

All modelled regions imposed emission regulations on the inland navigation sector for the emissions of NO$_x$, HC, CO, and PM, with the strictest regulations and earliest implementation by the US EPA Tiers, following by the European Nonroad Machinery Regulations and the China Emission Stages. Emission regulations are imposed on ships at the time of their initial registration. Therefore the age structure of the fleet has a significant impact when developing fleet emission factors. We extracted the age structures of the database of Clarksons Research and developed an average fleet emission factor under the assumption that the machinery complies with the relevant standards at the time of registry. Depending on the engine characteristics and maintenance by the crew, the emission limits might not be met in operation. Therefore the emission factors impose a tendency of underestimation.

3.3 Aviation

The accuracy of the modelled aviation emission inventory is influenced by a number of different aspects: both the availability and quality of different input data as well as methodological uncertainties in connection with simplifications and assumptions. The quality of the input data varies regionally, e.g. due to spatially limited availability of routing data and taxiing time statistics. Also the quality of data on the worldwide aircraft fleet varies, e.g. due to the quality differences between the underlying aircraft performance models and the engine-specific availability of emission factors.

For these reasons, the quality assessment in aviation is carried out individually at the grid cell level and is based on the number of included trajectory segments that fulfil certain quality standards. In general, an uncertainty factor of 1 is assigned to a grid cell when the relative frequency of included trajectory segments with reduced data quality exceeds a defined threshold, otherwise a value of zero is assigned. Multiple independent uncertainty factors of the included trajectory segments are weighted and finally summed up to the grid cell uncertainty score.

3.3.1 Activity data for aviation

The uncertainties of activity data depend on several criteria. First, the air traffic scenario for 2019 is based on various databases and modelling assumptions: for passenger air traffic, the demand and schedules, the airline network and fleet are considered to be of higher quality compared to the cargo subsector, where a higher degree of modelling is needed because of a lower availability of data. Furthermore, non-scheduled flights, helicopter flights, military air traffic, and general aviation such as private jets and business aviation are not included in the ELK emission inventory. However, the modelled subsectoral split of total CO_2 emissions is similar as derived by Graver et al. (2020). The most dominant uncertainty factor with regard to the gridded emission inventory is the quality of the applied aircraft performance model for trajectory modelling: these models affect the fuel flow rate, thrust, speed, as well as the climb and descend rate. BADA4 aircraft performance models cover the entire flight envelope and are more complex regarding flight physics than BADA3 models, which only cover the envelope at nominal conditions. Therefore, BADA4 models have an enhanced accuracy (Nuic et al., 2010; Poles et al., 2010). Due to the larger proportion of aircraft modelled using BADA3 models, the resulting emission inventories for regional and cargo subsectors have higher uncertainties. Further uncertainties occur from the aircraft performance-engine model combination. In order to keep the computational effort moderate, we only use one aircraft performance model per aircraft type and apply it for all scheduled flights. We allocate the engine emissions data for the engine, that is specified in the performance data. In cases where more than one aircraft performance model with dedicated engine data is available per aircraft type, we use the aircraft-engine combination with the highest market share in year 2019 from Cirium (2019) for all flights. Comparative calculations of the different aircraft performance model-engine combinations of the same aircraft type show deviations in mission fuel burn between 1 % and 7 %. Besides the aircraft performance models, the applied Total Energy Model for trajectory simulation considering the aircraft as a point mass is another simplification. The simplification of the detailed trajectory to a RedEmP has only minor effects on the trajectory accuracy. Sensitivity studies show that the impact on emissions due to deviations between the seat load factor from the flight plan and the discrete load factor from RedEmP are rather small. Changes in seat load factor by ± 0.05 in a global flight plan affect the worldwide total CO_2 and NO_x emissions by ± 1.2 % and ± 1.7 %, respectively. For some flights with higher payloads or flight lengths close to the aircraft-specific and payload-dependent maximum range, the load factor has to be reduced or the initially assigned cruise altitude has to be changed to enable the trajectory simulation. This leads to a potential underestimation of the flight-specific emissions. If this occurs more frequently within a grid cell, the uncertainty score is increased.

Real flight path data is available for North America, Europe and inbound/outbound flights from the European airspace. Incorporating this data implicitly accounts for effects of air traffic management (ATM), enables a weighted multi-route pattern, and results in a more realistic routing. In contrast to this, missing detailed flight path data for the African and South American continent, necessitating the assumption of standardised great circle routes. In such cases, a horizontal route dispersion, detours and further routing inefficiencies are not considered and the vertical dispersion of flight levels is generic. Since idealised great circle routes lead to an underestimation of the emission quantities, an increased uncertainty score is attributed to the affected grid cells.

However, despite the fact that RedEmP are projected along a detailed horizontal flight path, in the vertical dimension the trajectories follow either a fuel-optimized or a constant cruise flight level over the entire cruise phase instead of depicting the exact ATM-affected altitude pattern of the route profile. This can lead to considerable deviations from real flight paths in individual cases. The permanent assumption of fuel-optimized cruise altitudes leads to a potential underestimation of emissions and constant cruise altitudes rather to an overestimation as the reality will probably be in between both modes due to ATM processes. Furthermore, RedEmP have only been calculated for the most common cruise altitudes of each aircraft type (29 000–41 000 ft for jets, 16 000–25 000 ft for turboprops); outliers of cruise flight levels in real route profiles cannot be taken into account. Therefore, for about 10 % of the flight movements in the inventory, flight profiles are modelled with a cruise altitude deviating from the main cruise flight level as defined in the underlying flight path dataset – as a tendency, this leads to an underestimation of emission quantities in cases where a higher cruise altitude is underlain (and vice versa).

Another regional uncertainty factor is the availability of taxiing time statistics, which are available for most important airports in Europe and some busy airports on other continents. However, the median taxiing time does not represent daily conditions at the airport. For all other flights, standard taxi-in and taxi-out time from LTO cycle (ICAO, 2008) are used which do not consider individual airport size, capacity and runway layout. In contrast to most other emission inventories, ELK inventories consider emissions due to taxiing and use available data for local taxiing times to reduce uncertainties.

Air distance is corrected by wind effects, that are statistically modelled based on ERA-5 reanalysis data (Hersbach et al., 2023). For small aircraft with low cruise speeds, wind impact could not be derived. This results in a slight underestimation of the flown distance on average (Linke, 2016). Uncertainties of the wind speeds and their spatial distribution depend on the accuracy of the gridded 3D wind fields used. While ERA-5 data have the same horizontal resolution as the ELK aviation emission inventory of $0.25° \times 0.25°$, the vertical resolution of layers declines with increasing altitude due

to the pressure levelling. Thus, the data resolution of the wind fields on common cruise flight levels is rather coarse. We follow the methodology of Swaid et al. (2024), who propose to statistically capture the wind effects on air distance for an annual period and on a fuel-optimized cruise flight level. Note that the annual mean wind effect does not represent the actual daily wind situation along the detailed 3D route profile. Further inaccuracies are introduced by the usage of the ISA for trajectory simulations instead of real atmospheric background data.

3.3.2 Emission factors for aviation

Uncertainties in the derivation of emission factors are mainly driven by the accuracy of the underlying input emission data and the robustness of the applied extrapolation and interpolation method. The uncertainty scores vary per emission species. The constant emission factors for CO_2 and H_2O are considered to be reliable and robust. SO_2 emissions are directly affected by fuel sulphur content values and vary according to the used fuel sample both regionally and over time. To reduce uncertainties, in ELK we use available fuel sulphur content values quantified on continental level (CRC, 2012), which does not represent local fuel properties but should be more accurate compared to the assumption of a global average value. For state-of-the-art jets and piston engines, input emission factors for NO_x, HC/NMVOC, CO, and particles (BC, nvPM) originate from test bench measurements for four engine thrust settings as defined in LTO cycle (ICAO, 2008). The emission factor measurements contain small inaccuracies for jet engines depending on the used fuel specification (EASA, 2023). The uncertainties of the measured piston emission factors are higher (FOCA, 2007). For modelling turboprops, only constant values from overall fleet averages are available, which do not predominantly represent turboprop engines. This leads to increased inaccuracies and higher uncertainty scores, and mainly affects the results of regional and cargo subsectors where 51 % and 35 % of flight movements, respectively, are operated by turboprop aircraft and contribute to 38 % and 7 % of the regional and cargo air traffic CO_2 emissions. The extrapolation of emissions from on-ground measurements for the LTO cycle to in-flight conditions is done using fuel flow correlations, methods whose inaccuracies are discussed in the literature (e.g. Schulte et al., 1997; DuBois and Paynter, 2006). For the emission factors of BC, nvPM mass and number, uncertainties occur due to the application of constant emission factors from fleet averages for all engines, where no measurements are available; this affects in particular older turbojets, some piston aircraft and all turboprops. For the affected grid cells, higher uncertainty scores are assigned.

3.4 Energy for transport

For the representation of energy-related indirect transport emissions from refining, a large share of the data rely on reported refinery-level or country-level emission data. Due to the complexity of estimating refinery emissions, reports are considered the most reliable data source for the emission inventories. Reported data is mostly available for countries in Europe, North America, Oceania and Russia which make up the majority of global CO_2 emissions (61 %). For the remaining countries, emissions are calculated using refinery fuel consumption data and emission factors. Therefore, depending on the method for determining the emissions, the data carry different uncertainty factors which will be explained in the following.

3.4.1 Activity data for energy for transport

Uncertainties regarding refinery activity data arise from the lack of available information on the properties of individual refineries. Activities and product quantities of a refinery depend on various aspects, e.g. the crude oil used, the refinery complexity or the preference of refinery operators. This aspect influences the uncertainty of the emission inventories in several ways. To determine the share of transport-induced refinery emissions from total refinery emissions, we use product shares based on country-level refinery product quantities from the IEA Extended Energy Balances from 2019 to distribute refinery emissions to single refinery products, although to a certain extent they might differ from one refinery to another within a country. Therefore, this aspects leads to moderate uncertainty in the spatial distribution of emissions in all countries. Furthermore, when emissions from refineries are determined on country-level, we use the oil processing capacity of single refineries as a proxy despite the fact that other refinery-specific characteristics are also relevant, although to a less noticeable extent. For Europe, the US and Canada we used reported total refinery-level emission data as a basis for our estimations. To approximate the share caused by combustion process activities from total refinery emissions, we applied species-specific factors from Sun et al. (2019). These shares represent an average of US refineries and do not take into account individual emission characteristics of a refinery, e.g. due to the refinery setup, varying crude oils used or country-specific emission standards. We assume that the shares of combustion emissions in total refinery emissions of each species are well represented in its general tendency, thereby resulting in a moderate level of uncertainty. Since these shares apply to US refineries, the uncertainty for refineries in the EU and Canada are expected to be slightly higher. To our best knowledge, no monthly profiles for refinery processes are available. Therefore, we used the consumption profiles of land transport, the most consumption-intensive transport subsector, to allocate annual emissions to individual months. Since transport fuel

consumption is usually relatively evenly distributed, the uncertainty can be considered low. Annual emission estimations are not affected by this uncertainty.

3.4.2 Emission factors for energy for transport

For a part of the globe, we used default emission factors for refinery combustion processes to determine refinery emissions. These emission factors do not represent the emission standards and limits given in individual countries and could both over- or underestimate real emissions. This applies to developing countries in South and Central America, Africa and Asia, representing about 34 % of the global CO_2 emissions from refineries in the inventory. The uncertainty can be considered high in these countries for air pollutants and lower for CO_2, since CO_2 is usually released into the atmosphere uncontrolled. To estimate global emissions for the selected set of species, the emission quantities of some species are derived from those of another species, as they may not be equally available in all regions ("gap filling approach"). This is done using country-specific emission factor ratios between a known and an unknown species. In Europe, especially CO and PM emissions are gap-filled in many cases from other species. Due to the individuality of emission factors of each refinery, this approximation leads to moderate uncertainties especially when species are derived from other non-related species (e.g. PM from CO_2) instead of related species (e.g. $PM_{2.5}$ from PM_{10}). Similarly, missing emission species in reported country-level data is gap-filled by approximating them using country-specific emission ratios. When reported emission data from refineries or countries are used, sometimes not all particulate matter categories targeted in the emission inventories are included in the emission datasets (e.g. $PM_{2.5}$ and BC in EU refineries and BC in Canadian refineries). To fill these gaps and provide an estimate of BC and $PM_{2.5}$ emissions in these cases, we approximated them from emissions of other particulate matter categories, based on the share of BC emission factors relative to $PM_{2.5}$ or PM_{10}. For EU refineries, also $PM_{2.5}$ emissions are derived from the reported PM_{10} emission totals. The emission quantities of the derived species carry a medium level of uncertainty since related species (other particulate matter categories) are used for the approximation. For Canadian and US-refineries, we used the reported VOC emission data to represent NMVOC emissions in the inventory. Since VOC emissions include methane emissions which are excluded in NMVOC emissions, we expect emissions in our inventory to be slightly overestimated in these regions. The uncertainty is relatively low, since methane is usually burned in the combustion process and the share of methane in VOC emissions is therefore low.

4 Results and comparison with other inventories

In this section, the ELK inventory is presented for the different sectors and compared with other well-established global inventories. For this comparison we consider CEDS (Community Emissions Data System; Hoesly et al., 2018) in the v2021-04-21 release (O'Rourke et al., 2021) and, for aviation, in the updated v2023-04-18 release (Prime et al., 2023), which includes the correction by Thor et al. (2023); CAMS-GLOB (Soulie et al., 2024), consisting of CAMS-GLOB-ANT_v5.3 (for land transport), CAMS-GLOB-SHIP_v3.2 (for shipping) and CAMS-GLOB-AIR_v2.1 (for aviation); and EDGAR8 (Crippa et al., 2024) consisting of v8.0 (for GHGs) and v8.1 (for SLCFs). Note that these inventories are not completely independent of each other, as for example CAMS is partly based on an earlier version of EDGAR and includes data from the CEDS inventory as well. Nevertheless, they provide different emission totals, making it valuable to compare the ELK results with all of them. Additional datasets are considered for specific sectors and variables and are outlined in the respective subsections below. The comparison is generally conducted based on aggregated emissions, both at the global and the regional level. For the latter, we consider the IPCC AR6 scientific regions depicted in Fig. S2.

4.1 Land transport

The global CO_2 emissions of land transport in the ELK inventory are shown in Fig. 6 for the sector as a whole and for each subsector. The emissions are particularly high in the Northern Hemisphere, especially over Europe, the eastern US, India and eastern China. Emission peaks are clearly visible in correspondence with the major population centres and along major roads and highways, both in the Northern and, to a lower extent, in the Southern Hemisphere. The global CO_2 emissions of land transport amount to 6639 Tg in the reference year 2019 (Table 5) and 7382 Tg when considering the contribution of biofuels (CO_2-total). The CO_2 land transport emissions are dominated by cars, sharing 45 % of the total with a geographical pattern closely matching that of the total land transport emissions (Fig. 6b), and by heavy freight trucks with 33 % of the total (see Table S4, for details). Compared to the emission distribution of cars, which are quite spread over large areas, LCVs and HFTs emissions are more concentrated along major roads and highways (Fig. 6c and d). The other subsectors are responsible for less than 10 % of the total emissions, although they are important in specific regions, such as for instance 2-wheelers in India or bus transport in North America. Bus transport also shows high emissions spots in major urban areas. The rail transport contribution to land transport emissions is minor (about 1 % for CO_2) and is mostly due to freight. Emission maps of other species are shown in Figs. S3–S22, with the totals and the shares of each subsector given in Table S4. The emission shares of the

Table 5. Globally aggregated emissions of the four sectors considered in the ELK inventory. CO_2 emissions do not include the share of biofuels, which is accounted for in CO_2-total (for land transport only). The species nvPMm and nvPMn indicate non-volatile particle matter mass and number, respectively. Units are Tg(species), $Tg(NO_2)$ for NO_x and particles for PN and nvPMn.

Species	Land transport	Shipping	Aviation	Energy
BC	0.46	0.29	0.009	0.002
CH_4	0.86	0.02	–	–
CO	46.82	1.59	0.84	0.16
CO_2	6638.60	822.17	851.04	533.03
CO_2-total	7382.04	–	–	–
H_2O	–	–	333.25	–
HC	4.97	–	–	–
N_2O	0.28	0.05	–	–
NH_3	0.69	–	–	–
NMVOC	8.50	0.75	0.08	0.02
NO_2	3.14	–	–	–
NO_x	25.51	13.86	3.74	0.50
nvPMm	–	–	0.01	–
nvPMn	–	–	1.18×10^{26}	–
OC	0.32	–	0.005	–
PM_{10}	0.94	1.48	–	0.03
PM_{10} brake wear	0.22	–	–	–
PM_{10} tire wear	0.24	–	–	–
$PM_{2.5}$	0.75	–	–	0.02
$PM_{2.5}$ brake wear	0.08	–	–	–
$PM_{2.5}$ tire wear	0.16	–	–	–
PN	4.05×10^{26}	–	–	–
PN brake wear	8.30×10^{24}	–	–	–
SO_2	1.01	10.62	0.20	0.53

SLCFs show interesting differences with respect to CO_2: the largest share of BC, NO_x, and PN emissions, for example, is by heavy-freight trucks, due the predominance of diesel engines among these vehicles, while 2-wheelers dominate the emissions of CO, CH_4, HC, and OC, due the widespread usage of two-stroke engines in this category.

The comparison of the ELK land transport emissions with other global inventories is summarised in the heat map in Fig. 7, showing the relative difference in the globally aggregated emissions between ELK and each of the three inventories considered for the comparison (CEDS, CAMS-GLOB and EDGAR8). This analysis reveals the excellent agreement of ELK with these inventories for CO_2, with deviations within a few percent. Breaking down this comparison in the different world regions (Fig. S26) reveals, however, that this agreement actually results from a compensation between higher ELK emissions in some regions (mostly South and East Asia) and lower ELK emissions in other regions (mostly Western and Central North America). These regional discrepancies are consistent across the three inventories used for the comparison, revealing a rather peculiar geographical distribution of the land transport CO_2 emissions in the ELK inventory.

The deviations between emission estimates in the inventories are larger for non-CO_2 species, not only with respect

to ELK but also across the other inventories, as a result of the higher uncertainties in the emission factors of these species. The differences can be partly explained by the use of a bottom-up approach in the ELK inventory, which incorporates emission factors at the subsector level. The largest differences are observed with the CEDS inventory, showing deviations greater than 50 % for BC, CO, N_2O, NH_3, NMVOC, and SO_2. CAMS-GLOB and EDGAR8 are more aligned with the ELK aggregated emissions, although the latter shows a very large discrepancy for SO_2: the regional analysis (Fig. S34) indicates that this deviation can be attributed to a factor-116 difference between ELK and EDGAR8 in Southeast Asia, which accounted for 22 % of the total SO_2 land transport emissions in ELK.

Figure 8 shows the uncertainty scores for CO_2 land transport emissions assessed with the method outlined in Sect. 3, which for this sector is based on an analysis at the country level. Based on this analysis, the lowest uncertainty (score 1) is assigned to most of the developed countries, with a few exceptions, while other countries are assigned an uncertainty score of 2 or, in a few cases, an uncertainty score of 3 due to very limited knowledge of the corresponding activity data. The uncertainty scores for the other species mostly follow the same geographical pattern (see Fig. S35), although they are generally higher, in particular for BC, HC, NMHC, and PN. Significantly higher uncertainty scores are assigned to the non-exhaust mass emissions from tire and break wear, with a best uncertainty score of 2 assigned only to a few European countries and higher uncertainty scores up to 4 assigned to most of the other countries. These are even higher for non-exhaust number emissions, where only Europe and US are assigned a best uncertainty score of 3.

4.2 Shipping

In the ELK inventory shipping emissions are resolved into international (ocean-going) shipping and domestic navigation, although the latter is only modelled for Europe, US and China (Fig. 9). The distribution of international shipping emissions follows the major shipping routes in the Northern Pacific, Northern and Southern Atlantic, with significant activity in the Indian Ocean and off the coasts of South and East Asia. A striking feature are the high emissions along the coastlines, especially in the North Sea and Baltic Sea, in the Mediterranean and along China and South-East Asian countries. Two world-record-breaking traffic zones are located in Europe, which is reflected in the emissions: the English Channel, the world's busiest natural waterway, and the Kiel Canal, the world's busiest artificial waterway. As for the land transport sector, there is a significant difference between Northern and Southern Hemisphere. The global CO_2 emissions from shipping amount to 822 Tg in the reference year 2019, with an overwhelming dominance (93 %) of international shipping. This share remains above $\sim 85\%$ for all species (Table S5), with the notable exception of CO,
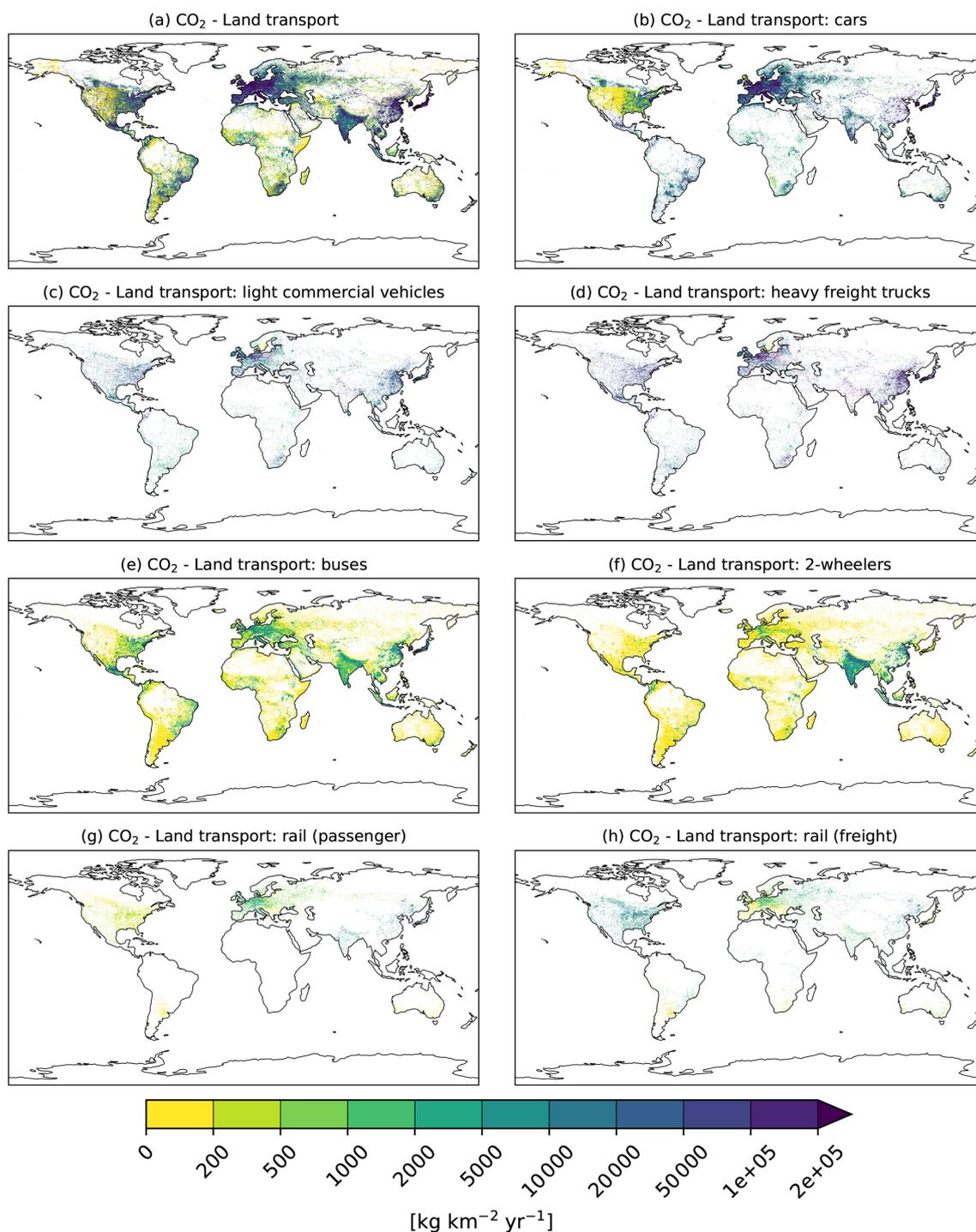
Figure 6. CO_2 emissions from land transport **(a)** and related subsectors **(b–h)**, not considering the share of biofuels (see Fig. S6 for the total CO_2 emissions of land transport including biofuels).

for which domestic navigation contributes 65 %. This can be explained with the fact that the inland vessel fleet contains many old ships and engines without emission standards. Furthermore, smaller engines are often operated with higher fuel-to-air mixtures, which can lead to incomplete combus-

tion and increased emissions of CO. The geographical distribution of the emissions is similar for all species, although for SO_2 the ELK inventory considers the reduced fuel sulphur content in the Sulphur Emissions Control Areas (SECAs), implemented in 2010 following the regulations of the IMO
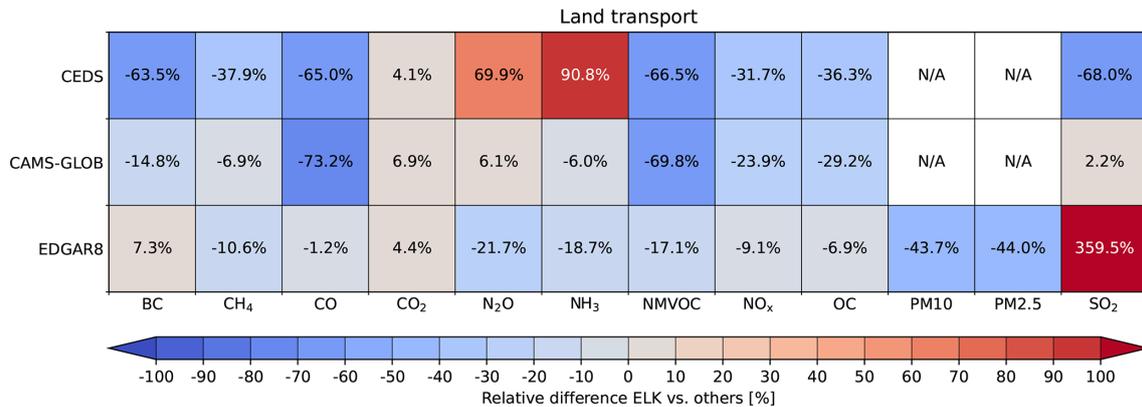
Figure 7. Relative difference of globally aggregated land transport emissions between ELK and the other global inventories: positive (negative) values indicate higher (lower) emissions in ELK. Note that the CEDS inventory includes inland navigation as part of the land transport sector.
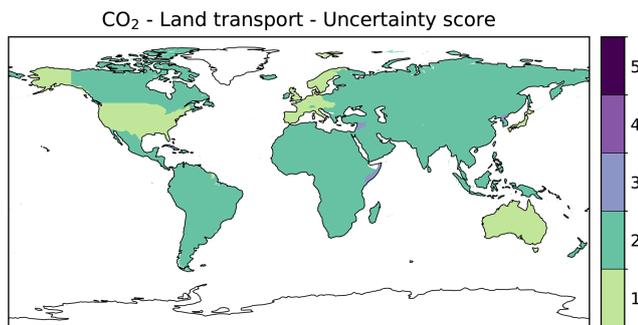
Figure 8. Uncertainty scores for the CO_2 land transport emissions, ranging from 1 (very low uncertainties) to 5 (very high uncertainties).

on shipping fuels to improve air quality in coastal regions. This is an important feature of the inventory, particularly in the context of the recent debate on the impact of the IMO regulations on climate (Jordan and Henry, 2024; Gettelman et al., 2024; Quaglia and Visioni, 2024).

The comparison with the other inventories shows a generally good agreement for the three species with the highest emissions, namely CO_2, NO_x, and SO_2 (Fig. 10). For this comparison we also include the shipping-specific high-resolution inventory by the Shipping Emission Inventory Model (SEIM; Yi et al., 2025). ELK global CO_2 emissions are 5 %–9 % lower than in the other inventories. The agreement is also remarkably good for SO_2, with differences of only a few percent in comparison to CEDS and CAMS-GLOB, while ELK has 17 % lower emissions than EDGAR8, since this inventory does not account for the IMO regulations in the SECAs, which obviously have an impact on the total SO_2 emissions. SO_2 in ELK are 13 % lower than in SEIM: this can be partly explained by the 7 % lower CO_2 emissions in ELK, but could also be due to different allocation of fuel types to the fleet, which affects the fuel sulphur content. The

NO_x emissions in ELK are about 20 %–30 % lower than in all other inventories, which could be due to incompleteness in the technical data: as the NO_x emission factor strongly depends on the ship construction date and on the engine's RPM (Faber et al., 2020), incompleteness of this data can have a large impact on the resulting emissions. The deviations for the other species are considerably larger, especially for BC and NMVOC. However, there is considerable disagreement across the other inventories as well, indicating a high level of uncertainty in the emission factors for these species in the shipping sector. The emissions of these species are nevertheless low compared to three key species discussed above (see Table 5), which are also the most relevant SLCFs in terms of climate impact (Righi et al., 2023; Mertens et al., 2024). The analysis of the deviations at the regional level shows a predominantly uniform distribution across the most important regions in CAMS-GLOB, EDGAR8 and SEIM (Fig. S47), while large regional differences are found in the comparison with CEDS: in this case the ELK inventory shows much larger emissions in the Mediterranean, around the Arabian Peninsula, and in East and Southeast Asia, and lower emissions in the North Pacific and North Atlantic ocean. This is somewhat surprising, since all inventories are supposed to be based on similar activity data from AIS and, at least for CO_2, they should use similar emission factors. One reason could be the allocation of the activity data to the different types of vessels and the corresponding assumptions drawn on their technical parameters, impacting fuel consumption and, in turn, CO_2 emissions. This could also be a reason for the higher global CO_2 emissions in ELK compared with the other inventories. The distribution of the regional deviations is similar for NO_x and SO_2 (Figs. S50 and S52, respectively), again pointing to the activity data, in particular the assumptions about the ships technical features in each ship category, as the possible reason for these deviations.

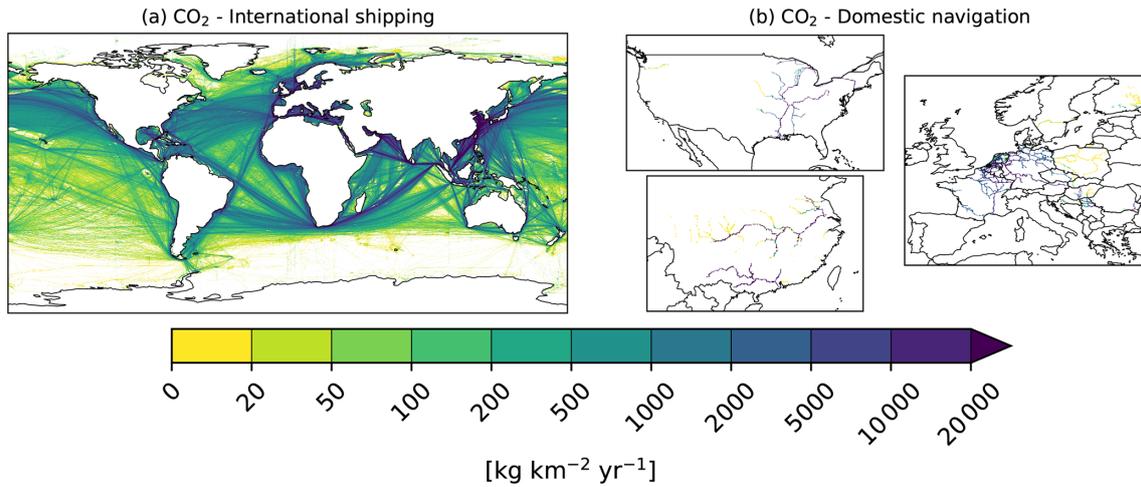The uncertainty in the activity data for the ELK inventory can be inferred from the uncertainty score for the CO_2 in-

Earth Syst. Sci. Data, 18, 1619–1664, 2026

https://doi.org/10.5194/essd-18-1619-2026

Figure 9. CO_2 emissions from shipping: **(a)** international shipping, **(b)** inland navigation.
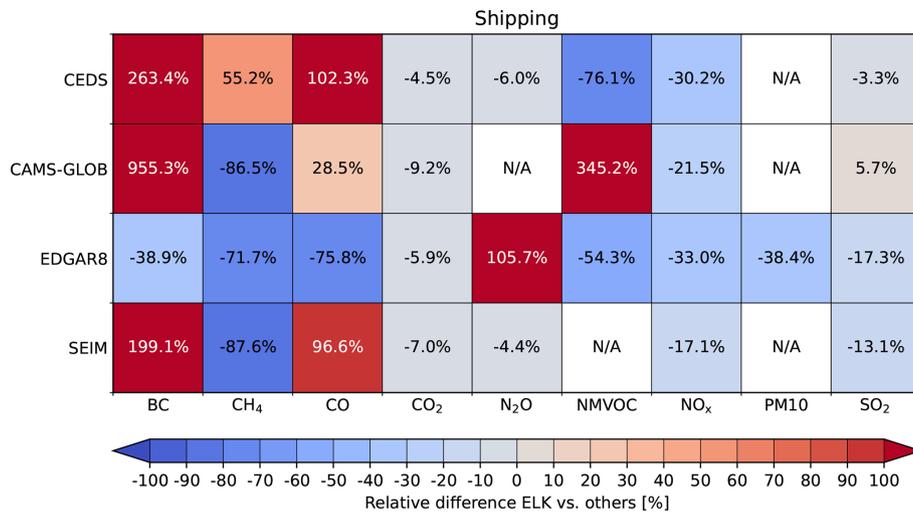

Figure 10. As in Fig. 7, but for shipping emissions. Note that the CEDS and EDGAR8 inventories do not include inland navigation in the shipping sector.

ternational shipping emissions shown in Fig. 11a. In our uncertainty assessment, we assign score 1 for the CO_2 emission factor worldwide, such that the overall score for this species is only determined by the uncertainty in the activity data. For the latter, we consider the fact that our emission model accounts neither for wave heights, which are particularly significant at the mid-latitudes, located between the Tropic of Cancer and the Arctic Circle as well as between the Tropic of Capricorn and the Antarctic Circle (Timmermans et al., 2020). We also assume that AIS data has a lower vessel coverage along the coastlines of certain regions due to unreported activities (Paolo et al., 2024). Combining all these factors results in an uncertainty score 2 over most of the globe, with a score 1 limited only to a few regions around Europe, US, South America, Africa and Australia. The scores are similar for SO_2 and considerably higher for other species

(Fig. S53), consistent with the comparison with the other inventories discussed above.

For CO_2 emissions from domestic navigation (Fig. 11b), we assess a score 2 for the US and Europe and a score 3–4 for China. The uncertainty of this subsector primarily arises from the assessment of activity data based on the input transportation statistics, which vary in spatial and temporal resolution. For China, we applied a combination of transportation statistics and AIS data, which is affected by the limited AIS availability and blind spots where no signals are received. This leads to a higher uncertainty score compared to Europe and the US The energy intensities of river transportation in the ELK inventory are set to a characteristic value within each modelling region, hence not capturing local phenomena such as increased energy intensity due to varying ship operating speeds, higher river flow velocities or location-specific
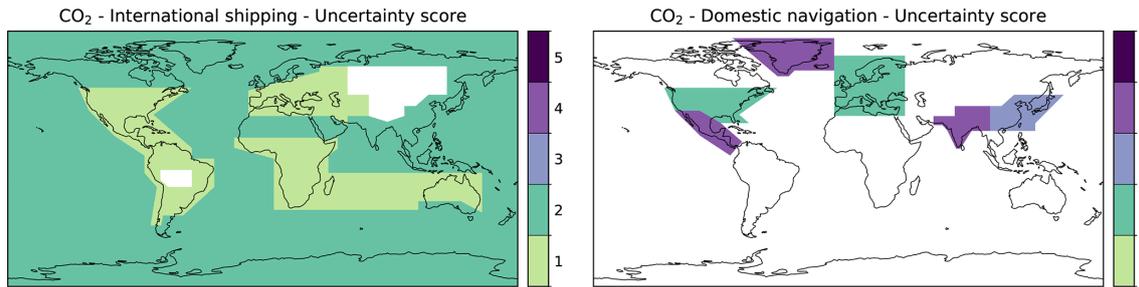
Figure 11. Uncertainty scores for the CO_2 shipping emissions, ranging from 1 (very low uncertainties) to 5 (very high uncertainties).

fleet characteristics. The emission factors for NO_x, CO, HC, and PM are calculated based on the fleet age structure and region specific emission limits, under the assumption that these limits are met. In reality ships might not comply to the regulations, leading to a tendency of underestimation in our inventory. Other emission factors are aligned with those of the international shipping sector and are therefore subject to the same uncertainties.

4.3 Aviation

The ELK inventory for aviation considers four subsectors or aircraft types, namely wide-body, single-aisle, regional and cargo aircraft (Fig. 12). Wide-body aircraft dominate the long-distance intercontinental traffic between North America, Europe, and East Asia, predominantly in the Northern Hemisphere. These three regional hotspots are also evident in the single-aisle route patterns, which are mostly concentrated in these regions almost exclusively above the continents, with a few routes in the North Atlantic and in the Pacific connecting Hawaii with North America. Regional flights are frequent in the US and Europe and limited to a few routes in the other regions of the world, thus marking a difference between developed and developing countries as well as in the population density. Cargo flights also have a long-distance pattern, with routes mainly connecting North America, Europe and China. The vertical stripes over the North Atlantic, especially visible in Fig. 12a and b, are a consequence of the reduced flight radar coverage over the North Atlantic and thus a reduced density of waypoints (at 10° longitude intervals) along the North Atlantic tracks. The various transatlantic routes are therefore mainly concentrated on the available waypoints and are approximated by great circle segments between these points.

The zonal maps (Fig. 13) show a peak in the CO_2 emissions at the typical cruise altitude of 10–12 km at northern mid-latitudes for all subsectors, with the exception of regional aircraft, which tend to fly lower, with a peak at around 6 km. This is due to the often very short flight distances of regional aircraft, which prevent them from reaching higher cruise altitudes, as well as the fact that a significant number of regional routes are operated by turboprop and piston

aircraft, which have lower cruising altitudes for technical reasons. Wide-body aircraft tend to follow higher-latitude routes (50–60° N) compared to single-aisle aircraft (40° N). Due to limited range, transatlantic flights of single-aisle aircraft only commute between US East Coast and Central Europe along the North Atlantic Track System, whereas wide-body flights also occur between the Middle East and the west coast of North America, resulting in more northward operations.

The global CO_2 emissions from aviation amount to 851 Tg (Table 5), almost completely due to wide-body (46 %) and single-aisle aircraft (48 %), see Table S6. Interestingly, only 3.3×10^6 wide-body aircraft flights (8.5 % of the total) contribute to a similar share of emissions as the 27.8×10^6 single-aisle aircraft flights. This is due to the higher distance-specific fuel consumption of wide-body aircraft in consequence of their higher weights that require more powerful engines. The large shares of emission from wide-body and single-aisle aircraft are also evident for the other species, although for CO and NMVOC the share of single-aisle and regional aircraft is significantly larger, since about one third of NMVOC and CO emissions are caused by taxiing activities on the ground when the engines are running in idle mode, as these activities have relatively higher impact for flights with shorter cruise phase. The ELK emission inventory for aviation also includes hourly data representative of the average diurnal variation of the emissions over the reference year 2019. This kind of data is useful for modelling of contrail cirrus and their impact on climate (e.g. Burkhardt and Kärcher, 2011; Bickel et al., 2025), especially concerning the emissions of H_2O as well as flight distance and propulsion efficiency. The diurnal variation for H_2O is shown in Fig. 14 for the four aviation subsectors. It shows a main peak around 14:00 UTC, mainly driven by the daily maximum of single-aisle emissions. At this time of the day, domestic traffic is intense in the three busy regions of Europe, North America and Asia. On the US East Coast, the morning increase in flight movements begins around this time. A second peak can be seen at 01:00 UTC and is due to the diurnal maximum of wide-body aircraft: this is the time of morning air traffic peak in East Asia and many North Atlantic crossings also take place at this time. However, the daily amplitude of wide-body H_2O emissions is lower compared to the other
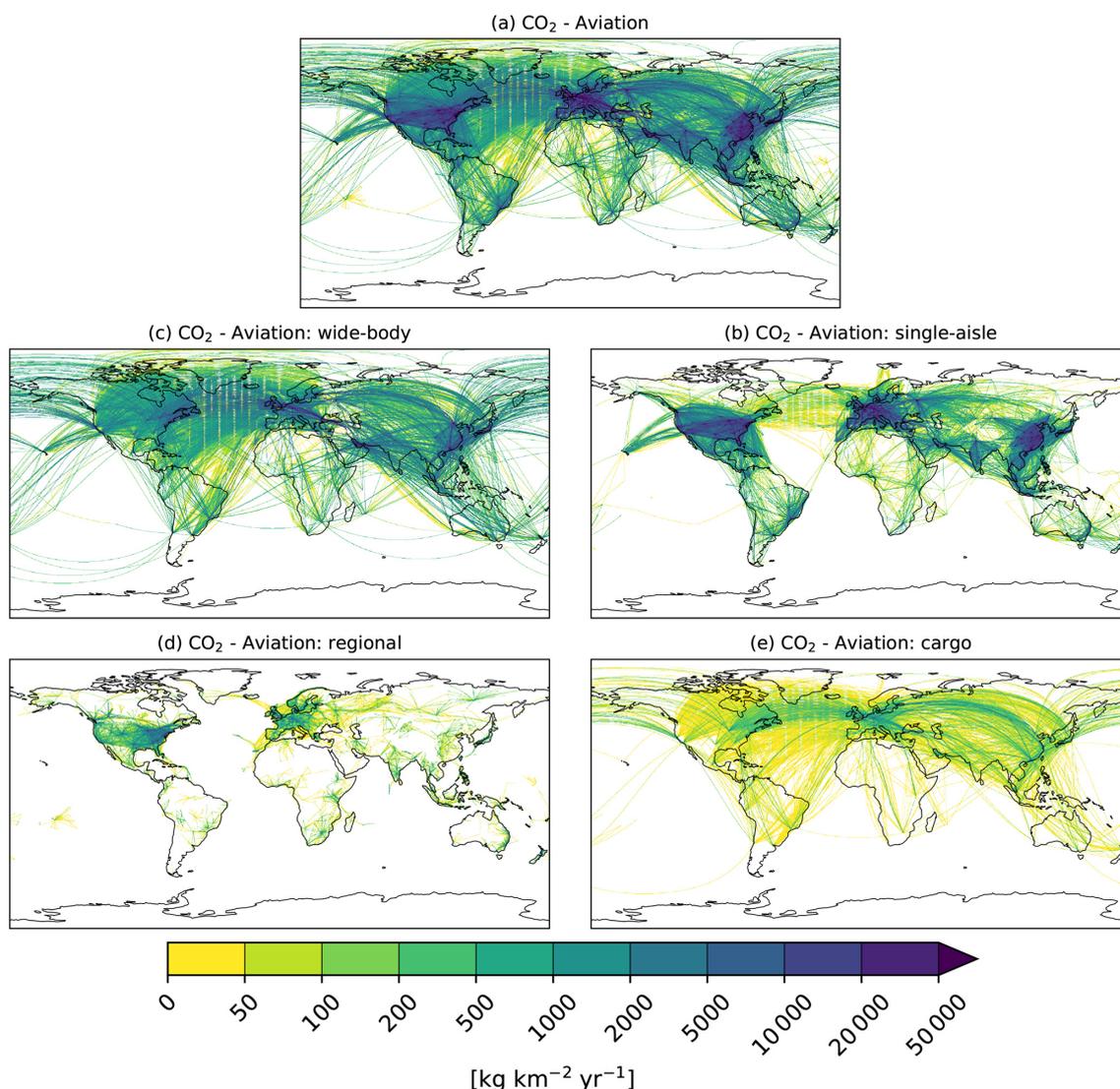
Figure 12. Vertically integrated CO_2 emissions from aviation (**a**) and related subsectors (**b–e**).

subsectors, because intercontinental and long-range flights take place at any time of the day. In contrast, the daily minimum of the overall aviation sector and of the single-aisle subsector occurs at 22:00 UTC, when nocturnal airport closures in Central European airports markedly reduce the European domestic air traffic. The contribution from regional traffic is high between 13:00–21:00 UTC, i.e. the morning time in the subsector's dominant area of North America. Cargo traffic is evenly distributed throughout the day, with slight peaks at night time in East Asia, morning in North America and evening in Europe.

For the comparison against other inventories, we include three additional aviation-specific datasets: the predecessor inventory TraK, developed in a previous DLR project, the dataset by Quadros et al. (2022) using telemetry data provided by Flightradar24, and the GAIA dataset (Teoh et al., 2024). The comparison (Fig. 15) shows that aviation has the

best agreement with the other inventories among the three transport sectors, with deviations within 50 % and mostly within 20 % for all species. The ELK inventory calculates lower aviation emissions than the other inventories in most cases, while it has generally larger emissions than the predecessor inventory TraK. This is due to the consideration of substantial parts of global cargo traffic volume, on the one hand, and due to various methodological improvements in ELK, on the other hand. The latter includes the statistical dispersion of the flight-specific emissions along different flight altitudes, including those at which the aircraft does not operate optimally in terms of fuel, the prevailing routing along real flight paths instead of great circle routes, and the wind-induced scaling of the air distance. This leads to longer flight distances and higher fuel consumption and hence to increased emissions in ELK compared to TraK. However, both the ELK and the TraK inventories are developed using
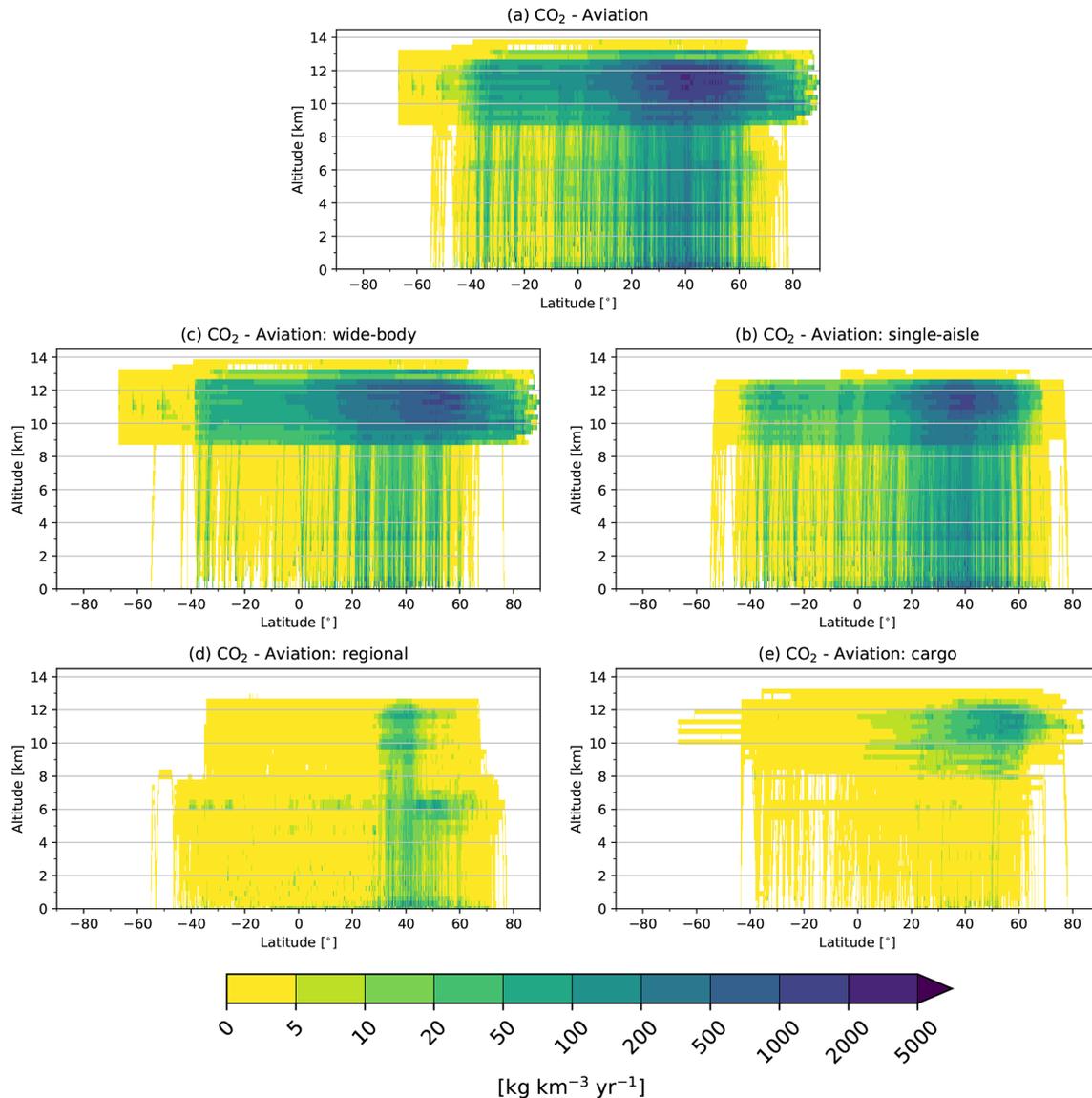
Figure 13. Zonally averaged CO_2 emissions from aviation **(a)** and related subsectors **(b–e)**.

a bottom-up approach, where the transport demand and the quantity structures are modelled individually and in great detail at the airport-pair level, so that, for example, a higher volume of air traffic is assumed for Asia due to a higher resolution of the traffic structure (which could explain the large differences of ELK against the other inventories in this region, see Fig. S80). The other inventories, on the contrary, mainly follow top-down approaches at a lower level of detail. Another reason for the higher ELK emissions in Asia could be related to the recent increase in activity in this region, which is not fully captured by the other inventories, since they possibly rely on less up-to-date activity data. The largest deviations are found for SO_2, with ELK showing lower emissions than all others. The emissions of this species mainly depend on the assumed fuel sulphur content. For the ELK inventory,

regionally varying sulphur concentrations in the fuel varying from 275 to 635 ppm taken from CRC (2012) are used to calculate the SO_2 emission factor depending on the geographical location of the departure airport, while other inventories often assume a globally averaged constant fuel sulphur content (e.g. Wilkerson et al., 2010; Simone et al., 2013; Quadros et al., 2022; Teoh et al., 2024). Large deviations are also found for BC: the ELK inventory considers flight phase-dependent information on engine thrust along the trajectory, which is included in the applied soot particle mass calculation in the form of relative thrust. The TraK inventory approximates the relative engine thrust using the ratio of the flight-phase-specific fuel flow to the maximum fuel flow at take-off, which is subject to uncertainties.
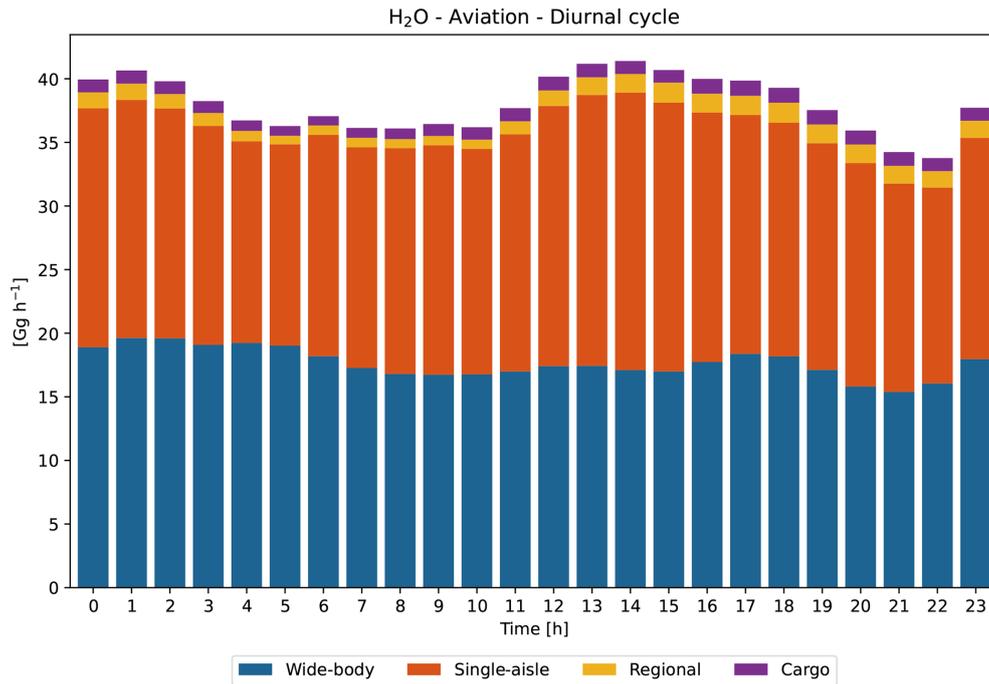
Figure 14. Aviation: Diurnal cycle of annual total aviation H_2O emissions by hour (UTC) and subsector for an average day.
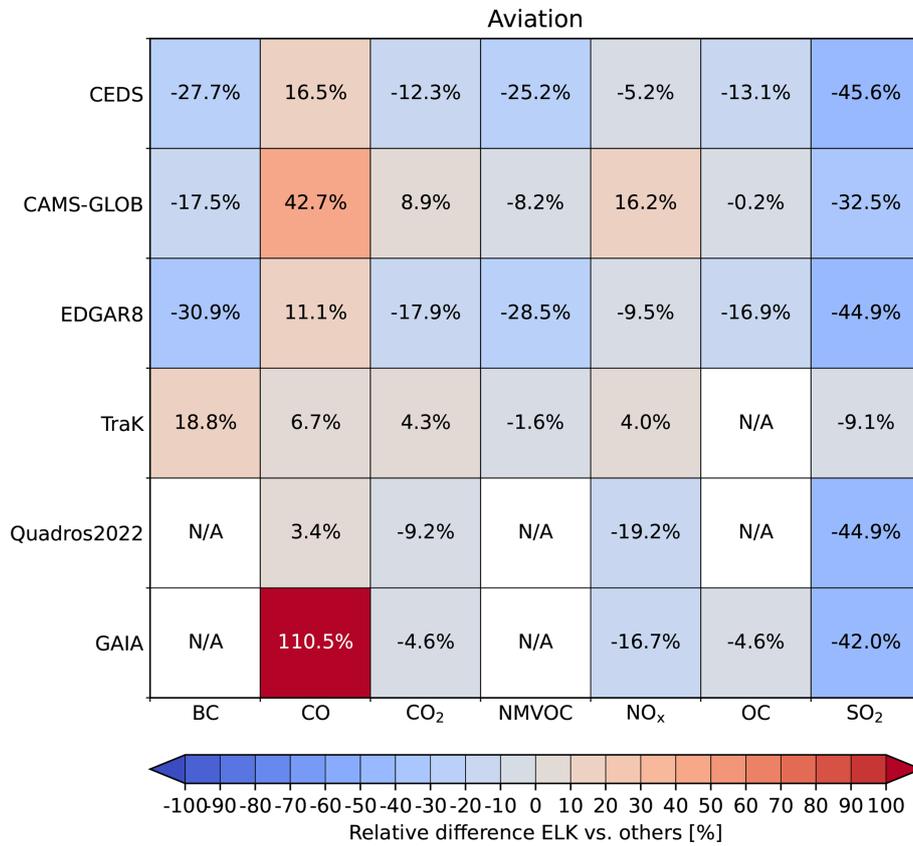
Figure 15. As in Fig. 7, but for aviation emissions.
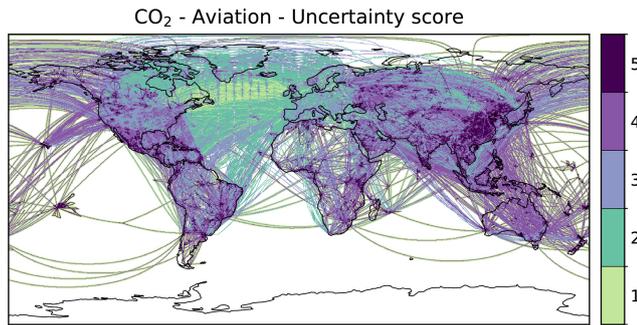
Figure 16. Uncertainty scores for the vertically integrated CO_2 aviation emissions, ranging from 1 (very low uncertainties) to 5 (very high uncertainties).

Figure 17. CO_2 emissions from the energy-for-transport sector.

Unlike the other transport sectors discussed above, the uncertainty analysis for aviation is performed on a grid cell basis, thus providing geographically resolved uncertainty scores on the same grid as the emissions. The vertically aggregated uncertainty scores (Fig. 16) reveal a generally low uncertainty, with a score of 2 along most routes. The lowest uncertainty (score 1) is calculated over the North Atlantic, due to the high availability of real flight path data and the enhanced quality of performance models of operating aircraft for this region. In contrast, larger uncertainties are assigned over China, India, Mexico and Africa, where the coverage of flight path data and taxiing times statistics is limited. For particle emissions (BC and nvPM, Fig. S85), the uncertainties are generally higher compared to the other species, because engine-specific emission factors are not available for some aircraft and emission factors from fleet averages have to be applied instead.

4.4 Energy for transport

The global CO_2 emissions from transport-related refining activities are shown in Fig. 17. Although the data is provided on the same grid as the land transport and shipping emissions, the figure shows the individual emission point sources to enhance their visibility on the map. The emissions are large in industrialized and highly populated regions, like US, Europe, Russia, Middle East, East China and Japan, while they are low in less developed and populated regions, e.g. Africa, South America and rural regions of Australia, Canada and Russia. Generally, the emission sources are concentrated along coastal areas (e.g. the North Sea coast of Belgium and the Netherlands) and big rivers (e.g. the Mississippi in the US), as refineries are often built at strategic locations to facilitate the transportation of refinery products. The total CO_2 emissions from the energy-for-transport sector in 2019 amount to 533 Tg (Table 5), which adds to the direct CO_2 emissions of the three transport sectors (8312 Tg). Hence, the energy-for-transport sector contributes an additional 6.4 % of indirect CO_2 emissions, underscoring the importance of con-

sidering the emissions from this sector for a comprehensive assessment of the transport impacts on climate.
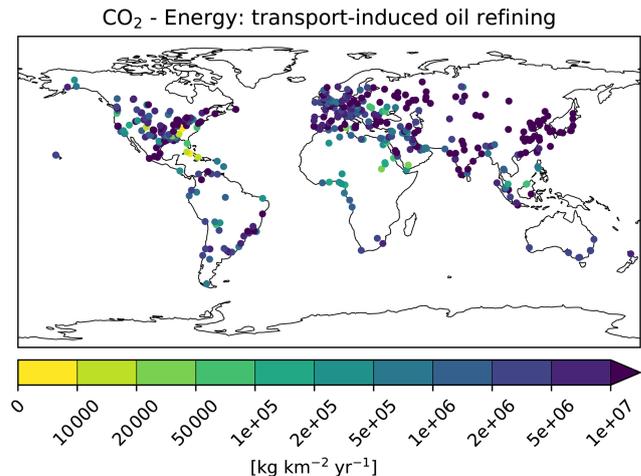
Since we focus solely on the fraction of energy emissions related to transport, a comparison with other inventories is not appropriate, as they report total emissions from the energy sector rather than just the transport-related share. To validate the energy for transport emissions, other sources are considered instead, although a fully consistent comparison with the ELK data is not feasible. One dataset that can be used for a plausibility check is the one by Ma et al. (2022), who calculated the overall CO_2 emissions from refineries in different countries. This is compared to the ELK energy emissions in Fig. 18a and shows generally higher values. This can partly be explained with the fact that Ma et al. (2022) accounted for the emissions from all refinery activities and not only the transport-related combustion emissions. In the ELK inventory, the transport-related emissions are on average responsible for about 50 % of the total emissions. Ma et al. (2022) also included further sources of emissions, like processing, flaring, and fugitive emissions, which are not considered in ELK and, according to Sun et al. (2019), are expected to contribute about 13 % of total CO_2 emissions. Furthermore, Ma et al. (2022) comprises all GHG emissions, while the ELK values are for CO_2 only. Given these differences, it is not surprising that the ELK emissions in the energy-for-transport sector are lower, still this comparison is a useful quality check on the ELK energy emissions, ensuring that transport-related emissions from oil refining are below the overall emissions from the refinery sector. Figure 18a also shows data for some countries from the UNFCCC (https://unfccc.int/ghg-inventories-annex-i-parties/2023, last access: 10 June 2025), reporting total fuel combustion emissions from petroleum refining (IPCC sector 1.A.1.b). Also in this case, the ELK emissions, which consider only the transport-
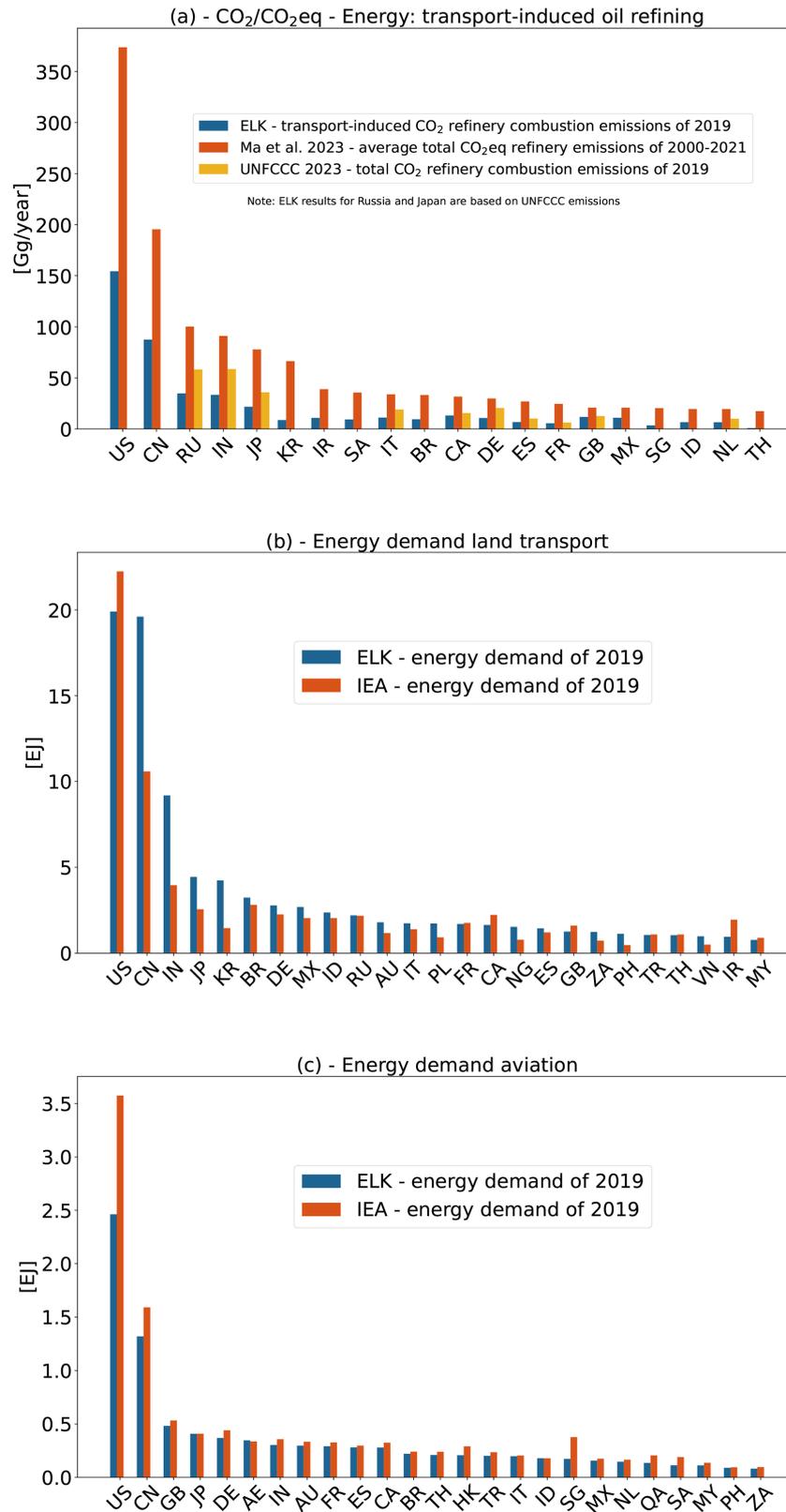
Figure 18. Comparison of **(a)** CO_2 emissions from energy for transport with CO_2eq emissions in Ma et al. (2022) and reported CO_2 emission data from the UNFCCC; energy demand of the land transport **(b)** and aviation **(c)** sectors in ELK compared with data from the IEA Extended Energy Balances from 2019.
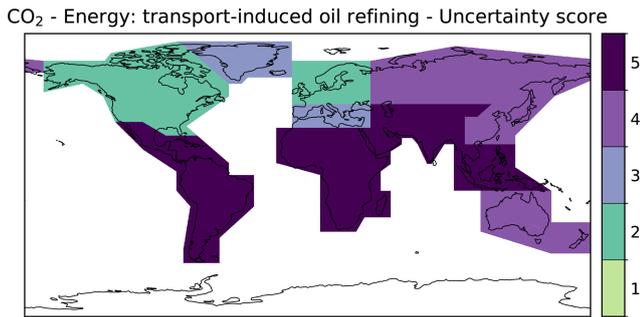
CO$_2$ - Energy: transport-induced oil refining - Uncertainty score

Figure 19. Uncertainty scores for the CO$_2$ energy for transport emissions, ranging from 1 (very low uncertainties) to 5 (very high uncertainties).

related fraction of the total combustion emissions, are below the UNFCCC figures.

We further compare the energy demand estimated in the ELK land transport and aviation sectors against the IEA Extended Energy Balances (https://www.iea.org/data-and-statistics/data-product/world-energy-balances, last access: 10 June 2025) in Fig. 18b and c, respectively. The IEA fuel consumption is fed into the estimation of the share of fuels from refineries used in the transport sector against total refinery products. For aviation this is realized by assigning the consumption to the departure country. For the shipping sector an attribution of fuel consumption to specific countries is not possible. The ELK inventory shows a larger (smaller) fuel consumption for land transport in Asia (North America) than the IEA data. For aviation, the ELK fuel consumption is lower than the IEA data in China and North America.

The uncertainty analysis of the CO$_2$ emissions from the energy-for-transport sector (Fig. 19) results in a low uncertainty score 2 only for US, Canada, Central and Northern Europe where point source emission data is available for refinery activities. Larger uncertainties are assessed in the other regions, e.g. Russia and Oceania due to uncertainties regarding refinery locations, and are particularly high (score 5) in Central and South America, Africa, South and East Asia where a default approach is applied to estimate emissions.

5 Data availability

The ELK emission inventory is available at https://doi.org/10.15489/d9dswthdix21 (Ehrenberger et al., 2025, for land transport), https://doi.org/10.15489/lhqawfes5755 (Banyś et al., 2025, for shipping), https://doi.org/10.15489/86s8uwpxik95 (Weder et al., 2025, for aviation), and https://doi.org/10.15489/gixadaq6ds98 (Draheim et al., 2025, for energy-for-transport). Users are kindly requested to cite the present paper if using the data for scientific publications.

6 Conclusions

This paper documents the ELK global emission inventory for the transport sectors, incorporating land transport, shipping, aviation, and energy-for-transport emissions from oil refineries. The methodology for emission calculation described here offers several advantages over existing global inventories, including a consistent bottom-up methodology applying, whenever possible, common underlying data across the transport sectors, the consideration of indirect transport emissions in the energy sector, and a higher sectoral resolution to resolve the emissions from specific vehicles or aircraft types, which opens interesting perspectives for assessing the effects of different transport categories, like passenger vs. freight. Furthermore, the ELK inventory provides more comprehensive information than commonly found in global inventories. This includes, for instance, aviation-specific quantities, that are particularly valuable for the aviation climate modelling community, and non-exhaust emissions of particulate matter by land transport, whose impact will gain importance with the transition to electric vehicles. The ELK inventory is complemented with a geographically resolved uncertainty score resulting from a thorough characterisation of uncertainty factors, to facilitate informed usage of the emission data.

In the ELK inventory land transport emissions are dominated by cars and heavy freight trucks, which are responsible of 45 % and 33 %, respectively, of the sector's CO$_2$ emissions globally. Other categories are relevant at the regional level, for instance 2-wheelers emissions in India and buses in North America, but the global contribution of each of them is below 10 %. The emissions of the short-lived species reveal the importance of specific technologies for certain categories, like the widespread usage of diesel engines for trucks and of 2-stroke engines by 2-wheelers. The emissions from the shipping sector in the ELK inventory are dominated by the international shipping, which contributes more than 85 % of the global emissions of all species, with the exception of CO, which to 65 % is attributed to domestic navigation. This is due to the old age of the inland shipping fleet, characterized by engines with no emission standards and small engines operating at higher fuel-to-air mixtures leading to incomplete combustion and higher CO emissions. The ELK inventory also accounts for the IMO regulations on fuel sulphur content, resulting in lower SO$_2$ emissions in the SECA regions. The ELK aviation inventory shows that wide-body and single-aisle aircraft are responsible for 94 % of the global CO$_2$ aviation emissions, although wide-body flights are only 8.5 % of the total. Regional differences are also remarkable across the different aircraft categories in ELK, with wide-body and cargo flights dominating the long-distance routes, while single-aisle and regional aicraft fly shorter routes. Regional aircraft also tend to fly lower, with a peak around 6 km, in contrast to the typical flight altitude at 10–12 km of the other types. These considerations apply to all aviation

emitted species, although exception exists, for instance for CO and NMVOC, which are caused to a relevant extent by taxiing activities, on which short-range flights have a larger impact. The energy-for-transport sector emissions, a key feature of the ELK inventory, contribute an additional 6.4 % to the global transport CO_2 emissions, with the emissions concentrated in the developed countries, mostly around coastlines and big rivers, where refineries are located to facilitate the trade of refining products.

The ELK inventory is validated against established global emission inventories, yielding generally consistent results with minor discrepancies for CO_2 and larger biases for non-CO_2 species. The latter can largely be attributed to differences in assumptions and methodologies across these inventories, or to intrinsically large uncertainties for certain species, which are common across different inventories. Although the emission data presented here target the present-day (year 2019), the ELK emission models are designed to easily accommodate future projections under various scenarios and storyline assumptions.

Despite the added value of the ELK inventory demonstrated in this work, several improvements are possible and should be considered in future versions. Various components of the land transport emission calculation methodology and data sources could be enhanced. The calculation of the emission factors of CO_2 and SO_2 could be improved by considering country- and segment-specific fuel consumption data. As more databases become available, emission factors for other pollutants should be refined by incorporating additional country-based emission factors. Improved datasets would be particularly useful for 2-wheelers and for heavy and light commercial vehicles, especially in developing countries. A limitation of the current approach for rail transport is its inability to reflect country-level exceptions, particularly those with highly electrified rail networks relative to their regional representation. This can be improved with the availability of harmonised global datasets and activity reporting. The current spatial disaggregation model is limited to countries with available open data on nationwide traffic counts and applies only to passenger cars. Expanding this model to include heavy and light commercial vehicles would be a much required improvement. Furthermore, as more traffic count data become available in other regions, the model could be extended and validated to deliver improved spatial disaggregation of emissions.

In the shipping sector, using the best available AIS data source is essential for ensuring accurate emission calculations. Increasing the number of vessel movements in the input data will enhance the completeness of the dataset. Future expansion of the AIS data exchange system capabilities would allow to increase the number of satellite transmission channels, thereby improving coverage in remote areas. New research findings on alternative fuels and propulsion systems are needed to improve the accuracy of emission factors. Future changes to IMO regulations and improved emission in-

ventories might require shipping companies to register emissions data onboard vessels and transmit it via binary messages, eliminating the need for manual estimates. No additional reception equipment updates would be required for this purpose, as the AIS binary transmission protocol can be received in the same way as it is currently the case for position data. The domestic navigation emissions in the ELK inventory are limited to Europe, US and China. To extend the coverage to additional regions such as South America, India, and Southeast Asia, improved transport statistics would be crucial. However, such data is either not public available or difficult to access, and support from local authorities may be needed to obtain further information. Additionally, improvements to the domestic navigation dataset could benefit from further development of the SAR detection concept discussed in this work, along with an improved interpolation method for inland water vessels. This could complement the AIS data, especially in regions with limited coverage.

For the aviation sector, follow-up research should focus on novel aircraft concepts and engine technologies, such as the application of sustainable aviation fuels (SAF), electric and hydrogen-powered engines. This could be integrated into the aviation emission model, thus enabling the assessment of the environmental effects of future aviation scenarios. The underlying aviation emission model GRIDLAB should be extended to reliably simulate flights with short distances below 150 nautical miles. Depending on the available computational resources, the resolution of the aviation inventory could be further increased, enhancing its applicability in high-resolution atmospheric models.

With the expected increasing shift to electric vehicles, the assessment of transport-related emissions in the energy sector, specifically in the electricity generation, needs to be included in the energy emission inventory for the upcoming years. In addition to the emission from refineries, other upstream processes, like oil extraction, significantly contribute to the emissions and should be considered in future versions. Other sources, like fugitive and process-related emissions, could also be added with reasonable effort, although these are more difficult to determine. Some species, like CH_4, NH_3, and OC, were not included in the ELK energy inventory due to inconsistent data availability across different regions. Future investigations would be required to assess data availability and expand the inventory by additional species.

The method developed here for assessing uncertainty could be further refined by incorporating additional sources of uncertainties, addressing them at the subsector level, and by improving the robustness of the scores by applying different weights to the activity data and for the emission factors. As the uncertainty of the activity level and the emission factors might vary substantially within the relatively coarse spatial classification scheme adopted here, increasing the spatial resolution of the uncertainty scores would significantly increase their applicability.

The ELK inventory is released on a Creative Commons license and the scientific community is welcome to use this newly developed datasets for assessment studies and decision-making analyses, and to provide feedback for improvements on future versions of the dataset.

Author contributions. MR led the ELK project, contributed to defining the requirements and structure of the emission inventories, performed the analysis and validation of the results, contributed to the concept for the uncertainty assessment and coordinated the writing of the manuscript with input by all co-authors. SE created the emission inventory for global land transport, contributed to the uncertainty assessment and coordinated the generation of the emission datasets for all sectors. SB contributed to the requirements definition, to the analysis and the validation of the emission inventories. JHen defined the requirements and structure of the emission inventories, and contributed to their analysis and validation. JHel developed the method for the uncertainty assessment and coordinated its implementation for all sectors. PBa programmed the IMO algorithms for maritime emission calculation and carried out the emission calculation for international shipping. ID developed the method for the spatial distribution of the land transport emissions, created the emission inventory for global land transport and contributed to the uncertainty assessment. PD created the emission inventory for the energy sector and contributed to the uncertainty assessment and the validation. AF created the emission inventory for domestic navigation and contributed to the uncertainty assessment. ML contributed to the uncertainty assessment of non-exhaust emissions. TP co-developed the concept for the energy sector emission inventory. YS co-developed the concept for the energy sector emission inventory, especially with respect to spatio-temporal data and data processing. AS co-led the ELK project and contributed to the emission inventory for European land transport. BS contributed to the emission inventory for domestic navigation. NT created the emission inventory for European land transport, prepared the socioeconomic base data, and contributed to the uncertainty assessment. CMW extended the methodology of air traffic emission modelling, categorized the worldwide aircraft fleet into subsectors, quantified the aviation emissions, derived the methodology for the aviation uncertainty assessment, created the aviation emission inventory data and contributed to the validation. PBe modelled the air traffic demand and fleet composition for passenger and cargo transport and provided worldwide flight plans to the aviation emission modelling. MC validated and updated the database of emissions factors and improved the model capabilities and performance of the aviation emission model. MG modelled the air traffic demand and fleet composition for passenger and cargo transport and provided worldwide flight plans to the aviation emission modelling. AL provided air traffic data and performed their post-processing and interpretation for the application in the aviation emission inventory. FL originally developed the applied methodology of air traffic emission modelling and conceptualized the methodological improvements of the aviation emission methodology. SM provided data on regionally varying sulphur content in aviation fuel for the aviation emission modelling. ZLZ performed comprehensive and detailed trajectory simulations for the aviation emission modelling.

References

ACI: Traffic statistics, Tech. rep., Airport Council International, https://aci.aero/resources/data-center/ (last access: 6 Febraury 2026), 2019.

Al-Falahi, M., Tarasiuk, T., Jayasinghe, S., Jin, Z., Enshaei, H., and Guerrero, J.: AC ship microgrids: control and power management optimization, Energies, 11, 1458, https://doi.org/10.3390/en11061458, 2018.

Allekotte, M., Biemann, K., C., H., Colson, M., and Knörr, W.: Aktualisierung der Modelle TREMOD/TREMOD-MM für die Emissionsberichterstattung 2020 (Berichtsperiode 1990–2018): Berichtsteil TREMOD, Tech. rep., ifeu – Institut für Energie- und Umweltforschung, Heidelberg, Germany, https://www.umweltbundesamt.de/publikationen/aktualisierung-tremod-2019 (last access: 27 February 2026), 2020.

Aritua, B., Cheng, L., van Liere, R., and de Leijer, H.: Blue Routes for a New Era: Developing Inland Waterways Transportation in China, Tech. rep., World Bank, Washington, DC, USA, https://doi.org/10.1596/978-1-4648-1584-3, 2020.

Banyś, P., Heymann, F., and Gucma, M.: Occurrence of unknown sensor data within AIS dynamic messages, Naše More, 67, 126–137, https://doi.org/10.17818/NM/2020/2.5, 2020.

Banyś, P., Gucma, M., and Shradha Fowdur, J.: Assessment of possible misidentification of AIS transponders within AIS data due to bit inversions of MMSI, Naše More, 71, 30–37, https://doi.org/10.17818/nm/2024/1.5, 2024.

Banyś, P., Fitz, A., Suhr, B., Hellekes, J., Brinkop, S., Hendricks, J., Schulz, A., and Righi, M.: ELK – Global Emission Inventory – Shipping Sector, 2019, DLR [data set], https://doi.org/10.15489/lhqawfes5755, 2025.

BASt: Automatic counting stations 2019, https://www.bast.de/DE/Themen/Digitales/HF_1/Massnahmen/verkehrszaehlung/Daten/2019_1/Jawe2019.html?nn=414410 (last access: 6 February 2026), 2019.

Belzer, D. B.: A Comprehensive System of Energy Intensity Indicators for the U.S. Methods, Data and Key Trends, Tech. Rep. PNNL-22267, Pacific Northwest National Laboratory, Richland, WA, USA, https://www.pnnl.gov/main/publications/external/technical_reports/pnnl-22267.pdf (last access: 27 February 2026), 2014.

Bickel, M., Ponater, M., Burkhardt, U., Righi, M., Hendricks, J., and Jöckel, P.: Contrail cirrus climate impact: from radiative forcing to surface temperature change, J. Climate, 38, 1895–1912, https://doi.org/10.1175/JCLI-D-24-0245.1, 2025.

BMV: Verkehr in Zahlen 2025/2026, https://www.bmv.de/SharedDocs/DE/Anlage/G/verkehr-in-zahlen25-26-pdf.pdf?__blob=publicationFile (last access: 6 February 2026), 2025.

Bray, L. G., Dager, C. A., Henry, R. L., and Koroa, M. C.: River efficiency, fuel taxes, and modal shifts: Tennessee Valley Authority model assists policy makers, TR News, 18–22, https://onlinepubs.trb.org/onlinepubs/mb/TRNews221Features.pdf (last access: 27 February 2026), 2002.

Burkhardt, U. and Kärcher, B.: Global radiative forcing from contrail cirrus, Nat. Clim. Change, 1, 54–58, https://doi.org/10.1038/nclimate1068, 2011.

CARB: EMFAC 2021, Tech. rep., California Air Resources Board, https://ww2.arb.ca.gov/our-work/programs/msei/emfac2021-model-and-documentation (last access: 6 February 2026), 2021.

CCNR: Annual Report 2023: Inland Navigation in Europe Market Observation, Tech. rep., Central Commission for the Navigation of the Rhine, https://inland-navigation-market.org/wp-content/uploads/2023/10/CCNR_annual_report_EN_2023_WEB-1.pdf (last access: 6 February 2026), 2023.

Cirium: Cirium Fleets Analyzer, Tech. rep., Cirium, London, UK, https://www.cirium.com/analytics-services/fleets-analyzer/ (last access: 6 February 2026), 2019.

Corbett, J. J. and Fischbeck, P.: Emissions from ships, Science, 278, https://doi.org/10.1126/science.278.5339.823, 1997.

CRC: Update of the survey of sulfur levels in commercial jet fuel: Final Report, Tech. Rep. 605, CRC Project AV-1-10, Coordinating Research Council, https://crcao.org/wp-content/uploads/2019/05/CRCFinalReportProjectAV-1-10November2012.pdf (last access: 27 February 2026), 2012.

Crippa, M., Solazzo, E., Huang, G., Guizzardi, D., Koffi, E., Muntean, M., Schieberle, C., Friedrich, R., and Janssens-Maenhout, G.: High resolution temporal profiles in the emissions database for global atmospheric research, Sci. Data, 7, https://doi.org/10.1038/s41597-020-0462-2, 2020.

Crippa, M., Guizzardi, D., Schaaf, E., Monforti-Ferrario, F., Quadrelli, R., Risquez Martin, A., Rossi, S., Vignati, E., Muntean, M., Brandao De Melo, J., Oom, D., Pagani, F., Banja, M., Taghavi-Moharamli, P., Köykkä, J., Grassi, G., Branco, A., and San-Miguel, J.: GHG emissions of all world countries – 2023, Tech. rep., European Commission, Luxembourg, https://doi.org/10.2760/953322, 2023.

Crippa, M., Guizzardi, D., Pagani, F., Schiavina, M., Melchiorri, M., Pisoni, E., Graziosi, F., Muntean, M., Maes, J., Dijkstra, L., Van Damme, M., Clarisse, L., and Coheur, P.: Insights into the spatial distribution of global, national, and subnational greenhouse gas emissions in the Emissions Database for Global Atmospheric Research (EDGAR v8.0), Earth Syst. Sci. Data, 16, 2811–2830, https://doi.org/10.5194/essd-16-2811-2024, 2024.

Crisp, D.: The State-of-the-Art in Ship Detection in Synthetic Aperture Radar Imagery, AD-a426 096, Australian Government – Department of Defence, https://apps.dtic.mil/sti/tr/pdf/ADA426096.pdf (last access: 6 February 2026), 2004.

Dahl, A., Gharibi, A., Swietlicki, E., Gudmundsson, A., Bohgard, M., Ljungman, A., Blomqvist, G., and Gustafsson, M.: Traffic-generated emissions of ultrafine particles from pavement–tire interface, Atmos. Environ., 40, 1314–1323, https://doi.org/10.1016/j.atmosenv.2005.10.029, 2006.

Deidewig, F., Doepelheuer, A., and Lecht, M.: Methods to assess aircraft engine emissions in flight, in: 20th Congress of the Int. Council of the Aeronautical Sciences 1996 (ICAS), Sorrento, Italy, https://elib.dlr.de/38317/ (last access: 26 February 2026), 1996.

DfT: Road Traffic Statistics, Tech. rep., UK Department for Transport, https://storage.googleapis.com/dft-statistics/road-traffic/all-traffic-data-metadata.pdf (last access: 6 February 2026), 2014.

DfT: Average annual daily flow (AADF) – major and minor roads, Tech. rep., UK Department for Transport, https://storage.googleapis.com/dft-statistics/road-traffic/downloads/data-gov-uk/dft_traffic_counts_aadf.zip (last access: 6 February 2026), 2019.

Döpelheuer, A.: Anwendungsorientierte Verfahren zur Bestimmung von CO, HC und Ruß aus Luftfahrttriebwerten, Tech. Rep. DLR Forschungsbericht 2002–10, DLR Institut für Antriebstechnik, https://elib.dlr.de/49148/ (last access: 27 February 2026), 2002.

Draheim, P., Pregger, T., Scholz, Y., Hellekes, J., Brinkop, S., Hendricks, J., Schulz, A., and Righi, M.: ELK – Global Emission Inventory – Energy-for-Transport Sector, 2019, DLR [data set], https://doi.org/10.15489/gixadaq6ds98, 2025.

DuBois, D. and Paynter, G.: Fuel Flow Method2 for estimating aircraft emissions, J. Aerosp., 115, 1–14, https://doi.org/10.4271/2006-01-1987, 2006.

EASA: Introduction to the ICAO Engine Emissions Databank, Tech. Rep. TE.GEN.00301-006, European Union Aviation Safety Agency (EASA), Cologne, Germany, https://www.easa.europa.eu/en/downloads/45576/en (last access: 6 February 2026), 2023.

Ehrenberger, S., Dasgupta, I., Thomsen, N., Hellekes, J., Löber, M., Brinkop, S., Hendricks, J., Schulz, A., and Righi, M.: ELK – Global Emission Inventory – Land Transport Sector, 2019, DLR [data set], https://doi.org/10.15489/d9dswthdix21, 2025.

Eurostat: Statistical regions in the European Union and partner countries – NUTS and statistical regions 2021–2022 edition, Publications Office of the European Union, https://doi.org/10.2785/321792, 2022.

Eyers, C., Addleton, D., Atkinson, K., Broomhead, M., Christou, R., Elliff, T., Falk, R., Gee, I., Lee, D., Marizy, C., Michot, S., Middel, J., Newton, P., Norman, P., Plohr, M., Raper, D., and Stanciou, N.: AERO2k Global Aviation Emissions Inventories for 2002 and 2025, Tech. rep., QinetiQ LtD, Farnborough, Hants, UK, https://www.yumpu.com/en/document/read/7313363/aero2k-global-aviation-emissions-inventories-for-2002-and-2025 (last access: 27 February 2026), 2005.

Eyring, V., Köhler, H. W., van Aardenne, J., and Lauer, A.: Emissions from international shipping: 1. The last 50 years, J. Geophys. Res.-Atmos., 110, https://doi.org/10.1029/2004JD005619, 2005.

Faber, J., Hanayama, S., Zhang, S., Pereda, P., Comer, B., Hauerhof, E., van der Loeff, W. S., Smith, T., Zhang, Y., Kosaka, H., Adachi, M., Bonello, J.-M., Galbraith, C., Gong, Z., Hirata, K., Hummels, D., Kleijn, A., Lee, D. S., Liu, Y., Lucchesi, A., Mao, X., Muraoka, E., Osipova, L., Qian, H., Rutherford, D., de la Fuente, S. S., Yuan, H., Perico, C. V., Wu, L., Sun, D., Yoo, D.-H., and Xing, H.: Fourth IMO Greenhouse Gas Study 2020, Tech. rep., International Maritime Organization, London, UK, https://www.imo.org/en/ourwork/environment/pages/fourth-imo-greenhouse-gas-study-2020.aspx (last access: 26 February 2026), 2020.

Feng, L., Smith, S. J., Braun, C., Crippa, M., Gidden, M. J., Hoesly, R., Klimont, Z., van Marle, M., van den Berg, M., and van der Werf, G. R.: The generation of gridded emissions data for CMIP6, Geosci. Model Dev., 13, 461–482, https://doi.org/10.5194/gmd-13-461-2020, 2020.

FHWA: Traffic Monitoring Guide, Tech. rep., Federal Highway Administration, https://rosap.ntl.bts.gov/view/dot/74643 (last access: 6 February 2026), 2022a.

FHWA: U.S Traffic Volume Data : Special Tabulations, Tech. rep., Federal Highway Administration, https://www.fhwa.dot.gov/

policyinformation/tables/tmasdata/#y22 (last access: 6 February 2026), 2022b.

Fiore, A. M., Naik, V., Spracklen, D. V., Steiner, A., Unger, N., Prather, M., Bergmann, D., Cameron-Smith, P. J., Cionni, I., Collins, W. J., DalsØren, S., Eyring, V., Folberth, G. A., Ginoux, P., Horowitz, L. W., Josse, B., Lamarque, J.-F., MacKenzie, I. A., Nagashima, T., O'Connor, F. M., Righi, M., Rumbold, S. T., Shindell, D. T., Skeie, R. B., Sudo, K., Szopa, S., Takemura, T., and Zeng, G.: Global air quality and climate, Chem. Soc. Rev., 41, 6663, https://doi.org/10.1039/c2cs35095e, 2012.

FOCA: Aviation Policy and Strategy, Environmental Affairs; Aircraft Piston Engine Emissions, Tech. rep., Federal Department of the Environment, Transport, Energy and Communications DETEC; Federal Office of Civil Aviation, Bern, Switzerland, https://downloads.regulations.gov/EPA-HQ-OAR-2007-0294-0103/content.pdf (last access: 27 February 2026), 2007.

Fruhwirt, D., Sturm, P., Nöst, T., Leonhardt, P., Bode, G., Michael, S., and Rodler, J.: PM emissions from railways – results of tests on a wheel-rail test bench, Transport. Res. D-Tr. E., 122, 103858, https://doi.org/10.1016/j.trd.2023.103858, 2023.

Gately, C. K. and Hutyra, L. R.: Large uncertainties in urban-scale carbon emissions, J. Geophys. Res.-Atmos., 122, 11242–11260, https://doi.org/10.1002/2017JD027359, 2017.

Gelhausen, M. C., Berster, P., and Wilken, D.: Airport Capacity Constraints And Strategies For Mitigation – A global Perspective, Academic Press, https://doi.org/10.1016/C2016-0-01894-6, 2019.

Gettelman, A., Christensen, M. W., Diamond, M. S., Gryspeerdt, E., Manshausen, P., Stier, P., Watson Parris, D., Yang, M., Yoshioka, M., and Yuan, T.: Has reducing ship emissions brought forward global warming?, Geophys. Res. Lett., 51, https://doi.org/10.1029/2024gl109077, 2024.

Ghosh, A.: Possibilities and challenges for the inclusion of the electric vehicle (EV) to reduce the carbon footprint in the transport sector: a review, Energies, 13, 2602, https://doi.org/10.3390/en13102602, 2020.

Graver, B., Rutherford, D., and Zheng, S.: CO$_2$ emissions from commercial aviation: 2013, 2018, and 2019, Tech. rep., The International Council on Clean Transportation (ICCT), https://theicct.org/wp-content/uploads/2021/06/CO2-commercial-aviation-oct2020.pdf (last access: 27 February 2026), 2020.

Hagberg, A. A., Schult, D. A., and Swart, P. J.: Exploring network structure, dynamics, and function using NetworkX, in: Proceedings of the 7th Python in Science Conference, edited by: Varoquaux, G., Vaught, T., and Millman, J., Pasadena, CA, USA, 11–15, https://doi.org/10.25080/TCWV9851, 2008.

Hersbach, H., Bell, B., Berrisford, P., Biavati, G., Horányi, A., Muñoz Sabater, J., Nicolas, J., Peubey, C., Radu, R., Rozum, I., Schepers, D., Simmons, A., Soci, C., Dee, D., and Thépaut, J.-N.: ERA5 hourly data on pressure levels from 1940 to present Copernicus Climate Change Service (C3S) Climate Data Store (CDS) [data set], https://doi.org/10.24381/cds.bd0915c6, 2023.

Hiraishi, T., Nyenzi, B., Odingo, R., Galbally, I., Paciornik, N., and Tichy, M.: Annex 1: Conceptual Basis for Uncertainty Analysis: IPCC Good Practice Guidance and Uncertainty Management in National Greenhouse Gas Inventories, https://www.ipcc.ch/

site/assets/uploads/2018/03/A1_Conceptual-1.pdf (last access: 27 February 2026), 2000a.

Hiraishi, T., Nyenzi, B., Odingo, R., Penman, J., Habetsion, S., Abel, K., Eggleston, S., and Pullus, T.: Chapter 6: Quantifying Uncertainties in Practice: IPCC Good Practice Guidance and Uncertainty Management in National Greenhouse Gas Inventories, https://www.ipcc.ch/site/assets/uploads/2018/03/6_Uncertainty-1.pdf (last access: 27 February 2026), 2000b.

Hoesly, R. M., Smith, S. J., Feng, L., Klimont, Z., Janssens-Maenhout, G., Pitkanen, T., Seibert, J. J., Vu, L., Andres, R. J., Bolt, R. M., Bond, T. C., Dawidowski, L., Kholod, N., Kurokawa, J.-I., Li, M., Liu, L., Lu, Z., Moura, M. C. P., O'Rourke, P. R., and Zhang, Q.: Historical (1750–2014) anthropogenic emissions of reactive gases and aerosols from the Community Emissions Data System (CEDS), Geosci. Model Dev., 11, 369–408, https://doi.org/10.5194/gmd-11-369-2018, 2018.

Huang, H., Zhou, C., Huang, L., Xiao, C., Wen, Y., Li, J., and Lu, Z.: Inland ship emission inventory and its impact on air quality over the middle Yangtze River, China, Sci. Total Environ., 843, 156770, https://doi.org/10.1016/j.scitotenv.2022.156770, 2022.

IATA: Air Freight Bills (CASS), Tech. rep., International Air Transport Association, Montreal, Canada, https://www.iata.org/en/services/finance/cass/ (last access: 6 February 2026), 2019.

ICAO: Manual of the ICAO Standard Atmosphere: Extended to 80 Kilometres (262 500 Feet), Doc (International Civil Aviation Organization), International Civil Aviation Organization, https://books.google.de/books?id=4RgKxAEACAAJ (last access: 6 February 2026), 1993.

ICAO: Annex 16 to the Convention on International Civil Aviation – Environmental Protection – Volume II: Aircraft Engine Emissions, 3rd edn., Tech. rep., International Civil Aviation Organization, https://www.bazl.admin.ch/dam/de/sd-web/2zooNDDnJSFa/icao_annex_16_environmentalprotectionvolumeii-aircraftengineemis.pdf (last access: 27 February 2026), 2008.

IEA: The Future of Trucks: Implications for energy and the environment, Tech. rep., IEA, Paris, https://www.iea.org/reports/the-future-of-trucks (last access: 6 February 2026), 2017.

IMO: Carriage requirements for shipborne navigational systems and equipment (SOLAS Chapter V, Regulation 19.2), Tech. rep., https://www.navcen.uscg.gov/sites/default/files/pdf/AIS/SOLAS.V.19.2.1-5.pdf (last access: 6 February 2026), 2004.

INFRAS: Handbook emission factors for road transport (HBEFA), https://www.hbefa.net/e/index.html, last access: 6 February 2026.

IPCC: Reporting Tables, in: 2006 IPCC Guidelines for National Greenhouse Gas Inventories, Prepared by the National Greenhouse Gas Inventories Programme, edited by: Eggleston, H., Buendia, L., Miwa, K., Ngara, T., and Tanabe, K., book section 8A.2, IGES, Japan, https://www.ipcc-nggip.iges.or.jp/public/2006gl/pdf/1_Volume1/V1_8x_Ch8_An2_ReportingTables.pdf (last access: 27 February 2026), 2006.

ITU: Recommendation ITU-R M.1371-5 Technical characteristics for an automatic identification system using time division multiple access in the VHF maritime mobile frequency band, Tech. rep., International Telecommunication Union, https://www.itu.int/dms_pubrec/itu-r/rec/m/R-REC-M.1371-5-201402-I!!PDF-E.pdf (last access: 6 February 2026), 2014.

Iturbide, M., Gutiérrez, J. M., Alves, L. M., Bedia, J., Cerezo-Mota, R., Cimadevilla, E., Cofiño, A. S., Di Luca, A., Faria, S. H., Gorodetskaya, I. V., Hauser, M., Herrera, S., Hennessy, K., Hewitt, H. T., Jones, R. G., Krakovska, S., Manzanas, R., Martínez-Castro, D., Narisma, G. T., Nurhati, I. S., Pinto, I., Seneviratne, S. I., van den Hurk, B., and Vera, C. S.: An update of IPCC climate reference regions for subcontinental analysis of climate model data: definition and aggregated datasets, Earth Syst. Sci. Data, 12, 2959–2970, https://doi.org/10.5194/essd-12-2959-2020, 2020.

Jaghdani, T. J. and Ketabchy, M.: The Strategic significance of the Russian Volga River System, Russian Analytical Digest, 304, 22–27, https://doi.org/10.3929/ethz-b-000643679, 2023.

Jalkanen, J.-P., Brink, A., Kalli, J., Pettersson, H., Kukkonen, J., and Stipa, T.: A modelling system for the exhaust emissions of marine traffic and its application in the Baltic Sea area, Atmos. Chem. Phys., 9, 9209–9223, https://doi.org/10.5194/acp-9-9209-2009, 2009.

Janssens-Maenhout, G., Crippa, M., Guizzardi, D., Muntean, M., Schaaf, E., Dentener, F., Bergamaschi, P., Pagliari, V., Olivier, J. G. J., Peters, J. A. H. W., van Aardenne, J. A., Monni, S., Doering, U., Petrescu, A. M. R., Solazzo, E., and Oreggioni, G. D.: EDGAR v4.3.2 Global Atlas of the three major greenhouse gas emissions for the period 1970–2012, Earth Syst. Sci. Data, 11, 959–1002, https://doi.org/10.5194/essd-11-959-2019, 2019.

Jaramillo, P., Kahn Ribeiro, S., Newman, P., Dhar, S., Diemuodeke, O., Kajino, T., Lee, D., Nugroho, S., Ou, X., Hammer Strømman, A., and Whitehead, J.: Transport, in: Climate Change 2022: Mitigation of Climate Change. Contribution of Working Group III to the Sixth Assessment Report of the Intergovernmental Panel on Climate Change, edited by: Shukla, P., Skea, J., Slade, R., Khourdajie, A. A., van Diemen, R., McCollum, D., Pathak, M., Some, S., Vyas, P., Fradera, R., Belkacemi, M., Hasija, A., Lisboa, G., Luz, S., and Malley, J., Cambridge University Press, Cambridge, UK and New York, NY, USA, https://doi.org/10.1017/9781009157926.012, 2022.

Jelinek, F., Carlier, S., and Smith, J.: Advanced Emission Model (AEM3) v1.5 Validation Report, Tech. rep., EUROCONTROL Experimental Centre, Breitgny sur Orge, France, https://www.eurocontrol.int/sites/default/files/library/016a_AEM_Validation.pdf (last access: 27 February 2026), 2004.

Johansson, L., Jalkanen, J.-P., and Kukkonen, J.: Global assessment of shipping emissions in 2015 on a high spatial and temporal resolution, Atmos. Environ., 167, 403–415, https://doi.org/10.1016/j.atmosenv.2017.08.042, 2017.

Jordan, G. and Henry, M.: IMO2020 regulations accelerate global warming by up to 3 years in UKESM1, Earths Future, 12, e2024EF005011, https://doi.org/10.1029/2024EF005011, 2024.

Knörr, W., Heidt, C., Schmied, M., and Notte, B.: Aktualisierung der Emissionsberechnung für die Binnenschifffahrt und Übertragung der Daten in TREMOD, https://www.ifeu.de/fileadmin/uploads/IFEU-INFRAS-2013-Aktualisierung-der-Emissionsberechnung-für-die-Binnenschifffahrt-und-Übertragung-der-Daten-in-TREMOD3.pdf (last access: 26 February 2026), 2013.

Lamb, W. F., Wiedmann, T., Pongratz, J., Andrew, R., Crippa, M., Olivier, J. G. J., Wiedenhofer, D., Mattioli, G., Khourdajie, A. A., House, J., Pachauri, S., Figueroa, M., Saheb, Y., Slade, R., Hubacek, K., Sun, L., Ribeiro, S. K., Khennas, S., de la Rue du

Can, S., Chapungu, L., Davis, S. J., Bashmakov, I., Dai, H., Dhakal, S., Tan, X., Geng, Y., Gu, B., and Minx, J.: A review of trends and drivers of greenhouse gas emissions by sector from 1990 to 2018, Environ. Res. Lett., 16, 073005, https://doi.org/10.1088/1748-9326/abee4e, 2021.

Lee, D., Fahey, D., Skowron, A., Allen, M., Burkhardt, U., Chen, Q., Doherty, S., Freeman, S., Forster, P., Fuglestvedt, J., Gettelman, A., De León, R., Lim, L., Lund, M., Millar, R., Owen, B., Penner, J., Pitari, G., Prather, M., Sausen, R., and Wilcox, L.: The contribution of global aviation to anthropogenic climate forcing for 2000 to 2018, Atmos. Environ., 244, 117834, https://doi.org/10.1016/j.atmosenv.2020.117834, 2021.

Lekaki, D., Kastori, M., Papadimitriou, G., Mellios, G., Guizzardi, D., Muntean, M., Crippa, M., Oreggioni, G., and Ntziachristos, L.: Road transport emissions in EDGAR (Emissions Database for Global Atmospheric Research), Atmos. Environ., 324, 120422, https://doi.org/10.1016/j.atmosenv.2024.120422, 2024.

Lewis, P., Donahue, K., Benitez, J., Doyle, A., Gomez, R., Narukullapati, S. S., O'Brien, T., Olson, B., Reuter, J., Schildt, S., Suico, G., Vij, A., and Vu, K.: Waterborne Competitiveness: U.S. and Foreign Investments in Inland Waterways, Tech. rep., Eno Center for Transportation, https://enotrans.org/wp-content/uploads/2023/02/Waterborne-Competitiveness-Eno-Center-for-Transportation.pdf (last access: 6 February 2026), 2022.

Linke, F.: Ökologische Analyse operationeller Lufttransportkonzepte, PhD, Technische Universität Hamburg, https://elib.dlr.de/103182/ (last access: 27 February 2026), 2016.

Löber, M., Bondorf, L., Grein, T., Reiland, S., Wieser, S., Epple, F., Philipps, F., and Schripp, T.: Investigations of airborne tire and brake wear particles using a novel vehicle design, Environ. Sci. Pollut. Res., 31, 53521–53531, https://doi.org/10.1007/s11356-024-34543-9, 2024.

Lund, M. T., Aamaas, B., Stjern, C. W., Klimont, Z., Berntsen, T. K., and Samset, B. H.: A continued role of short-lived climate forcers under the Shared Socioeconomic Pathways, Earth Syst. Dynam., 11, 977–993, https://doi.org/10.5194/esd-11-977-2020, 2020.

Ma, S., Lei, T., Meng, J., Liang, X., and Guan, D.: Contributions of key countries, enterprises, and refineries to greenhouse gas emissions in global oil refining, 2000–2021, Innovation (Camb), 4, 100361, https://doi.org/10.1016/j.xinn.2022.100361, 2022.

Mastrandrea, M. D., Field, C. B., Stocker, T. F., Edenhofer, O., Ebi, K. L., Frame, D. J., Held, H., Kriegler, E., Mach, K. J., Matschoss, P. R., Plattner, G.-K., Yohe, G. W., and Zwiers, F. W.: Guidance Note for Lead Authors of the IPCC Fifth Assessment Report on Consistent Treatment of Uncertainties, https://pure.mpg.de/rest/items/item_2147184/component/file_2147185/content (last access: 27 February 2026), 2010.

Mathissen, M., Grigoratos, T., Gramstat, S., Mamakos, A., Vedula, R., Agudelo, C., Grochowicz, J., and Giechaskiel, B.: Interlaboratory study on brake particle emissions part II: particle number emissions, Atmosphere-Basel, 14, 424, https://doi.org/10.3390/atmos14030424, 2023.

Matthias, V., Bieser, J., Mocanu, T., Pregger, T., Quante, M., Ramacher, M. O., Seum, S., and Winkler, C.: Modelling road transport emissions in Germany – current day situation and scenarios for 2040, Transport. Res. D-Tr. E., 87, 102536, https://doi.org/10.1016/j.trd.2020.102536, 2020.

McDonald, B. C., McBride, Z. C., Martin, E. W., and Harley, R. A.: High-resolution mapping of motor vehicle carbon dioxide emissions, J. Geophys. Res.-Atmos., 119, 5283–5298, https://doi.org/10.1002/2013JD021219, 2014.

Meijer, J., Huijbregts, M., and Schotten, C.: Global patterns of current and future road infrastructure, Environ. Res. Lett., 13, 064006, https://doi.org/10.1088/1748-9326/aabd42, 2018.

Mertens, M., Brinkop, S., Graf, P., Grewe, V., Hendricks, J., Jöckel, P., Lanteri, A., Matthes, S., Rieger, V. S., Righi, M., and Thor, R. N.: The contribution of transport emissions to ozone mixing ratios and methane lifetime in 2015 and 2050 in the Shared Socioeconomic Pathways (SSPs), Atmos. Chem. Phys., 24, 12079–12106, https://doi.org/10.5194/acp-24-12079-2024, 2024.

Milios, A., Bereta, K., Chatzikokolakis, K., Zissis, D., and Matwin, S.: Automatic fusion of satellite imagery and AIS data for vessel detection, in: 2019 22th International Conference on Information Fusion (FUSION), https://doi.org/10.23919/FUSION43075.2019.9011339, 1–5, 2019.

Monks, P., Allan, J., Reeves, C., Williams, M., and Carruthers, D.: Non-Exhaust Emissions from Road Traffic, Tech. rep., Department for Environment, Food and Rural Affairs; Scottish Government; Welsh Government; and Department of the Environment in Northern Ireland, https://uk-air.defra.gov.uk/assets/documents/reports/cat09/1907101151_20190709_Non_Exhaust_Emissions_typeset_Final.pdf (last access: 6 Febrary 2026), 2019.

Morales, M., Gonzalez-García, S., Aroca, G., and Moreira, M. T.: Life cycle assessment of gasoline production and use in Chile, Sci. Total Environ., 505, 833–843, https://doi.org/10.1016/j.scitotenv.2014.10.067, 2015.

Nuic, A., Poles, D., and Mouillet, V.: BADA: an advanced aircraft performance model for present and future ATM systems, Int. J. Adapt. Control Signal Process., 24, 850–866, https://doi.org/10.1002/acs.1176, 2010.

OECD: Passenger Transport by Mode (Rail, Road, Cars, Buses), https://data-viewer.oecd.org/?chartId=68958164-16bd-4f7a-9e70-3f39bb05cbb0 (last access: 6 February 2026), 2025.

O'Rourke, P., Smith, S., Mott, A., Ahsan, H., McDuffie, E., Crippa, M., Klimont, Z., Mcdonald, B., Wang, S., Nicholson, M., Hoesly, R., and Feng, L.: CEDS v_2021_04_21 Gridded emissions data, PNNL [data set], https://doi.org/10.25584/PNNLDataHub/1779095, 2021.

Paolo, F. S., Kroodsma, D., Raynor, J., Hochberg, T., Davis, P., Cleary, J., Marsaglia, L., Orofino, S., Thomas, C., and Halpin, P.: Satellite mapping reveals extensive industrial activity at sea, Nature, 625, 85–91, https://doi.org/10.1038/s41586-023-06825-8, 2024.

Paxian, A., Eyring, V., Beer, W., Sausen, R., and Wright, C.: Present-day and future global bottom-up ship emission inventories including polar routes, Environ. Sci. Technol., 44, 1333–1339, https://doi.org/10.1021/es9022859, 2010.

Peng, X., Ding, Y., Yi, W., Laroussi, I., He, T., He, K., and Liu, H.: The inland waterway ship emission inventory modeling:

the Yangtze River case, Transport. Res. D-Tr. E., 129, 104138, https://doi.org/10.1016/j.trd.2024.104138, 2024.

Perricone, G., Alemani, M., Wahlström, J., and Olofsson, U.: A proposed driving cycle for brake emissions investigation for test stand, P. I. Mech. Eng. D-J. Aut., 234, 122–135, https://doi.org/10.1177/0954407019841222, 2020.

Poles, D., Nuic, A., and Mouillet, V.: Advanced aircraft performance modeling for ATM: analysis of BADA model capabilities, in: 29th Digital Avionics Systems Conference, https://doi.org/10.1109/DASC.2010.5655518, 1.D.1–1–1.D.1–14, 2010.

Press Information Bureau, Government of India: Cargo movement through waterways: 9.11 million tonnes on National Waterway-1 (Ganga) in 2019–20, https://www.pib.gov.in/PressReleasePage.aspx?PRID=2003047 (last access: 27 February 2026), 2023.

Prime, N., Smith, S. J., Ahsan, H., Hoesly, R. M., Mott, A., O'Rourke, P. R., McDuffie, E. E., Crippa, M., Klimont, Z., McDonald, B., Wang, S., Nicholson, M. B., and Feng, L.: CEDS Version 2021-04-21 Aircraft Emissions Fix, Zenodo [code], https://doi.org/10.5281/zenodo.7846185, 2023.

Quadros, F. D. A., Snellen, M., Sun, J., and Dedoussi, I. C.: Global civil aviation emissions estimates for 2017–2020 using ADS-B data, J. Aircraft, 59, 1394–1405, https://doi.org/10.2514/1.C036763, 2022.

Quaglia, I. and Visioni, D.: Modeling 2020 regulatory changes in international shipping emissions helps explain anomalous 2023 warming, Earth Syst. Dynam., 15, 1527–1541, https://doi.org/10.5194/esd-15-1527-2024, 2024.

Radmilovic, Z. and Dragovic, B.: The inland navigation in Europe: basic facts, advantages and disadvantages, J. Marit. Res., 4, 31–46, 2007.

Rahman, M. M., Canter, C., and Kumar, A.: Well-to-wheel life cycle assessment of transportation fuels derived from different North American conventional crudes, Appl. Energ., 156, 159–173, https://doi.org/10.1016/j.apenergy.2015.07.004, 2015.

Rayner, N. A., Parker, D. E., Horton, E. B., Folland, C. K., Alexander, L. V., Rowell, D. P., Kent, E. C., and Kaplan, A.: Global analyses of sea surface temperature, sea ice, and night marine air temperature since the late nineteenth century, J. Geophys. Res.-Atmos., 108, https://doi.org/10.1029/2002JD002670, 2003.

Reed Travel Group: Official Airline Guide (OAG), Tech. rep., Reed Travel Group, Dunstable, UK, https://www.oag.com (last access: 6 February 2026), 2019.

Righi, M., Hendricks, J., and Brinkop, S.: The global impact of the transport sectors on the atmospheric aerosol and the resulting climate effects under the Shared Socioeconomic Pathways (SSPs), Earth Syst. Dynam., 14, 835–859, https://doi.org/10.5194/esd-14-835-2023, 2023.

Sabre: Data Based on Market Information Data Tapes (MIDT), Tech. rep., Sabre AirVision Market Intelligence (MI), Southlake, UK, https://www.sabre.com/products/suites/pricing-and-revenue-optimization/market-intelligence/ (last access: 6 February 2026), 2019.

S&P Global Mobility: Global Vehicles in Operation (VIO), https://www.spglobal.com/mobility/en/products/worldview.html (last access: 6 Febrary 2026), 2021.

Schaefer, M. and Bartosch, S.: Overview on fuel flow correlation methods for the calculation of NO_x, CO and HC emissions and their implementation into aircraft performance software, Tech.

Rep. IB-325-11-13, German Aerospace Center (DLR), Cologne, Germany, 2013.

Schäfer, M., Strohmeier, M., Lenders, V., Martinovic, I., and Wilhelm, M.: Bringing up OpenSky: a large-scale ADS-B sensor network for research, in: Proceedings of the 13th International Symposium on Information Processing in Sensor Networks, IPSN '14, IEEE Press, 83–94, https://doi.org/10.1109/IPSN.2014.6846743, 2014.

Schulte, P., Schlager, H., Ziereis, H., Schumann, U., Baughcum, S. L., and Deidewig, F.: NO emission indices of subsonic long-range jet aircraft at cruise altitude: in situ measurements and predictions, J. Geophys. Res.-Atmos., 102, 21431–21442, https://doi.org/10.1029/97JD01526, 1997.

Schumann, U.: On conditions for contrail formation from aircraft exhausts, Meteorol. Z., 5, 4–23, https://doi.org/10.1127/metz/5/1996/4, 1996.

Schumann, U., Penner, J. E., Chen, Y., Zhou, C., and Graf, K.: Dehydration effects from contrails in a coupled contrail–climate model, Atmos. Chem. Phys., 15, 11179–11199, https://doi.org/10.5194/acp-15-11179-2015, 2015.

Segers, L.: Mapping inland shipping emissions in time and space for the benefit of emission policy development: a case study on the Rotterdam-Antwerp corridor, https://resolver.tudelft.nl/uuid:a260bc48-c6ce-4f7c-b14a-e681d2e528e3 (last access: 6 February 2026), 2021.

Simone, N. W., Stettler, M. E., and Barrett, S. R.: Rapid estimation of global civil aviation emissions with uncertainty quantification, Transport. Res. D-Tr. E., 25, 33–41, https://doi.org/10.1016/j.trd.2013.07.001, 2013.

Skolnik, M.: Radar Handbook, in: 3rd edn., McGraw-Hill New York, NY, USA, ISBN 9780071485470, 2008.

Smith, S. J., McDuffie, E. E., and Charles, M.: Opinion: Coordinated development of emission inventories for climate forcers and air pollutants, Atmos. Chem. Phys., 22, 13201–13218, https://doi.org/10.5194/acp-22-13201-2022, 2022.

Smith, T. W. P., Jalkanen, J. P., Anderson, B. A., Corbett, J. J., Faber, J., Hanayama, S., O'Keeffe, E., Parker, S., Johansson, L., Aldous, L., Raucci, C., Traut, M., Ettinger, S., Nelissen, D., Lee, D. S., Ng, S., Agrawal, A., Winebrake, J. J., Hoen, M., Chesworth, S., and Pandey, A.: Third IMO Greenhouse Gas Study 2014, Tech. rep., International Maritime Organization, London, UK, https://www.imo.org/en/ourwork/environment/pages/greenhouse-gas-studies-2014.aspx (last access: 27 February 2026), 2014.

Solazzo, E., Crippa, M., Guizzardi, D., Muntean, M., Choulga, M., and Janssens-Maenhout, G.: Uncertainties in the Emissions Database for Global Atmospheric Research (EDGAR) emission inventory of greenhouse gases, Atmos. Chem. Phys., 21, 5655–5683, https://doi.org/10.5194/acp-21-5655-2021, 2021.

Soulie, A., Granier, C., Darras, S., Zilbermann, N., Doumbia, T., Guevara, M., Jalkanen, J.-P., Keita, S., Liousse, C., Crippa, M., Guizzardi, D., Hoesly, R., and Smith, S. J.: Global anthropogenic emissions (CAMS-GLOB-ANT) for the Copernicus Atmosphere Monitoring Service simulations of air quality forecasts and reanalyses, Earth Syst. Sci. Data, 16, 2261–2279, https://doi.org/10.5194/essd-16-2261-2024, 2024.

Stettler, M., Eastham, S., and Barrett, S.: Air quality and public health impacts of UK airports.

https://doi.org/10.5194/essd-18-1619-2026

Earth Syst. Sci. Data, 18, 1619–1664, 2026

Part I: Emissions, Atmos. Environ., 45, 5415–5424, https://doi.org/10.1016/j.atmosenv.2011.07.012, 2011.

Stettler, M. E. J., Boies, A. M., Petzold, A., and Barrett, S. R. H.: Global civil aviation black carbon emissions, Environ. Sci. Technol., 47, 10397–10404, https://doi.org/10.1021/es401356v, 2013.

Strohmeier, M., Olive, X., Lübbe, J., Schäfer, M., and Lenders, V.: Crowdsourced air traffic data from the OpenSky Network 2019–2020, Earth Syst. Sci. Data, 13, 357–366, https://doi.org/10.5194/essd-13-357-2021, 2021.

Sun, P., Young, B., Elgowainy, A., Lu, Z., Wang, M., Morelli, B., and Hawkins, T.: Criteria air pollutant and greenhouse gases emissions from U.S. refineries allocated to refinery products, Environ. Sci. Technol., 53, 6556–6569, https://doi.org/10.1021/acs.est.8b05870, 2019.

Swaid, M., Linke, F., and Gollnick, V.: A methodology for efficient statistical analysis of air distance in aviation, in: AIAA Aviation Forum and ASCEND, https://doi.org/10.2514/6.2024-3850, 2024.

Szopa, S., Naik, V., Adhikary, B., Artaxo, P., Berntsen, T., Collins, W., Fuzzi, S., Gallardo, L., Kiendler-Scharr, A., Klimont, Z., Liao, H., Unger, N., and Zanis, P.: Short-lived climate forcers, in: Climate Change 2021: The Physical Science Basis. Contribution of Working Group I to the Sixth Assessment Report of the Intergovernmental Panel on Climate Change, edited by: Masson-Delmotte, V., Zhai, P., Pirani, A., Connors, S. L., Péan, C., Berger, S., Caud, N., Chen, Y., Goldfarb, L., Gomis, M. I., Huang, M., Leitzell, K., Lonnoy, E., Matthews, J. B. R., Maycock, T. K., Waterfield, T., Yelekçi, O., Yu, R., and Zhou, B., Cambridge University Press, Cambridge, UK and New York, NY, USA, https://doi.org/10.1017/9781009157896.008, 2021.

Teoh, R., Schumann, U., Majumdar, A., and Stettler, M. E. J.: Mitigating the climate forcing of aircraft contrails by small-scale diversions and technology adoption, Environ. Sci. Technol., 54, 2941–2950, https://doi.org/10.1021/acs.est.9b05608, 2020.

Teoh, R., Engberg, Z., Shapiro, M., Dray, L., and Stettler, M. E. J.: The high-resolution Global Aviation emissions Inventory based on ADS-B (GAIA) for 2019–2021, Atmos. Chem. Phys., 24, 725–744, https://doi.org/10.5194/acp-24-725-2024, 2024.

Teske, S., Giurco, D., Morris, T., Nagrath, K., Mey, F., Briggs, C., Dominish, E., and Florin, N.: Achieving the Paris Climate Agreement goals: Global and regional 100% renewable energy scenarios with non-energy GHG pathways for +1.5°C and +2°C, Springer eBook Collection, Springer International Publishing, https://doi.org/10.1007/978-3-030-05843-2, 2019.

Thomsen, N.: ULTImodel, Zenodo [code], https://doi.org/10.5281/zenodo.7826486, 2023.

Thomsen, N. and Schulz, A.: Projecting traffic flows for road-based passenger transport in Europe for the analysis of climate impact, Eur. Transp. Res. Rev., 16, 33, https://doi.org/10.1186/s12544-024-00652-2, 2024.

Thomsen, N. and Seum, S.: Using open data for spatial transport emission modelling, in: European Transport Conference ETC 2021, https://elib.dlr.de/144436/ (last access: 27 February 2026), 2021.

Thor, R. N., Mertens, M., Matthes, S., Righi, M., Hendricks, J., Brinkop, S., Graf, P., Grewe, V., Jöckel, P., and Smith, S.: An inconsistency in aviation emissions between CMIP5 and CMIP6 and the implications for short-lived species and their radiative forcing, Geosci. Model Dev., 16, 1459–1466, https://doi.org/10.5194/gmd-16-1459-2023, 2023.

Timmermans, B. W., Gommenginger, C. P., Dodet, G., and Bidlot, J.-R.: Global wave height trends and variability from new multimission satellite altimeter products, reanalyses, and wave buoys, Geophys. Res. Lett., 47, e2019GL086880, https://doi.org/10.1029/2019GL086880, 2020.

Tings, B., da Silva, C. A. B., and Lehner, S.: Dynamically adapted ship parameter estimation using TerraSAR-X images, Int. J. Remote Sens., 37, 1990–2015, https://doi.org/10.1080/01431161.2015.1071898, 2016.

Townsin, R. L.: The ship hull fouling penalty, Biofouling, 19, 9–15, https://doi.org/10.1080/0892701031000088535, 2003.

Urjais, D.: DDR2 Reference Manual for Airline Users (ed. 2.9.11), Tech. rep., EUROCONTROL, Brussels, Belgium, https://www.eurocontrol.int/ddr (last access: 6 February 2026), 2022.

Vachon, P., Campbell, J., Bjerkelund, C., Dobson, F., and Rey, M.: Ship detection by the RADARSAT SAR: validation of detection model predictions, Can. J. Remote Sens., 23, 48–59, https://doi.org/10.1080/07038992.1997.10874677, 1997.

Waterborne Commerce Statistics Center: 2019 – State to State Commodity Tonnages Public Domain Database, https://ndclibrary.sec.usace.army.mil/resource?title=2019-State to State Commodity Tonnages Public Domain Database in EXCEL format& documentId=d1eafdfc-426d-4e47-bbf5-a638d4d8825e (last access: 27 February 2026), 2021.

Weder, C. M., Berster, P., Clococeanu, M., Gelhausen, M., Lau, A., Linke, F., Matthes, S., Zengerling, Z. L., Brinkop, S., Hendricks, J., Schulz, A., and Righi, M.: ELK – Global Emission Inventory – Aviation Sector, 2019, DLR [data set], https://doi.org/10.15489/86s8uwpxik95, 2025.

Wilkerson, J. T., Jacobson, M. Z., Malwitz, A., Balasubramanian, S., Wayson, R., Fleming, G., Naiman, A. D., and Lele, S. K.: Analysis of emission data from global commercial aviation: 2004 and 2006, Atmos. Chem. Phys., 10, 6391–6408, https://doi.org/10.5194/acp-10-6391-2010, 2010.

Woehler, S., Atanasov, G., Silberhorn, D., Fröhler, B., and Zill, T.: Preliminary Aircraft Design within a Multidisciplinary and Multifidelity Design Environment, in: Aerospace Europe Conference 2020, https://elib.dlr.de/185515/ (last access: 27 February 2026), 2020.

Yeh, S., Mishra, G. S., Fulton, L., Kyle, P., McCollum, D. L., Miller, J., Cazzola, P., and Teter, J.: Detailed assessment of global transport-energy models' structures and projections, Transport. Res. D-Tr. E., 55, 294–309, https://doi.org/10.1016/j.trd.2016.11.001, 2017.

Yi, W., Wang, X., He, T., Liu, H., Luo, Z., Lv, Z., and He, K.: The high-resolution global shipping emission inventory by the Shipping Emission Inventory Model (SEIM), Earth Syst. Sci. Data, 17, 277–292, https://doi.org/10.5194/essd-17-277-2025, 2025.

Zengerling, Z. L., Linke, F., Weder, C. M., and Dahlmann, K.: Climate-Optimised Intermediate Stop Operations: Mitigation Potential and Differences from Fuel-Optimised Configuration, Appl. Sci., 12, https://doi.org/10.3390/app122312499, 2022.